Global and Regional Sea Level Rise Scenarios for the United States

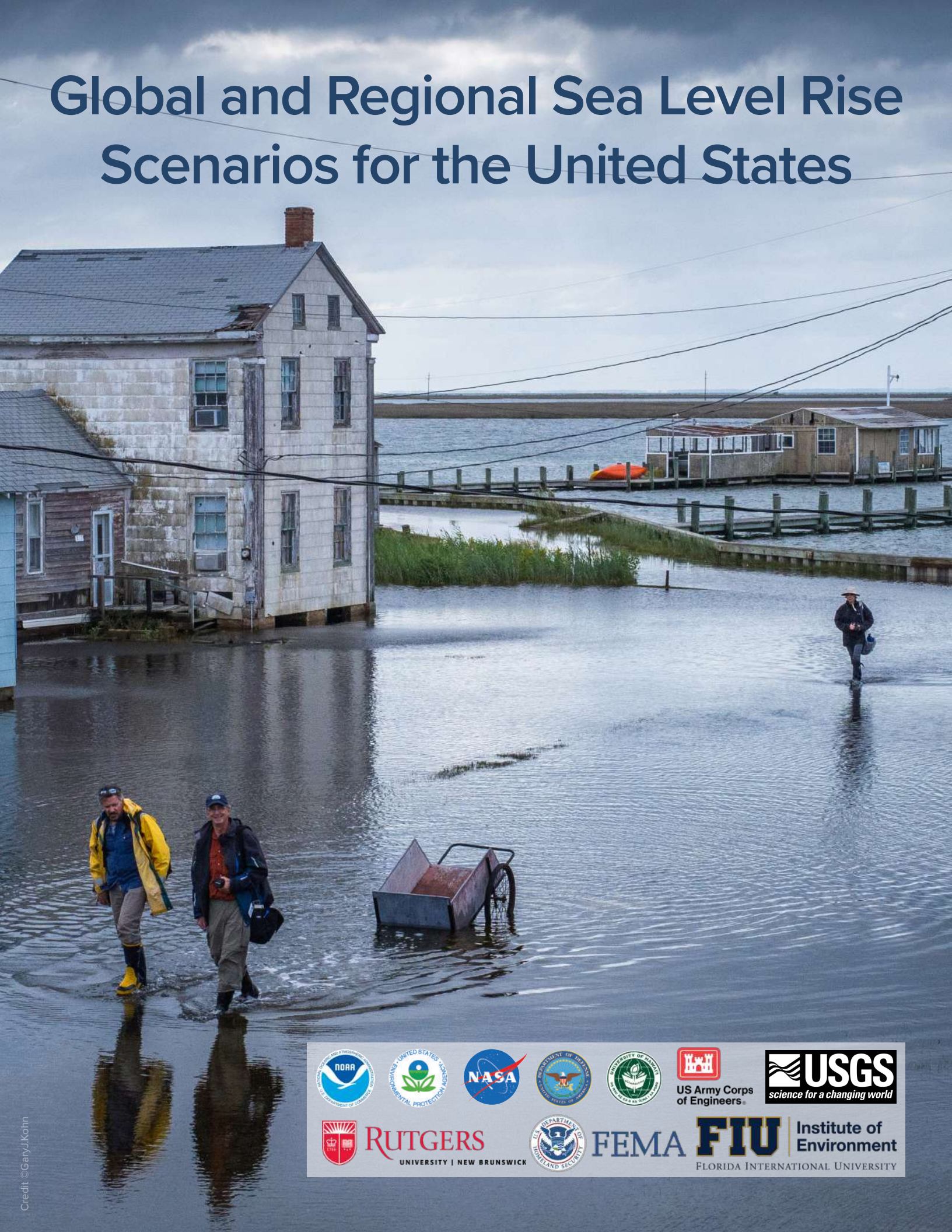

Credit ©Gary J. Kohn

NOAA · United States Environmental Protection Agency · NASA · Department of Defense · University of Hawai'i · US Army Corps of Engineers · USGS science for a changing world

Rutgers University | New Brunswick · U.S. Department of Homeland Security · FEMA · FIU Institute of Environment, Florida International University

Cover Image: Flooding from 15-knot northerly winds on Smith Island, Maryland, on November 23, 2015. Credit ©Gary J. Kohn

National Oceanic and Atmospheric Administration
U.S. Department of Commerce
National Ocean Service
Silver Spring, Maryland
February, 2022

Recommended Citation:
Sweet, W.V., B.D. Hamlington, R.E. Kopp, C.P. Weaver, P.L. Barnard, D. Bekaert, W. Brooks, M. Craghan, G. Dusek, T. Frederikse, G. Garner, A.S. Genz, J.P. Krasting, E. Larour, D. Marcy, J.J. Marra, J. Obeysekera, M. Osler, M. Pendleton, D. Roman, L. Schmied, W. Veatch, K.D. White, and C. Zuzak, 2022: Global and Regional Sea Level Rise Scenarios for the United States: Updated Mean Projections and Extreme Water Level Probabilities Along U.S. Coastlines. NOAA Technical Report NOS 01. National Oceanic and Atmospheric Administration, National Ocean Service, Silver Spring, MD, 111 pp. https://oceanservice.noaa.gov/hazards/sealevelrise/noaa-nos-techrpt01-global-regional-SLR-scenarios-US.pdf

Global and Regional Sea Level Rise Scenarios for the United States: Updated Mean Projections and Extreme Water Level Probabilities Along U.S. Coastlines

Authors

William V. Sweet
NOAA National Ocean Service

Benjamin D. Hamlington
NASA Jet Propulsion Laboratory,
California Institute of Technology

Robert E. Kopp
Rutgers University

Christopher P. Weaver
U.S. Environmental Protection Agency

Patrick L. Barnard
U.S. Geological Survey

David Bekaert
NASA Jet Propulsion Laboratory,
California Institute of Technology

William Brooks
NOAA National Ocean Service

Michael Craghan
U.S. Environmental Protection Agency

Gregory Dusek
NOAA National Ocean Service

Thomas Frederikse
NASA Jet Propulsion Laboratory
California Institute of Technology

Gregory Garner
Rutgers University

Ayesha S. Genz
University of Hawai'i at Mānoa, Cooperative Institute for Marine and Atmospheric Research

John P. Krasting
NOAA Geophysical Fluid Dynamics Laboratory

Eric Larour
NASA Jet Propulsion Laboratory,
California Institute of Technology

Doug Marcy
NOAA National Ocean Service

John J. Marra
NOAA National Centers for Environmental Information

Jayantha Obeysekera
Florida International University

Mark Osler
NOAA National Ocean Service

Matthew Pendleton
Lynker

Daniel Roman
NOAA National Ocean Service

Lauren Schmied
FEMA Risk Management Directorate

Will Veatch
U.S. Army Corps of Engineers

Kathleen D. White
U.S. Department of Defense

Casey Zuzak
FEMA Risk Management Directorate

Table of Contents

List of Figures

List of Tables

Executive Summary

This report and accompanying datasets from the U.S. Sea Level Rise and Coastal Flood Hazard Scenarios and Tools Interagency Task Force provide 1) sea level rise scenarios to 2150 by decade that include estimates of vertical land motion and 2) a set of extreme water level probabilities for various heights along the U.S. coastline. These data are available at 1-degree grids along the U.S. coastline and downscaled specifically at NOAA tide-gauge locations. Estimates of flood exposure are assessed using contemporary U.S. coastal flood-severity thresholds for current conditions (e.g., sea levels and infrastructure footprint) and for the next 30 years (out to year 2050), assuming no additional risk reduction measures are enacted.

This effort builds upon the 2017 Task Force report (Sweet et al., 2017). In particular, the set of global mean sea level rise scenarios from that report are updated and downscaled with output directly from the United Nations Intergovernmental Panel on Climate Change (IPCC) Sixth Assessment Report (AR6; IPCC, 2021a), through the efforts of the NASA Sea Level Change Team; updates include adjustments to the temporal trajectories and exceedance probabilities of these scenarios based upon end-of-century global temperatures. As with the 2017 report, these global mean sea level rise scenarios are regionalized for the U.S. coastline. In addition, methodology supporting the U.S. Department of Defense Regional Sea Level (DRSL) database[1] (Hall et al., 2016) is adapted for the extreme water level dataset newly developed for this report.

This report will be a key technical input for the Fifth National Climate Assessment (NCA5). These data and information are being incorporated into current and planned agency tools and services, such as NOAA's Sea Level Rise Viewer and Inundation Dashboard,[2] NASA's Sea Level Change Portal,[3] and others. Although the intent of this report is not to provide authoritative guidance or design specifications for a specific project, it is intended to help inform Federal agencies, state and local governments, and stakeholders in coastal communities about current and future sea level rise to help contextualize its effects for decision-making purposes.

Key Message #1:
Multiple lines of evidence provide increased confidence, regardless of the emissions pathway, in a narrower range of projected global, national, and regional sea level rise at 2050 than previously reported (Sweet et al., 2017).

- Both trajectories assessed by extrapolating rates and accelerations estimated from historical tide gauge observations, and model projections, fall within the same range in all cases, giving higher confidence in these relative sea level (RSL; land and ocean height changes) rise amounts by 2050.
- Relative sea level along the contiguous U.S. (CONUS) coastline is expected to rise on average as much over the next 30 years (0.25–0.30 m over 2020–2050) as it has over the last 100 years (1920–2020).
- Due to processes driving regional changes in sea level, there are similar regional differences in both the modeled scenarios and observation-based extrapolations, with higher RSL rise along the East (0–5 cm higher on average than CONUS) and Gulf Coasts (10–15 cm higher) as compared to the West (10–15 cm lower) and Hawaiian/Caribbean (5–10 cm lower) Coasts.
- The projections do not include natural year-to-year sea level variability that occurs along U.S. coastlines in response to climatic modes such as the El Niño–Southern Oscillation.

[1] https://drsl.serdp-estcp.org/
[2] https://coast.noaa.gov/digitalcoast/tools/slr.html
[3] https://sealevel.nasa.gov/

Key Message #2

By 2050, the expected relative sea level (RSL) will cause tide and storm surge heights to increase and will lead to a shift in U.S. coastal flood regimes, with major and moderate high tide flood events occurring as frequently as moderate and minor high tide flood events occur today. Without additional risk-reduction measures, U.S. coastal infrastructure, communities, and ecosystems will face significant consequences.

- Minor/disruptive high tide flooding (HTF; about 0.55 m above mean higher high water [MHHW][4]) is projected to increase from a U.S average frequency of about 3 events/year in 2020 to >10 events/year[5] by 2050.
- Moderate/typically damaging HTF (about 0.85 m above MHHW) is projected to increase from a U.S. average frequency of 0.3 events/year in 2020 to about 4 events/year in 2050.
- Major/often destructive HTF (about 1.20 m above MHHW) is projected to increase from a U.S. average frequency of 0.04 events/year in 2020 to 0.2 events/year by 2050.
- Across all severities (minor, moderate, major), HTF along the U.S. East and Gulf Coasts will largely continue to occur at or above the national average frequency.

Key Message #3:

Higher global temperatures increase the chances of higher sea level by the end of the century and beyond. The scenario projections of relative sea level along the contiguous U.S. (CONUS) coastline are about 0.6–2.2 m in 2100 and 0.8–3.9 m in 2150 (relative to sea level in 2000); these ranges are driven by uncertainty in future emissions pathways and the response of the underlying physical processes.

- With an increase in average global temperature of 2°C above preindustrial levels, and not considering the potential contributions from ice-sheet processes with limited agreement (low confidence) among modeling approaches, the probability of exceeding 0.5 m rise globally (0.7 m along the CONUS coastline) by 2100 is about 50%. With 3°–5°C of warming under high emissions pathways, this probability rises to >80% to >99%. The probability of exceeding 1 m globally (1.2 m CONUS) by 2100 rises from <5% with 3°C warming to almost 25% with 5°C warming.
- Considering low-confidence ice-sheet processes and high emissions pathways with warming approaching 5°C, probabilities rise to about 50%, 20%, and 10% of exceeding 1.0 m, 1.5 m, or 2.0 m of global rise by 2100, respectively. These processes are unlikely to make significant contributions with 2°C of warming, but how much warming might be required to trigger them is currently unknown.
- As a result of improved understanding of the timing of possible large future contributions from ice-sheet loss, the "Extreme" scenario from the 2017 report (2.5 m global mean sea level rise by 2100) is now viewed as less plausible and has been removed. Nevertheless, the potential for increased acceleration in the late 21st century and beyond means that the other high-end scenarios provide pathways that could reach this threshold in the decades immediately following 2100 (and continue rising).
- Regionally, the projections are near or higher than the global average in 2100 and 2150 for almost all U.S. coastlines due to the effects from vertical land motion (VLM); gravitational, rotational, and deformational effects due to land ice loss; and ocean circulation changes. Largely due to VLM, RSL projections are lower than the global amounts along the southern Alaska coast and are higher along the Eastern and Western Gulf coastlines.

[4] Mean higher high water (MHHW) level is estimated over the 1983–2001 tidal epoch period and, in this case, is considered a fixed elevation that does not change with sea level rise.

[5] The extreme value statistical methods in this report do not directly resolve frequencies >10 events/year.

Key Message #4

Monitoring the sources of ongoing sea level rise and the processes driving changes in sea level is critical for assessing scenario divergence and tracking the trajectory of observed sea level rise, particularly during the time period when future emissions pathways lead to increased ranges in projected sea level rise.

- Efforts are under way to narrow the uncertainties in ice-sheet dynamics and future sea level rise amounts in response to increasing greenhouse gas forcing and associated global warming.
- Early indicators of changes in sea level rise trajectories can serve to trigger adaptive management plans and are identified through continuous monitoring and assessment of changes in sea level (on global and local scales) and of the key drivers of sea level change that most affect U.S. coastlines, such as ocean heat content, ice-mass loss from Greenland and Antarctica, vertical land motion, and Gulf Stream system changes.

Section 1: Introduction

Sea level rise driven by global climate change is a clear and present risk to the United States today and for the coming decades and centuries (USGCRP, 2018; Hall et al., 2019). Sea levels will continue to rise due to the ocean's sustained response to the warming that has already occurred—even if climate change mitigation succeeds in limiting surface air temperatures in the coming decades (Fox-Kemper et al., 2021). Tens of millions of people in the United States already live in areas at risk of coastal flooding, with more moving to the coasts every year (NOAA NOS and U.S. Census Bureau, 2013). Rising sea levels and land subsidence are combining, and will continue to combine, with other coastal flood factors, such as storm surge, wave effects, rising coastal water tables, river flows, and rainfall (Figure 1.1), some of whose characteristics are also undergoing climate-related changes (USGCRP, 2017). The net result will be a dramatic increase in the exposure and vulnerability of this growing population, as well as the critical infrastructure related to transportation, water, energy, trade, military readiness, and coastal ecosystems and the supporting services they provide.

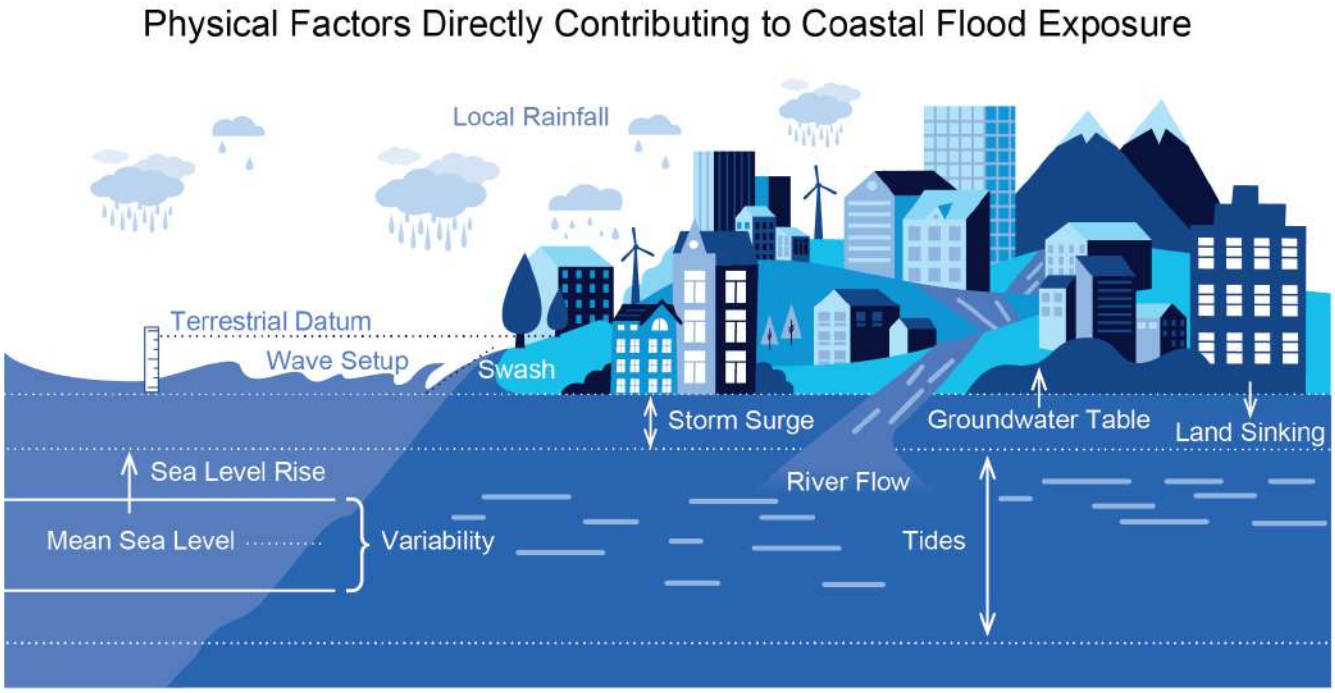

Figure 1.1: Schematic (not to scale) showing physical factors affecting coastal flood exposure. Due to the clear and strong relative sea level rise signal (i.e., combination of sea level rise and sinking lands), the probability of flooding and impacts are increasing along most U.S. coastlines.

Global mean sea level (GMSL) rise is a direct effect of climate change, resulting from a combination of thermal expansion of warming ocean waters and the addition of water mass into the ocean, largely associated with the loss of ice from glaciers and ice sheets. These processes are well understood for the recent past, and their contributions have been estimated for the 20th century (Figure 1.2a). With regard to increasing sea levels associated with climate change, the questions are when and how much, rather than if (USGCRP, 2017; Hall et al., 2019). Increases in GMSL provide an important indicator of the changing climate, but it is the sea level rise on local and regional scales—measured by the global network of tide gauges and satellites—that is most relevant for coastal communities around the world. Regional and local sea level rise has not been and will not be uniform in time or space. Rather, sea levels change locally for a variety of reasons, such as vertical land motion (VLM), which can exacerbate the effects of the rising ocean. For context, whereas GMSL has risen by about 17 cm over the last 100 years (1920–2020), with noted acceleration since about 1970, relative sea level (RSL) averaged along the contiguous United States (CONUS) has risen about 28 cm over the same period with similar onset of acceleration (Figure 1.2b).

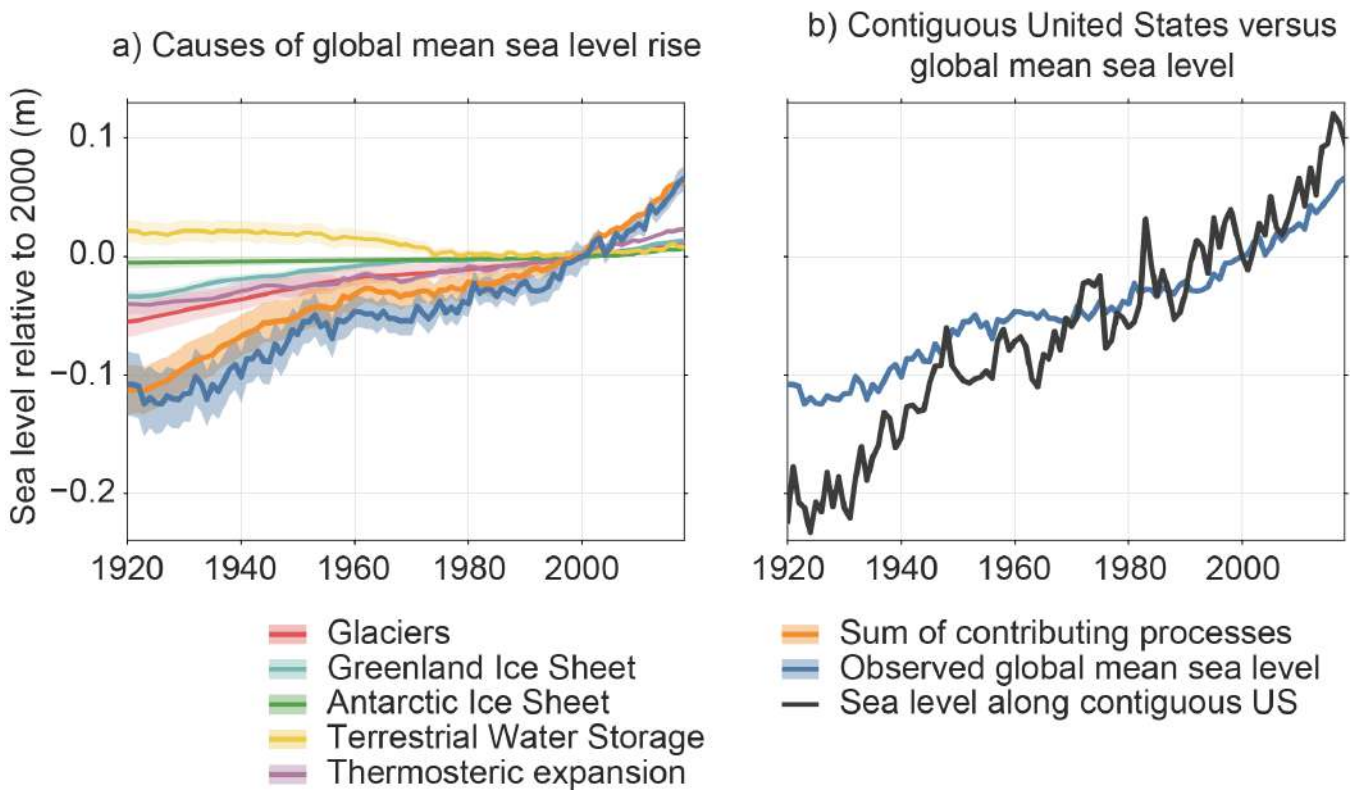

Figure 1.2: a) Observed annual global mean sea level (GMSL) change from global tide gauges (blue line), along with the sum (orange line) of contributions from thermal expansion (thermosteric) and four distinct water-mass-driven increases in GMSL. b) GMSL change (blue line) as shown in a) with the annual average relative sea level change measured by tide gauges around the contiguous United States (black line; with a linear regression estimate of 28 cm of sea level rise from 1920 to 2020). (Adaptation of Frederikse et al., 2020).

While this long-term and upward shift in mean RSL is the underlying driver of changes to the Nation's coasts, extreme water levels (EWLs) occurring against the background of this shifting sea level baseline are responsible for many of the recurring and event-based impacts. In this report, EWLs are explicitly assumed to be ocean-related changes measured by tide gauges (e.g., high tides and storm surges), which typically do not measure other contributors such as direct rainfall or river flow unless they are positioned upstream of major river systems (Moftakhari et al., 2016). Specifically, EWLs are considered as those occurring with an average event frequency between 0.01 events/year (often referred to as the 1% annual chance event) and 10 events/year. This range mostly spans the flood frequency of NOAA high tide flood (HTF) severity levels (minor, moderate, and major). HTF levels are nationally calibrated against NOAA's National Weather Service and local emergency managers' depth-severity thresholds used in weather forecasting and impact communications (NOAA, 2020) to provide a consistent coastal-climate resilience standard (Sweet et al., 2018).

Higher sea levels amplify the impacts of storm surge, high tides, coastal erosion, and wetland loss, even absent any changes in storm frequency and intensity. Because of threshold effects related to changes measured relative to a fixed elevation (Figure 1.3a), even the relatively small increases in sea level over the last several decades have led to greatly increased frequency of flooding[6] at many places along the U.S. coast (Figure 1.3b). Much of the coastline is already close to a flood regime shift, with respect to flood frequency (and presumably damages). That is, only about a 0.3–0.7 m height difference currently separates infrequent, moderate/typically-damaging and major/often-destructive HTF from minor/disruptive "nuisance" HTF (Sweet et al., 2018), whose impacts are already remarkable throughout dozens of densely populated coastal cities (Moore and Obradovich, 2020). Decades ago, powerful storms were what typically caused coastal flooding,

[6] The definition of a "flood" in this report is typically meant to refer to a water level associated with impacts rather than the occurrence of natural phenomena.

but today, due to RSL rise, even common wind events and seasonal high tides regularly cause HTF within coastal communities, affecting homes and businesses, overloading stormwater and wastewater systems, infiltrating coastal groundwater aquifers with saltwater, and stressing coastal wetlands and estuarine ecosystems.

At multiple locations along the U.S. coastline, the annual frequency of minor HTF is accelerating and has more than doubled over the past couple of decades, turning it from a rare event into a recurrent and disruptive problem (Sweet and Park, 2014; Sweet et al., 2018; USGCRP, 2018). For example, the trends in minor/disruptive HTF have grown from about 5 days in 2000 to 10–15 days in New York City and Norfolk, Virginia, in 2020; in Miami, Florida, and Charleston, South Carolina, annual frequencies have grown from 0–2 days to about 5–10 days over the same period. These increases will continue, further accelerate, and spread to more locations over the next couple of decades (Sweet et al., 2021; Thompson et al., 2021). Thus, accurate projections of ongoing and future sea level rise and assessments that integrate across processes and temporal and spatial scales are key inputs to planning efforts and a key goal of this report.

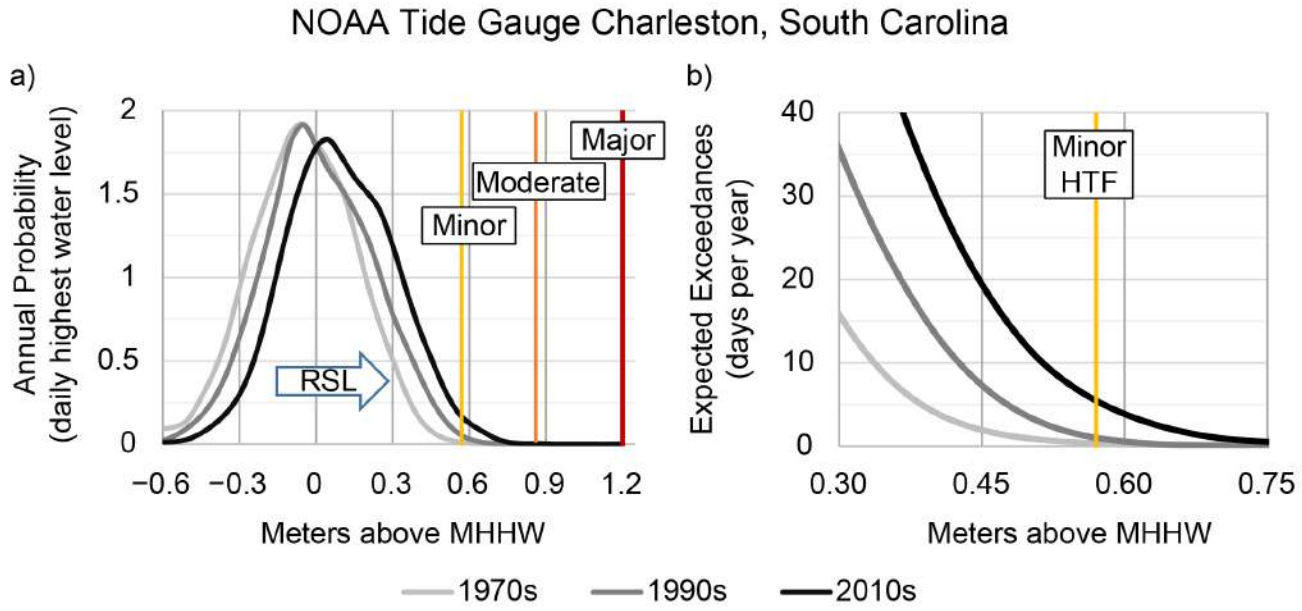

Figure 1.3: a) Annual probability density and b) annual expected exceedances for daily highest water levels relative to the 1983–2001 mean higher high water (MHHW) tidal datum showing increases in NOAA minor, moderate, and major high tide flooding (HTF) probabilities/frequencies due to relative sea level (RSL) rise at the NOAA tide gauge in Charleston, South Carolina.

The Sea Level Rise and Coastal Flood Hazard Scenarios and Tools Interagency Task Force (hereafter "Task Force") was jointly convened at the direction of the White House Resilience Council in 2015 under the U.S. Global Change Research Program (USGCRP), the Subcommittee on Ocean Sciences and Technology (SOST), and the National Ocean Council (NOC). This was in recognition of the strong need and demand for authoritative, consistent, and accessible sea level rise and associated coastal hazard information for the entire U.S. coastline, coordinated across the relevant Federal agencies, to serve as a starting point for on-the-ground coastal preparedness planning and risk management activities. The goal of the Task Force, since its inception, has been to develop the necessary products through sustained and coordinated participation of key agencies, based on the best available science, including regional science and expertise when possible and appropriate. The goal has also been to incorporate those products into user-friendly mapping, visualization, and analysis tools made easily accessible through existing agency portals serving specific partners and stakeholders, as well as interagency venues such as the National Climate Assessment (NCA), the U.S. Climate Resilience Toolkit, and others.

The Task Force focused its initial efforts on the development of an interagency report (Sweet et al., 2017), providing updated GMSL rise scenarios focused primarily on 2100 and integrating these GMSL rise scenarios with regional factors contributing to sea level change to produce, for the first time, a set of RSL scenarios for the entire U.S. coastline. These scenarios were also a major technical input to Volumes I and II of the Fourth NCA (NCA4; USGCRP 2017, 2018) and have been widely used in the development of state (e.g., Florida[7] and Virginia [CCRM, 2019]) and local agency adaptation plans (e.g., Pensacola, Florida,[8] and Portland, Maine [One Climate Future, 2019]), and processes for anticipating and managing future coastal risks.

The Task Force's first report (Sweet et al., 2017) built upon the most current scenarios at that time (e.g., Parris et al., 2012; Kopp et al., 2014; Hall et al., 2016) and estimated the full possible range for GMSL rise by 2100 as being bounded by 0.3 m on the low end, representing a simple linear extrapolation of the GMSL rate since the early 1990s, and by 2.5 m on the high end, representing an extreme ice-sheet melt/discharge scenario. This 0.3–2.5 m range was discretized and aligned with emissions-based, conditional probabilistic storylines and global model projections into six GMSL rise scenarios: Low, Intermediate-Low, Intermediate, Intermediate-High, High, and Extreme, corresponding to GMSL rise by 2100 of 0.3 m, 0.5 m, 1.0 m, 1.5 m, 2.0 m, and 2.5 m, respectively. These GMSL rise scenarios were then used to derive regional RSL responses on a 1-degree grid covering the coastlines of the U.S. mainland, Alaska, Hawai'i, the Caribbean, and the Pacific Island territories, as well as at the precise locations of tide gauges along these coastlines.

This current report takes the Sweet et al. (2017) report as its starting point, updating the GMSL scenarios and the associated local and regional RSL projections to reflect recent advances in sea level science, as well as expanding the types of scenario information provided to better serve stakeholder needs for coastal risk management and adaptation planning. As with the 2017 report, this iteration will also serve as a key technical input to the NCA, in this case NCA5. Specific updates in this report include the following:

- While this report still uses the same nomenclature as the NOAA 2017 GMSL scenarios, it draws upon new science of the Intergovernmental Panel on Climate Change (IPCC) Sixth Assessment Report (AR6; Fox-Kemper et al., 2021; Garner et al., 2021) to provide updated temporal trajectories and exceedance probabilities based on different levels of global warming. One effect is that the associated RSL projections for the U.S. coastline (gridded and at individual tide-gauge locations) differ in timing and magnitude as compared to the NOAA 2017 projections.
- In addition, in leveraging this updated science, including a longer observational record, improved understanding of ice-sheet dynamical processes, and better-constrained models, this report provides a more comprehensive and detailed assessment of the distinct types and range of uncertainties associated with the GMSL rise scenarios, particularly at the high end.
- By utilizing 50-year regional sets of tide-gauge data, observation-based rates and accelerations are extrapolated to the year 2050 to identify the scenario projections aligning with current RSL trajectories.
- Lastly, gridded EWL probabilities are provided, along with methods to localize them along most U.S. coastlines, to contextualize each of the regionalized sea level scenarios across a range of flood frequencies under current standards, from recurrent tidal flooding to major storm-surge flooding, out to 2050.

To frame the remainder of this report, it is important to emphasize the distinction between describing scientific progress, in terms of current understanding and key uncertainties, and translating such advances in the scientific knowledge base into actionable science. The latter requires sustained engagement by groups such as NOAA's Office of Coast Management and the Sea Grant program with users, stakeholder groups, and associated boundary organizations regarding their specific planning and decision contexts. Our development

[7] https://floridadep.gov/rcp/florida-resilient-coastlines-program/documents/proposed-rule-development-draft-62s-7-sea-level

[8] https://storymaps.arcgis.com/stories/e812723f69ad4a618c8f5f8b08cb208e

of scenarios in this report is grounded in the principles of risk-based framing for climate assessment (King et al., 2015; Weaver et al., 2017; Sutton, 2019; Kopp et al., 2019) and is consistent with adaptation pathways approaches for long-term planning. What we thus aim to provide are screening-level (suitable for first-order assessment) products appropriate for framing and bounding important problems in coastal risk assessment and management, along with contextualization of the underlying science and illustrative case studies. For example, consistent with this purpose, this report aims to provide the underlying scientific information to develop both planning- and bounding-type scenarios across the full spectrum of coastal risk; that is, 1) planning scenarios intended to frame near- to mid-term decision contexts and/or longer-term decisions with high-risk tolerance or ability to adjust plans, which address the question, What is most likely to happen? and 2) bounding scenarios designed to set the envelope of possible future outcomes, which can be used to stress-test long-term objectives, gauge the "when, not if" a given level of sea level rise might be reached, and address the question How bad could things get? *What this report does NOT provide is official guidance nor design specifications for a specific project.*

Section 2 describes advances in the understanding of the drivers of mean sea level since the 2017 report, discusses the use of observations for a near-term trajectory assessment, and provides the updated GMSL rise scenarios and their associated regional RSL projections. Section 3 focuses on high-frequency EWLs, including a regional frequency analysis of historical NOAA tide-gauge data to develop a set of EWL probabilities for assessing and projecting (to 2050) across a range of flood levels. Section 4 applies these scenarios and projections in illustrative use-case examples. Section 5 provides a summary of the report findings, as well as conclusions and next steps.

Section 2: Future Mean Sea Level: Scenarios and Observation-Based Assessments

Since Sweet et al. (2017), the observations and available data records of both sea level change and the associated processes have increased in number and length. In part due to these observations, our understanding of the drivers of sea level change has improved. There have also been significant advances in modeling how these processes will cause sea level to change in the future. This has led to an improved understanding of the possible trajectory of future sea level rise. In this report, these advances are reflected both in an update to the GMSL scenarios and a change in approach from Sweet et al. (2017). The primary change in approach is in separating this section into two different time periods: 1) near term (2020–2050) and 2) long term (2050–2150). There is also a section discussing divergence of the GMSL scenarios and tracking that is particularly relevant during the transition between the near- and long-term time periods. In the remainder of this section, a brief overview of the drivers of global and regional sea level rise is provided. Next, updates to Sweet et al. (2017) are discussed, and the motivation and scientific justification for these changes are given. Finally, the updated information for the two time periods, along with the transition between these periods, is provided.

2.1. Overview of Regional and Global Sea Level Rise

Over long, multidecadal to centennial timescales, the primary drivers of changes in GMSL are thermal expansion due to the heating of the ocean and the addition of water mass associated with ice-mass loss from the ice sheets and glaciers. Other changes in the movement of water between ocean and land, including from groundwater depletion and water impoundment, have a secondary impact on GMSL, although they can increase in importance for certain time periods (see Frederikse et al., 2020). During the 20th century, GMSL estimated from tide-gauge records has been explained by the individual processes contributing to it (see Figure 1.2a; Frederikse et al., 2020). More recently, observed GMSL from satellite altimetry over the past 15 years has been explained using the in situ measurements of the Argo profiling floats and the observations of water-mass change from the GRACE and GRACE-FO satellites (WCRP, 2018). On shorter timescales, considerable interannual and decadal variability in GMSL is linked primarily to variations in terrestrial water storage and driven heavily by the El Niño–Southern Oscillation (ENSO; Boening et al. 2012; Fasullo et al., 2013; Piecuch and Quinn, 2016; Hamlington et al., 2020a, 2020b].

At the regional level, rates of sea level rise can deviate significantly from the globally averaged rate. Sea level rise is not uniform across the globe; rather, it manifests as relative sea level (RSL) rise that also responds to several key factors important at regional and local scales (Kopp et al., 2014; Sweet et al., 2017; Hamlington et al., 2020a; Fox-Kemper et al., 2021). On short timescales and in short records, natural variations on interannual to decadal timescales can impact estimates of rates and accelerations. On long timescales, however, there are three primary causes of regional variations in estimated rates and accelerations: 1) sterodynamic sea level change; 2) gravitational, rotational, and deformational (GRD) changes due to contemporary ice-mass loss and the movement of water between land and ocean; and 3) vertical land movement (VLM; subsidence or uplift) due to glacial isostatic adjustment (GIA), tectonics, sediment compaction, groundwater and fossil fuel withdrawals, and other non-climatic factors. These three causes are discussed briefly below.

Sterodynamic sea level changes are those that arise from changes in the ocean's circulation (currents) and its density (temperature and salinity). Sea level rise associated with sterodynamic sea level change is the combination of global mean thermosteric rise associated with global ocean warming and local deviations from the global mean due to ocean dynamic processes. It is these changes in ocean dynamics that lead to regional differences. Focusing on possible causes of long-term sterodynamic sea level changes for the U.S. coastlines, future changes in the Atlantic meridional overturning circulation (AMOC) are particularly relevant. The IPCC AR6 (IPCC, 2021a) determined that it is *very likely* that the AMOC will decline in the future, although there is still disagreement as to the extent of this decline. A weakening AMOC will lead to an increase in sea level along the coastal Northeast and Southeast regions (Yin et al., 2009; Krasting et al.,

2016; see Figure A1.1 for region definitions). For the Northwest and Southwest coastal regions, ENSO plays a substantial role in interannual sea level change, although there is no clear evidence for a sustained shift in ENSO that will result in a long-term increase or decrease in sea level. Some models project future sea level changes associated with ocean dynamics to be large in magnitude in some locations, but these projections remain uncertain (Fox-Kemper et al., 2021).

The ice-mass loss from ice sheets and glaciers to the ocean has a strong influence on regional sea level. Changes in Earth's GRD responses dictate the spatial distribution of water across the global ocean (Farrell and Clark, 1976; Milne and Mitrovica, 1998; Mitrovica et al., 2001). These so-called sea level fingerprints are important to determining regional sea level rise. Mass loss causes a sea level fall in the near-field, a reduced sea level rise at intermediate distances, and a greater-than-global-average sea level rise at larger distances. For U.S. coastlines, particularly in the Northeast, this means that a similar amount of ice-mass loss in Antarctica will have a larger impact than ice-mass loss in Greenland. Similarly, ice-mass loss in Greenland leads to bigger increases in sea level along the Northwest and Southwest coastal regions than along the Northeast coastal region. At any time horizon, the regional sea level rise associated with GRD will be driven both by the amount of ice that is being lost and the source of that ice. These regional fingerprints are tied to projected trajectories of mass loss from the associated source. Changes in terrestrial water storage (groundwater withdrawal and dam building) also have an associated fingerprint, but the regional contribution is generally smaller than that from the ice sheets and glaciers.

Lastly, the VLM considered in this report refers to either subsidence or uplift that occurs in coastal regions and can lead to the change in the height of sea level relative to land. VLM is not a singular phenomenon but instead results from various processes that display different patterns in space and time. These patterns have different impacts from place to place, especially in coastal settings where many of them operate at the same time. For much of the coastal United States, subsidence is driven on local scales by groundwater and fossil fuel withdrawal and on larger scales by GIA. However, in some regions such as southern Alaska, GIA leads to high rates of uplift in coastal regions. GIA is the ongoing response of the solid earth due to ice-mass changes in the past, particularly the deglaciation after the last glacial maximum. GIA induces VLM, in particular subsidence along the U.S. East Coast, as well as changes in the gravity field, which cause local sea level changes. Accurate future projections of VLM require an understanding of the underlying processes and the time and space scales on which they vary. Currently, and in this report, VLM projections are based in part on analysis of past observations. If activities change in a particular location (e.g., reduction in groundwater pumping), an associated change in the rate of VLM will not necessarily be captured. Modeling of future VLM under a range of possible scenarios is not currently available over large scales. (See the vertical land motion use case in Section 4.4 for more information.)

Beyond these processes that impact long-term changes in sea level, there is also considerable natural (or "unforced") climate variability that can lead to significant, albeit temporary, changes to sea level on the order of years or even decades. In many of the available observational records, it can be a challenge to distinguish between these natural signals and those processes discussed above. As an example, in Figure 2.1, the regional rates of sea level rise along U.S. coastlines are shown for the first half (a, 1993–2006), second half (b, 2007–2020), and full (c, 1993–2020) satellite altimeter record (which do not measure VLM effects), along with overlaid tide-gauge rates (which measure VLM effects) measured over the same time period. A significant shift occurs from the first half of the record to the second half, with high sea level rise rates found along all coastlines of CONUS from 2007 to 2020. For the Northwest and Southwest coastal regions, in particular, the rate was near 0 for the first half of the record before shifting to almost 10 mm/year over the second half, driven by decadal variability linked to the Pacific Decadal Oscillation (PDO; e.g., Bromirski et al., 2011; Hamlington et al., 2021). For the full record, there is considerably less spatial variability, with most regions approaching the globally averaged rate of 3.1 mm/year.

In this section of the report, the contribution of natural variability is not assessed directly, but its importance and contribution should be considered when looking at observed rates and assessing possible sea level at a specific time in the future. In other words, there is an "envelope" of naturally occurring sea level variability on top of the sea level rise discussed here that needs to be included to estimate sea level at a particular location at a specific time in the future. A depiction of the relationship between sea level rise and this envelope is provided in Figure 1.3. The median of the distribution increases over time as a result of the rising sea levels, while other sea level variability on a range of timescales contributes to the spread around this central value.

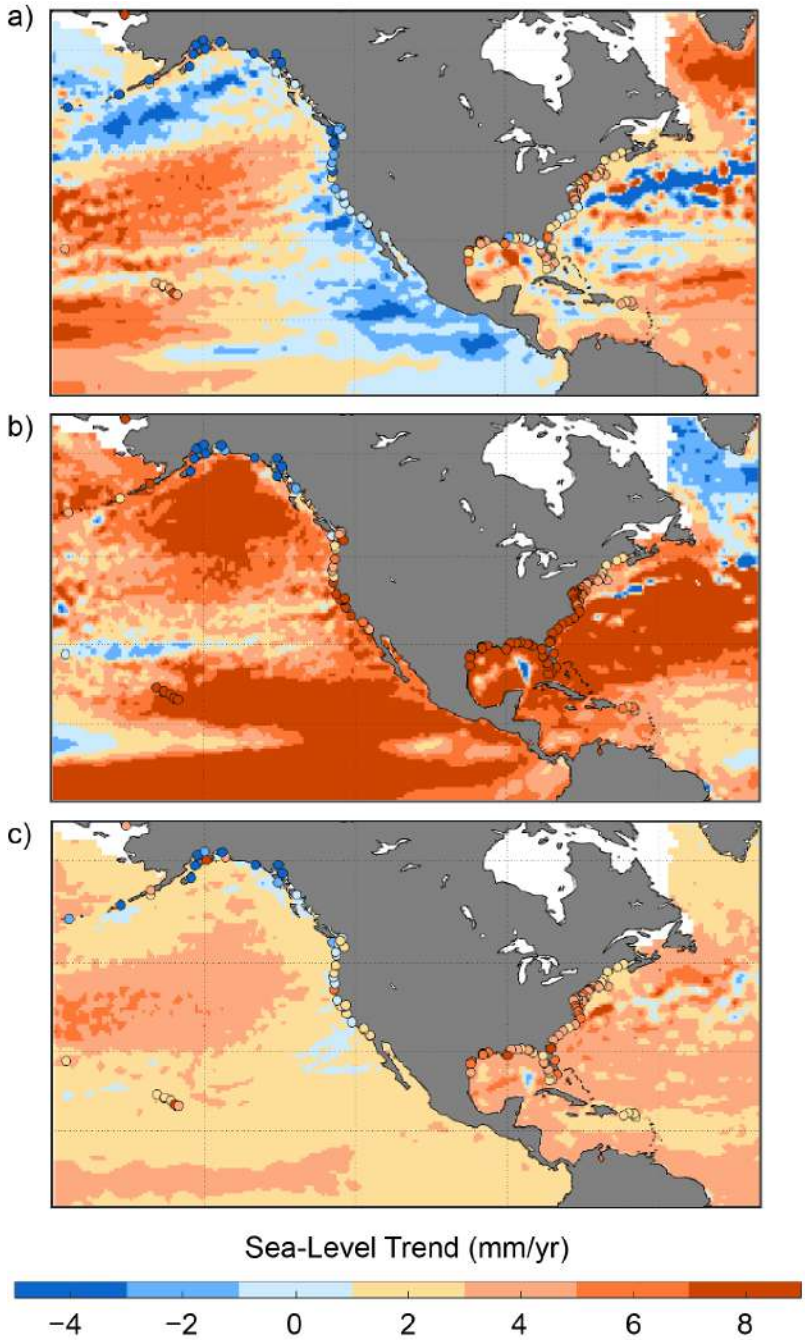

Figure 2.1: Regional sea level linear rates of rise (mm/year) from satellite altimetry over three different time periods: (a) 1993–2006, (b) 2007–2020, and (c) 1993–2020. Linear rates of change of relative sea level (ocean and land height changes) from tide gauges over the same time period are also shown (circles).

2.2. Updates from Sweet et al. (2017)

One of the main structural changes from the Sweet et al. (2017) report to this one is a specific emphasis on the near-term time period, 2020–2050. There is also a detailed discussion of GMSL scenario divergence and tracking that becomes particularly important in the transition from the near term to the long term. The motivation for the focus on these two topics is given below. Following this explanation, the primary advances in the sea level scenarios and assessments of future sea level are discussed in two subsections. The first provides an overview of the science and framework advancements that have led to an update of the scenarios first presented in Sweet et al. (2017). The second covers the inclusion of observation-based assessments of near-term sea level change for the first time.

2.2.1. Inclusion of Near-Term Time Period (2020–2050)

The dedicated focus on the near-term time period represents a new element in this report. Motivation for this change is provided briefly here. With increasing record lengths, the impact of natural sea level variability on estimated rates and accelerations diminishes, revealing more of the underlying climate change signal (see Figure 2.1c, for example). Tide gauges surrounding the U.S. coastlines provide records exceeding 100 years in some locations, and the satellite altimeter record is nearing three decades in length. Recent studies have assessed the degree to which rates and accelerations estimated from these records are reflective of the long-term increase in sea level (via satellite altimetry; e.g., Fasullo and Nerem, 2018; Richter et al., 2020) and RSL (via tide gauges; e.g., Wang et al., 2021). These studies suggest that with appropriate consideration of uncertainty, observation-based extrapolations can be informative in the near term. In this report, an assessment based solely on extrapolation of the observed rates and acceleration out to 2050 is used for trajectory tracking and a comparison to the GMSL and regional scenarios. These trajectories serve as an additional line of evidence for near-term sea level rise and provide a mostly independent (observational VLM information is shared in both) comparison to the model-based scenario. To maintain a distinction between estimates arising from observations and those coming from model-derived GMSL scenarios, the observation-based assessments are referred to in this report as “extrapolations” or “trajectories” and not as “projections.” These terms are also preceded by “observation-based” whenever used.

Beyond this renewed observational focus, the inclusion of this near-term time period is motivated by the fact that for certain decision types, short time horizons and nearer-term assessments are most relevant. For the typical lifetime of buildings and infrastructure in coastal areas, for example, a 30-year planning horizon has particular relevance (e.g., Fu, 2020; Hinkel et al., 2018). Additionally, flexible adaptation pathways and solutions typically require significant lead times on upgrades or replacements of coastal structures that necessitate assessments across a range of timescales. (Haasnoot et al., 2013, 2019; Bloeman et al., 2018; Werners et al., 2021; Hall et al., 2019). Knowing whether adaptation actions are required within the next 30 years or afterwards informs decisions about initial designs, the adaptations required, and the metrics that would trigger adaptation.

2.2.2. GMSL Scenario Divergence and Tracking

After 2050, the assessments and comparisons made using the observation-based extrapolations of future sea level rise become less informative and should be made with caution. This is because uncertainty in the current estimates of rates and accelerations leads to large projected ranges and because current estimates may not be reflective of shifts or process changes that may occur in the future with additional emissions and global warming, resulting in increasing divergence between the future GMSL scenarios after 2050. During the transition from near- to long-term assessments, an understanding of when the GMSL scenarios will diverge and what drives this divergence becomes increasingly important. Two types of uncertainty are important to consider in this context: uncertainty in physical processes and uncertainty in future emissions and ensuing warming. Although there are possible alternative definitions and framings, as used in this report, *process uncertainty* (Box 2.1) is associated with how well we currently understand why sea level has changed in the past and how it will change in the future. Stated another way, how well do we understand and model

the processes that will combine to impact sea level at a specific time and location in the future? This uncertainty is also reflected in the likely range of future sea level rise for a given GMSL scenario. The spread between the five GMSL rise scenarios is intended to reflect the range of potential future emissions pathways and associated warming levels that depends highly on global socioeconomic factors that have yet to unfold. This unknown future pathway leads to what is referred to here as *emissions uncertainty* (Box 2.1).

At some point in the future, the separation between GMSL rise scenarios will overtake the process uncertainty associated with individual GMSL rise scenarios. In other words, scenario dependence will emerge, and it will be possible to distinguish between the observation-based trajectories associated with two neighboring GMSL rise scenarios. In general, these time periods are important for connecting the near-term similarities between scenarios to the time period where scenarios diverge rapidly. An effort is made here to understand when divergence of the GMSL rise scenarios might occur and to link them to possible future warming and emissions pathways. This analysis then serves as the foundation for process-based monitoring that could be useful in determining the trajectory of ongoing sea level rise and, by extension, the possible future sea level rise out to 2150.

Box 2.1: Uncertainties

When assessing future changes in sea level, this report considers two main sources of uncertainty.

Process Uncertainty

An increase in emissions will cause ice-mass loss, ocean thermal expansion, and local ocean dynamic changes, but the sensitivity of these processes to these forcing changes comes with uncertainty. For example, the sensitivity of the Antarctic ice sheet is not yet fully understood, leading to a substantial uncertainty in how sea level reacts to forcing changes. Additionally, the future contributions from processes, such as changes in ocean circulation and VLM, that impact RSL change more locally have an associated uncertainty. This uncertainty in the contribution of these various processes to future RSL change is referred to in this report as *process uncertainty*.

Emissions Uncertainty

Increasing the amount of greenhouse gases (GHGs) in the atmosphere will trap more heat in the earth system. The amount of GHGs in the atmosphere determines the "forcing" of climate change and its effects, such as changes in temperature and sea level rise. Various forcing scenarios describe possible GHG emissions pathways, which range from quick emissions reduction to unmitigated future emissions. In the IPCC AR6 (IPCC, 2021a), these possible future pathways are referred to as Shared Socioeconomic Pathways (SSPs). The uncertainty in the future pathway is referred to as *emissions uncertainty*.

Uncertainties in this Report

In this report, emissions uncertainty and process uncertainty are combined to generate five sea level scenarios with GMSL target values in 2100: Low (0.3 m), Intermediate-Low (0.5 m), Intermediate (1 m), Intermediate-High (1.5 m), and High (2 m). These sea level scenarios are related to but distinct from the emissions pathway scenarios in the IPCC AR6.

Natural Variability

Next to sea level changes caused by changes in GHG forcing, many physical processes cause natural variations (e.g., ENSO). The scenarios and uncertainty ranges for each scenario and for the observation-based trajectories in this report do *not* include variations due to natural variability (the decadal scenario values are 19-year averages that remove most variability effects). Natural variability is not directly considered a source of uncertainty in the context of this report but does contribute to the uncertainty range in the observation-based extrapolations, as it can influence the estimated rates and accelerations in observational records. Natural, or non-forced, variations can also make significant contributions to sea level on a wide range of timescales. For example, along the U.S. West coast, sea levels are higher during El Niño years. When assessing sea level at a specific location and time in the future, the sea level contribution from natural variability must be combined with the scenarios and trajectories provided here.

2.2.3 Updates to the 2017 Sea Level Scenarios

In order to support decision-making efforts related to future sea level risks, past interagency efforts (Parris et al., 2012; Hall et al., 2016; Sweet et al., 2017) have defined a set of GMSL rise scenarios spanning a range from a Low scenario, consistent with no additional GMSL acceleration, to a worst-case, or high-end, Extreme scenario, judged to be at the physically plausible limits based on the scientific literature. In Sweet et al. (2017), these scenarios were developed to span a range of 21st-century GMSL rise from 0.3 m to 2.5 m. Sweet et al. (2017) built these scenarios upon the probabilistic emissions scenario–driven projections of Kopp et al. (2014). Kopp et al. (2014) combined a variety of different lines of evidence—global climate model (GCM) projections, the IPCC AR5 assessment of ice-sheet changes, and structured expert-judgment ice-sheet projections, among other sources of information—to generate distributions of future global and associated regional sea level changes consistent with low, medium, and high emissions scenarios. Sweet et al. (2017) filtered the ensemble of different future projections generated by Kopp et al. (2014) to identify those subsets consistent with 0.3 m, 0.5 m, 1.0 m, 1.5 m, 2.0 m, and 2.5 m of 21st-century GMSL rise. These subsets constituted the six Sweet et al. (2017) GMSL scenarios. For most purposes, Sweet et al. (2017) focused on the median of each subset, although 17th and 83rd percentile levels were also reported.

This report retains the Sweet et al. (2017) scenarios (except the Extreme 2.5 m scenario, discussed below), with the principal difference being updated temporal trajectories and exceedance probabilities now based on global warming levels rather than emissions scenarios. Linking to global warming levels provides a straightforward physical link for the GMSL scenarios and establishes a connection to global temperature monitoring efforts. The updates made in this report reflect the underlying ensemble of future projections based on methods used in the IPCC AR6 (Fox-Kemper et al., 2021; Garner et al., 2021) and listed in Table A1.1. As in Sweet et al. (2017), these projections are filtered based on 21st-century GMSL rise. In other words, projected pathways that intersect the GMSL scenario target values in 2100 are retained and then used to generate the GMSL scenarios from Low to High described here.

In addition to being updated based on the latest generation of GCMs and the IPCC AR6, this set of projections incorporates multiple methods of projecting future ice-sheet changes, which are the major sources of future sea level rise and pose the biggest source of uncertainty in projecting the timing and magnitude of future possible rise amounts. For Antarctica, this includes emulators derived from two different ice-sheet model intercomparison exercises (Edwards et al., 2021; Levermann et al., 2020), as well as from a single-model study focused on the potentially high-impact but uncertain-likelihood marine ice cliff instability (MICI) mechanism (DeConto et al. 2021) and a structured expert-judgment study (Bamber et al, 2019). For Greenland, this includes a single intercomparison-derived emulator (Edwards et al., 2021) and a structured expert-judgment study (Bamber et al., 2019). There is now a broader range of both Antarctic and Greenland potential contributions, compared to Sweet et al. (2017). Whereas the high-end scenarios of Sweet et al. (2017) were all dominated by Antarctic contributions, the potential for high Greenland contributions now also adds to these high-end scenarios, and due to its proximity, also drives larger differences along U.S. coastlines.

The use of multiple methods, including methods that consider mechanisms that could substantially increase ice-sheet sensitivity under high emissions scenarios, means that the time path of the higher GMSL scenarios is more realistic than in Sweet et al. (2017), which assumed (based on the underlying Kopp et al. [2014] projections) that ice-sheet loss would accelerate at a constant rate over the remainder of the century. A result is that there is less acceleration in the higher scenarios until about 2050 and greater acceleration toward the end of this century. This has two primary implications. First, despite maintaining the same target values and having the same range between scenarios in 2100, the range covered by the scenarios is smaller in the near term than in Sweet et al. (2017). Second, the likely (17th–83rd percentile) ranges of projections consistent with each scenario before and after the 2100 time point used to define the scenarios tend to be broader than in Sweet et al. (2017).

An important change from the Sweet et al. (2017) report is the exclusion of the Extreme (2.5 m) scenario in this report. Based on the most recent scientific understanding and as discussed in the IPCC AR6, the uncertain physical processes such as ice-sheet loss that could lead to much higher increases in sea level are now viewed as less plausible in the coming decades before potentially becoming a factor toward the end of the 21st century and beyond. A GMSL increase of 2.5 m by 2100 is thus viewed as less plausible, and the associated scenario has been removed from this report. Nevertheless, the increased acceleration in the late 21st century and beyond means that the other high-end scenarios provide pathways that potentially reach this threshold in the decades immediately following 2100 (and continue rising).

2.2.4. Observation-Based Extrapolations

As discussed above, the pathways of the updated GMSL scenarios differ from those presented in Sweet et al. (2017), and the range between the scenarios in the near term is now reduced. This report, for the first time, includes observation-based extrapolations to serve as a near-term (2020–2050) comparison for the scenarios. They can also be viewed as "trajectories" of current sea level rise. When interpreting these extrapolations, they should be considered as an additional line of evidence for near-term sea level rise alongside the model-based GMSL scenarios. They are not intended to replace the GMSL scenarios. Additionally, such observation-based extrapolations, or trajectories, can be potentially misleading if not appropriately constrained. This report makes no detailed assessment of whether the long-term rate and acceleration have emerged from the influence of natural variability in the observational record, although recent studies suggest this could be the case in some regions (Lyu et al., 2014; Richter et al., 2020; Fasullo and Nerem, 2018; Wang et al., 2021). Instead, the observation-based extrapolations are presented as computed and without interpretation after several methodological choices were made to generate extrapolations that can be compared to the scenarios and identify those scenarios that "bound" the 2050 extrapolations. These methodological choices are described briefly below.

First, the rates and accelerations are estimated from the tide-gauge records starting in 1970. Recent studies have shown a consistent acceleration in GMSL since 1970 (Dangendorf et al., 2019; Frederikse et al., 2020), and this is a primary motivator for the time period chosen. The impact of varying this start date on the regional scales relied on here was assessed and found to be negligible within a few years of 1970 (more below). This is not true, as a general statement, when using individual tide-gauge records. Second, the observation-based extrapolations are made only to 2050. Beyond that date, it is assumed that processes not fully represented in the observations could become dominant. Third, the uncertainty in the rate and acceleration associated with the influence of natural variability is accounted for as fully as possible and included in the extrapolation. Finally, the extrapolations are made for GMSL, the coastlines of CONUS, and 10 separate coastal regions around the United States and outlying islands (see Figure A1.1 for region definitions). By grouping tide gauges regionally, the influence of localized variability is reduced, and challenges associated with individual tide gauges with incomplete or short records are overcome, thus yielding more useful and narrower extrapolated ranges. These regional comparisons also fulfill the intent of providing an additional line of evidence and comparison point to the GMSL scenarios.

For each individual region, the observation-based extrapolation is performed as follows:

1. The tide gauges in the region are grouped and combined following the virtual station method (see Frederikse et al., 2020) to generate a monthly time series of RSL from 1920 to present.
2. Natural variability is partially removed through regression analysis using climate indices representing the El Niño–Southern Oscillation, Pacific Decadal Oscillation, and North Atlantic Oscillation (see Calafat et al., 2012; Hamlington et al., 2021).
3. The rate and acceleration from 1970 to present is computed, and the uncertainty on each term is assessed, accounting for the influence of remaining natural variability (see Hamlington et al., 2021) and serially correlated variability in the tide-gauge record (Bos et al., 2013, 2014).

4. The rates, accelerations, and uncertainties are used to generate an ensemble of 5,000 extrapolations with a baseline year of 2000 and extending to 2050. Median projections and a likely (17th–83rd) range are computed from this ensemble.

Following this procedure, observation-based extrapolations are obtained for GMSL, CONUS, and 8 coastal regions (Figure A1.1)—the Northeast (Maine to Virginia), the Southeast (North Carolina to the east coast of Florida), the Eastern Gulf (west coast of Florida to Mississippi), the Western Gulf (Louisiana to Texas), the Southwest (California), the Northwest (Oregon to Washington), the Hawaiian Islands, and the Caribbean. Elsewhere in the report, projections are discussed for the Pacific Islands, but due to the availability of tide-gauge data and the geographic range covered by the region, the extrapolations are conducted using only those gauges on the Hawaiian Islands. Observation-based extrapolations are also made for the southern and northern coasts of Alaska and mentioned in the text but not included in the tables below. Differential VLM heavily impacts the tide-gauge records along the southern coastline of Alaska and makes the creation of a regionally representative time series challenging. The observation-based extrapolations for Alaska are thus caveated with increased uncertainty in the underlying regional processes that heavily limit their utility as a comparison to the GMSL scenarios.

2.3. Near-Term Sea Level Change (2020–2050)

In Sweet et al. (2017), the range between the median values of the Low and High GMSL scenarios in 2020, 2030, 2040, and 2050 was 0.05 m, 0.12 m, 0.23 m, and 0.38 m, respectively. As a result of improved science and the updated framework and procedure for generating the GMSL scenarios, the time path of the scenarios—particularly the higher scenarios—is now more realistic and consistent with current process-based understanding. In this report, the range between the Low and High scenarios in 2020, 2030, 2040, and 2050 is now 0.02 m, 0.06 m, 0.15 m, and 0.28 m, respectively (Table 2.1). In other words, there is less divergence between the GMSL scenarios in this near-term time period, which reduces uncertainty in the projected amount of GMSL rise up to the year 2050. The Low scenario remains largely the same between this report and Sweet et al. (2017); this range reduction reflects a downward shift in the higher scenarios in 2050 and times prior, as discussed above. As an example, the projected value in 2050 for the High scenario in this report (~0.4 m) is the same as that for the Intermediate-High projected value in 2050 in Sweet et al. (2017). In short, while the scenarios continue to be defined by projected values of GMSL increase in 2100, it is important to note that the paths to get to these target values have changed in this report compared to the previous one.

Following the procedure outlined in Section 2.2.4, an observation-based extrapolation of GMSL is computed using the global tide-gauge reconstruction from Frederikse et al. (2020; Figure 2.2a; also see top row of Table 2.1). The extrapolated value of GMSL increase in 2050 relative to a baseline of 2000 is 0.24 m, with a likely (17th–83rd percentile) range between 0.19 m and 0.29 m. A similar extrapolation was made using GMSL data measured by satellite altimeters over 1993–2021, resulting in an estimate of 0.23 m of rise from 2000 to 2050 and in agreement with the results of the tide-gauge extrapolation. Based on the updated GMSL scenarios, the median of the 2050 observation-based extrapolation is bounded by (i.e., it falls between) the Intermediate-Low and Intermediate scenarios. The likely ranges for the Low and High scenarios do not overlap with the likely range of observation-based extrapolation in 2050, although the very likely ranges (5th–95th percentiles) do overlap. The likely range of the Intermediate-High scenario does overlap with the likely range of the observation-based extrapolation. A similar observation-based extrapolation is completed using only the tide gauges located around CONUS (Figure 2.2b), resulting in a projected increase of 0.38 m in 2050, with a likely range of 0.32 m to 0.45 m. This range for CONUS is again narrower than in Sweet et al. (2017). Similar to GMSL, this observation-based assessment is bounded by the Intermediate-Low and Intermediate scenarios in 2050.

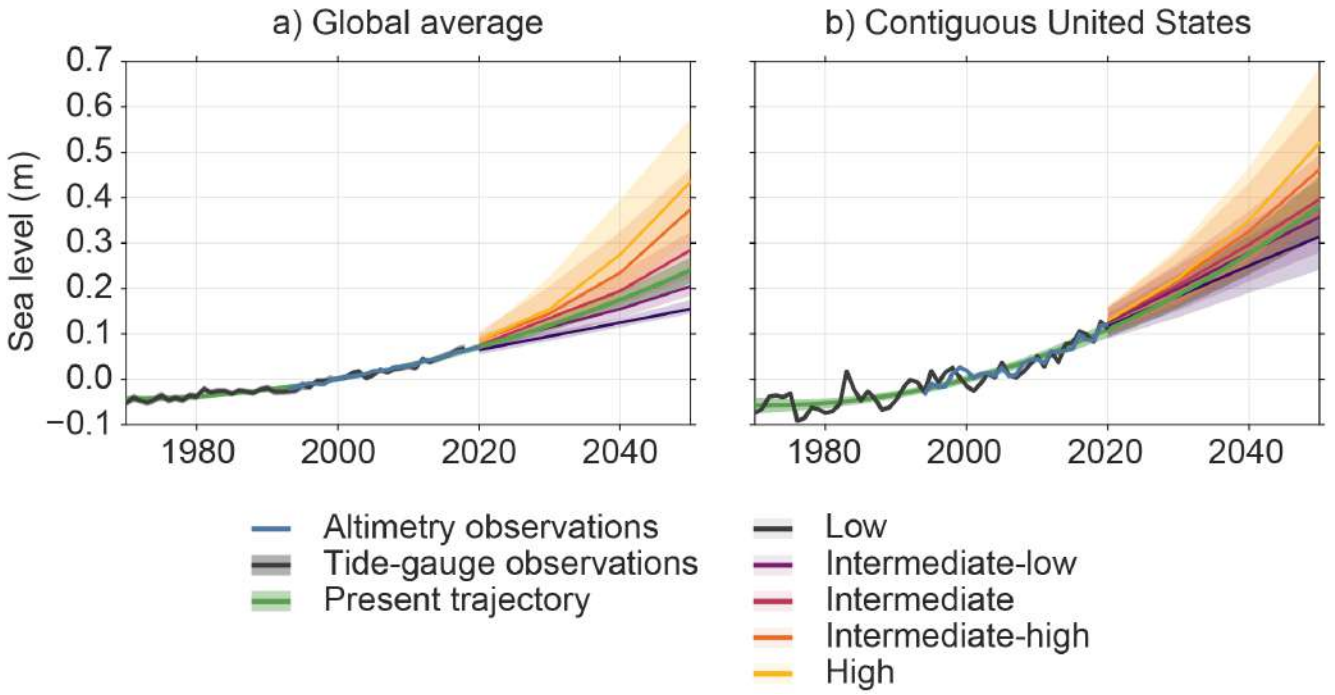

Figure 2.2: Observation-based extrapolations using tide-gauge data and five Scenarios, in meters, for a) global mean sea level and b) relative sea levels for the contiguous United States from 2020 to 2050 relative to a baseline of 2000. Median values are shown by the solid lines, while the shaded regions represent the likely ranges for the observation-based extrapolations and each scenario. Altimetry data (1993–2020) and tide-gauge data (1970–2020) are overlaid for reference.

As a result of the smaller region used and the increased influence of natural variability and VLM, the likely ranges in 2050 for CONUS in both the scenario projections and observation-based extrapolations are larger than those associated with the GMSL scenarios themselves. The likely range from the observation-based extrapolation does overlap with the likely ranges from both the Low and High scenarios. This is both a reflection of the larger range in the extrapolation for CONUS and the narrower range between the High and Low scenarios in this report. A key takeaway from this assessment is that on global and national scales, two lines of evidence (observations and GMSL scenarios) are consistent out to 2050 and support a narrower range in possible near-term sea level change than provided in Sweet et al. (2017). As discussed previously, this is consistent with and a result of the improved process-based understanding and projection approach that has been incorporated in this report.

The observation-based extrapolations are also computed for 10 coastal regions of the United States. Only 8 of these regions are shown in the tables and figures below, with the coastlines of Alaska covered separately in the text. As in the global and national cases, the observation-based extrapolations are extended out to 2050. Following the procedure outlined in section 2.2.4, tide gauges within each of these regions are combined into a single time series prior to extrapolating estimated rates and accelerations. Building on the discussion in section 2.2.4, the motivation for doing these assessments regionally as opposed to at each individual tide gauge location is two-fold. First, the observation-based extrapolations are intended to serve as a comparison to the model-based GMSL scenarios. Outside the possibility of very localized VLM, the processes included in the regionalized GMSL scenarios are generally spatially coherent over the regions considered. Indeed, the selection of specific regions is driven by process-based similarities mostly associated with ocean dynamics and large-scale VLM. Grouping the tide gauges and generating regional comparisons yields a closer analog to the information contained in the scenarios. The regional averages also reduce the influence of local signals—including VLM and other natural ocean variability—that can influence extrapolations and associated ranges. Second, some of the individual tide gauges around the U.S. coastlines have records that either do not span the full time period from 1970 to 2020 or contain data gaps. Generating

Table 2.1: Observation-based extrapolations and five scenarios, in meters, for global mean sea level and relative sea level for the contiguous United States from 2020 to 2050 relative to a baseline of 2000. Median [likely ranges] are shown.

Global Mean Sea Level				
	2020	2030	2040	2050
Obs. Extrapolation	0.07 [0.06, 0.08]	0.12 [0.11, 0.13]	0.18 [0.16, 0.19]	0.24 [0.19, 0.29]
Low	0.06 [0.05, 0.07]	0.09 [0.08, 0.10]	0.12 [0.11, 0.13]	0.15 [0.14, 0.17]
Intermediate-Low	0.07 [0.06, 0.07]	0.11 [0.09, 0.12]	0.15 [0.13, 0.17]	0.20 [0.18, 0.23]
Intermediate	0.07 [0.07, 0.09]	0.13 [0.11, 0.15]	0.19 [0.16, 0.23]	0.28 [0.22, 0.32]
Intermediate-High	0.08 [0.07, 0.10]	0.14 [0.11, 0.20]	0.23 [0.18, 0.32]	0.37 [0.27, 0.46]
High	0.08 [0.07, 0.10]	0.15 [0.11, 0.22]	0.27 [0.18, 0.39]	0.43 [0.31, 0.57]
Contiguous United States				
	2020	2030	2040	2050
Obs. Extrapolation	0.11 [0.09, 0.13]	0.19 [0.16, 0.21]	0.28 [0.23, 0.32]	0.38 [0.32, 0.45]
Low	0.12 [0.09, 0.15]	0.18 [0.14, 0.23]	0.25 [0.19, 0.31]	0.31 [0.24, 0.39]
Intermediate-Low	0.13 [0.10, 0.16]	0.20 [0.15, 0.25]	0.28 [0.22, 0.34]	0.36 [0.28, 0.44]
Intermediate	0.13 [0.10, 0.16]	0.21 [0.16, 0.26]	0.30 [0.23, 0.37]	0.40 [0.31, 0.49]
Intermediate-High	0.13 [0.10, 0.16]	0.22 [0.16, 0.28]	0.33 [0.24, 0.43]	0.46 [0.35, 0.61]
High	0.13 [0.10, 0.16]	0.22 [0.17, 0.29]	0.35 [0.26, 0.47]	0.52 [0.39, 0.68]

regional time series alleviates these challenges and allows us to provide generalized comparisons and assessments about the match between observations and model-based scenarios along the U.S. coastlines. These regional comparisons then provide an additional line of evidence for the possible overall trajectory of sea level in the near term. The result is shown in Figure 2.3, with corresponding values in Table 2.2 for each of the eight regions and compared to the scenarios in each region.

The regional differences in the observation-based extrapolations and scenarios in Figure 2.3 are consistent with the current process-based understanding of sea level rise. Processes such as ocean dynamics, the GRD response to contemporary ice-mass loss (i.e., fingerprints), and coastal VLM lead to differences between the eight regions. Additionally, uncertainty ranges on the extrapolations can be bigger or smaller depending on the number of tide gauges in a particular region and the influence of natural variability on the rate and acceleration estimates. To demonstrate this regionalization, Figure 2.4 shows these regional variations of sea level in 2050 for the Intermediate-Low and Intermediate-High scenarios. In 2050, the regional variation in future sea levels does not change significantly between scenarios. Although the values increase from the Intermediate-Low scenario to the Intermediate-High scenario, the east–west difference in sea level rise is similar. Higher values for both scenarios are found along the entire East and Gulf Coasts. Subsidence leads to the highest rates along the Gulf Coast, driven by regional and local factors, such as river sediment compaction and withdrawal of subsurface fluids (Dokka, 2011; NGS, 2001; Rydlund and Densmore, 2012). Along the East Coast, subsidence is generally associated with the large-scale process of GIA, with fluid extraction being an issue in some areas (Frederikse et al., 2017; Karegar et al., 2016). Beyond VLM, many of the regional differences are driven by differences in the ocean dynamic variability. For example, the sterodynamic contribution from 2000 to 2050 in the Northeast is more than double the sterodynamic contribution in the Southwest. This regional difference is similarly reflected in the observation-based extrapolations in 2050. It should be noted that this difference arises from higher-than-global-average projections for the Northeast as opposed to lower-than-global-average projections for the Southwest, which tracks very closely to the GMSL values shown in Table 2.1.

For the observation-based extrapolations, the largest estimates of sea level rise in 2050 are found along the entire Gulf Coast (Table 2.2). The Western Gulf has the highest extrapolated values in 2050, driven by high rates of coastal subsidence in the region and consistent with the scenarios discussed above. The Northwest and Southwest coastal regions have the lowest observation-based extrapolations to 2050. For the purposes of offering a comparison to the scenarios, the scenarios that either bound or track the median of the observation-based extrapolations are provided (denoted by red text or markers in Table 2.2). Two regions track the Intermediate-Low scenario (Northeast and Hawaiian Islands), and two regions track the Intermediate scenario (Southwest and Caribbean). The Intermediate-Low to Intermediate scenarios bound the Northwest, and the Intermediate to Intermediate-High scenarios bound the Southeast and Western Gulf regions. Finally, the Intermediate-High to High scenarios bound the Eastern Gulf region. With only the exceptions of the low-end scenarios in the Southwest and Eastern Gulf, the likely ranges from the observation-based extrapolations have at least some overlap with the likely ranges of all the scenarios within a given region. This is due to a combination of the larger uncertainty on the observation-based assessments at these regional levels for an individual scenario and the narrower ranges between the median values of each GMSL scenario found in this report compared to Sweet et al. (2017). While not shown in Table 2.2, the observation-based extrapolation for the northern coast of Alaska in 2050 (median value of 0.27 cm) is bracketed by the Intermediate and Intermediate-High scenarios. The extrapolation of the southern coast of Alaska leads to a large RSL decrease in 2050 and is inconsistent with the scenario median values. As mentioned above, this is a result of challenges in generating a representative tide-gauge time series to use in the extrapolation.

As a note on the interpretation of the results provided in this near-term section, the regional comparisons between the observation-based extrapolations and scenarios need to be considered in the context of the global comparison in Figure 2.2. The regional scenarios are intrinsically linked to their associated GMSL target values in 2100. In an ideal framework that perfectly represented the regionalization of these GMSL scenarios and the relevant regional processes, separate comparisons on a regional level would be unnecessary. In other words, all regions and locations would track the same GMSL scenario. Since this is not the case, if a particular region deviates from the others, it would be an indication that either the observation-based extrapolation for that region is biased high or low or that the framework used to generate the regionalization of the GMSL scenarios is not adequately representing the contribution of a regional process. Since the observed GMSL trajectory is near the Intermediate-Low scenario, as shown here, based on the current understanding of the processes driving regional RSL, it is not expected that a particular region would track a much higher scenario. These regional comparisons during the near-term time period then serve two potential purposes: 1) they provide an additional line of evidence along with the GMSL and CONUS comparisons for the near-term trajectory of sea level rise, and 2) they can serve to identify cases when the contributions of regional processes may be tracking differently than represented by the regionalization of the GMSL scenarios.

As a general assessment of these two purposes, the likely ranges of all but one of the regions are either bounded on one side by the Intermediate scenario or tracks a scenario neighboring the Intermediate scenario, showing some level of consistency with the GMSL and CONUS comparisons. This provides additional confidence in the narrower range (when compared to Sweet et al., 2017) of sea level rise at the regional level out to 2050 presented in this report. The Eastern Gulf is the only region bounded by the High scenario. The high observation-based extrapolation for the Eastern Gulf should be interpreted with caution, as it does not necessarily mean a higher scenario is applicable compared to other regions. As a possible explanation, unresolved natural ocean variability in the observational record could lead to an observation-based extrapolation that is biased high. Such variability would need to be low-frequency—or long period—to significantly impact a rate and acceleration estimated in a 50-year record. For all regions considered here, it is likely that natural variability still contributes to the median observation-based extrapolation, and as seen in Figure 2.1, this variability has a substantial impact on the coastlines of the United States. This influence of natural variability on rates and accelerations is captured to the extent possible in the likely ranges of the observation-based extrapolations, and these likely ranges should be considered in tandem with the median values

when assessing near-term trajectories. Beyond the possible influence of natural variability, there may also be a mismatch in the process representation between the observations and regionalized, model-based GMSL scenarios that leads to a projection that is too low in the latter. One possibility is non-linear or unresolved VLM in the region. The regionalized GMSL scenarios consider only long-term linear rates of VLM, while the observation-based extrapolations could represent a shift in the rate of VLM in the estimated acceleration.

An explanation of regional differences between observation-based extrapolations and model-based scenarios requires additional investigation, likely on a tide gauge-by-tide gauge basis. As a first step in this direction, the range between Low and High scenarios at each individual tide gauge (considering only the tide gauges with at least 30 years of data—102 of the full set of 121) is provided in Figure A1.2a, and the departure between the observation-based extrapolation and Intermediate scenario at each individual tide gauge is shown in Figure A1.2b. These figures show that the range between Low and High scenarios is generally lower than 20 cm in 2050 at the local level and that most observation-based extrapolations are within 15 cm of the Intermediate scenario in 2050. Of the 102 tide gauges used in this report, 65 have observation-based extrapolations that fall within the narrower Low to High ranges in 2050, and 80 of these 102 are within 15 cm of the Intermediate scenario. The majority of those falling below the Low scenario are found in the Northwest and southern Alaska regions, and the majority of those exceeding the High scenario are found in the two Gulf regions. This supports the regional comparisons shown in Figure 2.3 and Table 2.2 while also conveying that there is general agreement and consistency between the ranges of the observation-based extrapolations and regionalized GMSL scenarios even on a local, tide gauge-by-tide gauge level. A more definitive assessment of why some regions track higher (e.g., Eastern Gulf) or lower relative to others requires further analysis that should be done with consideration of the associated uncertainty and ranges.

As a general concluding statement on this near-term section, the link between the regional and global scenarios needs to be considered when drawing conclusions at the regional level based on the observation-based extrapolations. In practice, regionally identifying the scenario that upper-bounds the observation-based extrapolation at year 2050 (Table 2.2) may help compensate for potential interannual variability when projecting sea level for a particular location. The associated uncertainties in the approaches adopted here do emphasize the importance of ongoing monitoring using the observations and the need to update trajectories. As records continue to lengthen, likely ranges on near-term assessments will narrow. Additionally, satellite altimeter records are reaching sufficient length to be important in such monitoring. As a final note, the same framework used for extrapolating the observations forward can also be used to assess the increases—or offsets—observed over different recent time periods. These offsets are useful for adjusting baselines of the scenarios and are provided for each region in Table A1.2.

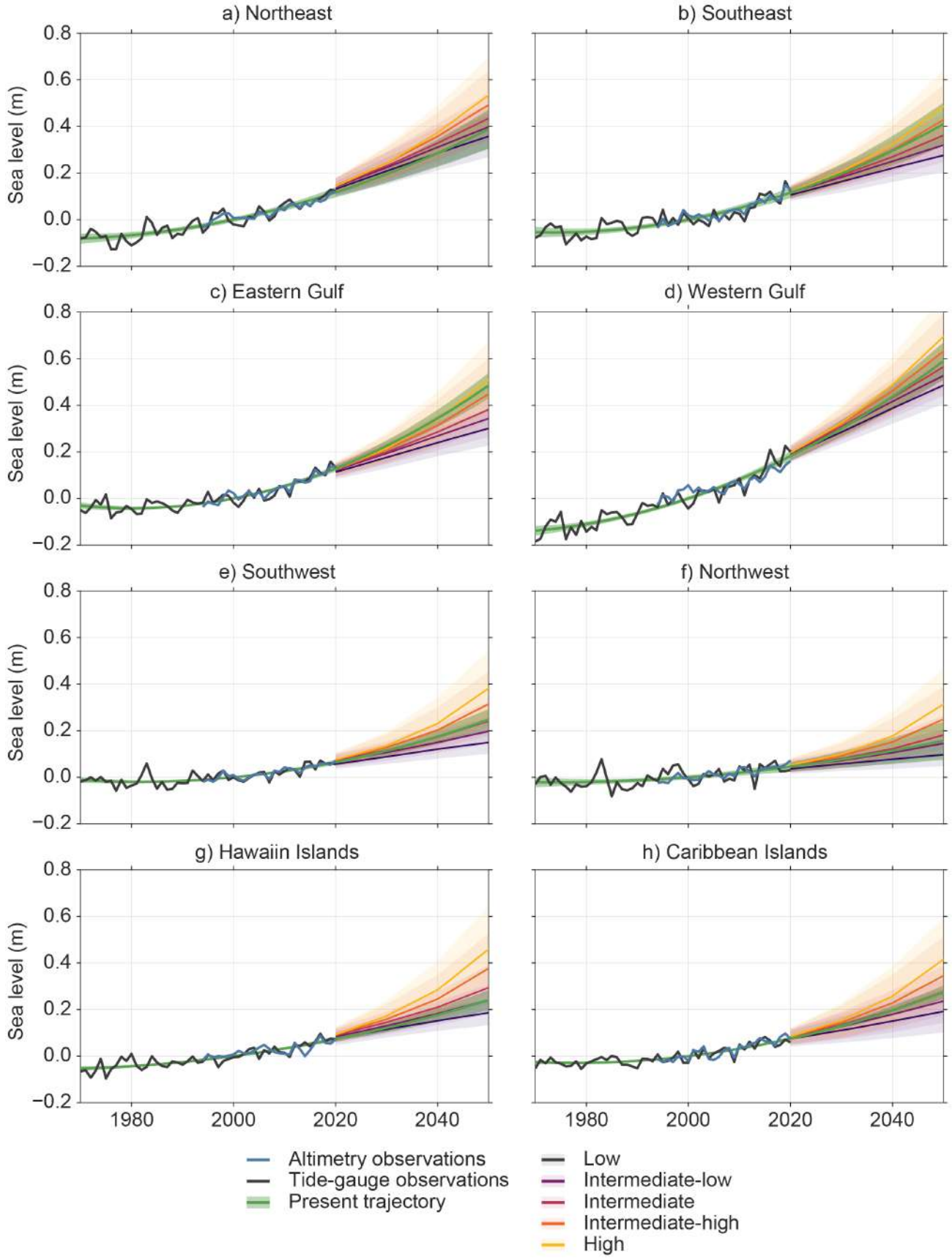

Figure 2.3: Observation-based extrapolations and five regionalized global mean sea level scenario projections, in meters, of relative sea levels for eight coastal regions around the United States from 2020 to 2050 relative to a baseline of 2000. Median values are shown by the solid lines, while the shaded regions represent the likely ranges for the observation-based extrapolations and each scenario. Tide-gauge data (1970 to 2020) are overlaid for reference, along with satellite altimetry observations, which do not include contributions from vertical land motion.

Table 2.2: Observation-based extrapolation and regionalized global mean sea level scenario–based estimates, in meters, of relative sea level in 2050 relative to a baseline of 2000 for eight coastal regions of the United States. Median [likely ranges] are shown. The two scenarios that bound the median observation-based extrapolation are also provided for each region and indicated by red dividing lines. In regions where the observation-based extrapolation is the same as a particular scenario, the scenario is indicated in red text and the bounding scenarios can be assumed to be the next higher or lower scenario (e.g., the Intermediate bounds the Northeast's observation-based extrapolation).

Observation Extrapolations	Low	Intermediate-Low	Intermediate	Intermediate-High	High	Median Bounding Scenarios
Northeast						
0.40 [0.30, 0.47]	0.36 [0.27, 0.45]	0.40 [0.31, 0.49]	0.43 [0.34, 0.54]	0.49 [0.38, 0.64]	0.54 [0.40, 0.69]	Int-Low
Southeast						
0.41 [0.32, 0.50]	0.28 [0.20, 0.35]	0.32 [0.25, 0.40]	0.36 [0.28, 0.46]	0.43 [0.32, 0.58]	0.49 [0.35, 0.64]	Int–Int-High
Eastern Gulf						
0.48 [0.43, 0.54]	0.30 [0.22, 0.38]	0.34 [0.26, 0.42]	0.38 [0.30, 0.48]	0.45 [0.34, 0.60]	0.51 [0.38, 0.68]	Int-High–High
Western Gulf						
0.59 [0.51,0.67]	0.49 [0.41, 0.57]	0.53 [0.44, 0.62]	0.57 [0.47, 0.67]	0.63 [0.51, 0.79]	0.69 [0.56, 0.87]	Int–Int-High
Southwest						
0.24 [0.20,0.29]	0.15 [0.10, 0.20]	0.20 [0.14, 0.26]	0.24 [0.18, 0.32]	0.31 [0.22, 0.45]	0.38 [0.26, 0.54]	Intermediate
Northwest						
0.16 [0.08, 0.24]	0.10 [0.05, 0.15]	0.15 [0.09, 0.20]	0.18 [0.12, 0.26]	0.25 [0.15, 0.39]	0.31 [0.19, 0.47]	Int-Low–Int
Hawaiian Islands						
0.24 [0.20, 0.28]	0.19 [0.13, 0.24]	0.24 [0.18, 0.31]	0.29 [0.22, 0.39]	0.38 [0.27, 0.53]	0.46 [0.31, 0.64]	Int-Low
Caribbean						
0.28 [0.24, 0.31]	0.19 [0.10, 0.29]	0.24 [0.14, 0.33]	0.28 [0.18, 0.39]	0.35 [0.22, 0.51]	0.42 [0.27, 0.59]	Intermediate

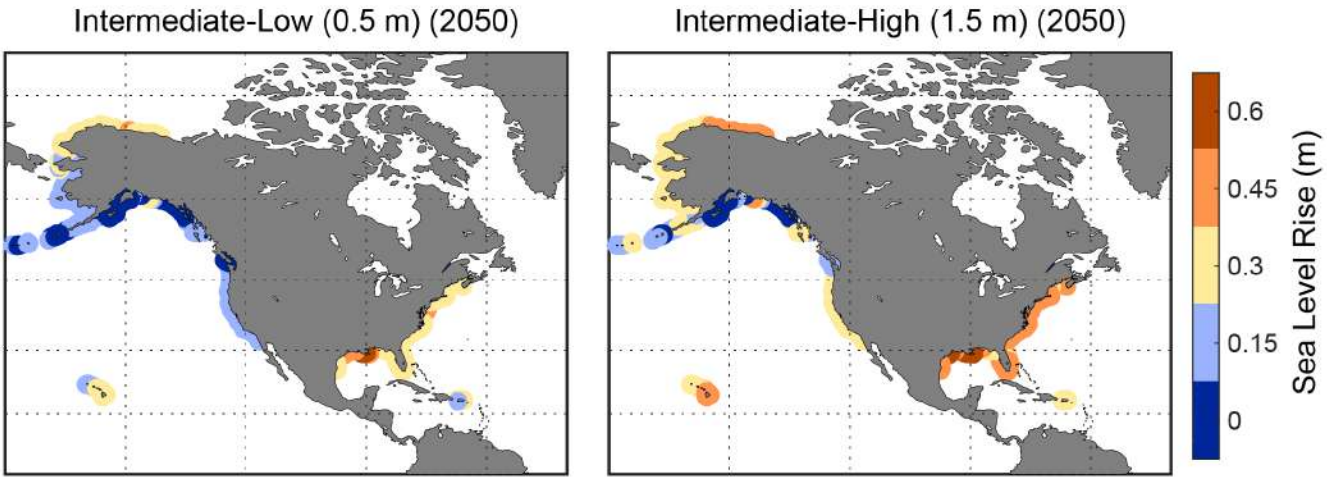

Figure 2.4: Relative sea level rise, in meters, in 2050 for the a) Intermediate-Low and b) Intermediate-High scenarios relative to the year 2000.

2.4. Long-Term Sea Level Change (2050–2150)

The updated GMSL values in 2050, 2100, and 2150 relative to a 2000 baseline are shown for each of the five scenarios in Table 2.3. Note that the current National Tidal Datum Epoch (NTDE) has a baseline of 1992 (midpoint of the 1983–2001 epoch). Comparisons between the projections here and calculations tied to the NTDE will require an adjustment between 1992 and 2000 (see Table A1.2 for offsets). Beyond the middle of this century, the differences between sea level scenarios become increasingly large, and the differences between sea level scenarios become more closely associated with differences in potential future GHG emissions pathways and associated global warming. Although the GMSL scenarios (names and their values) are the same at 2100 for this report and for Sweet et al. (2017), there is a narrowing in the range covered by the scenarios in both 2050 and 2150, driven primarily by a reduction in the values at those two target dates associated with the Intermediate-High and High scenarios in this report. As previously discussed, in 2050, the updated median value for the High scenario is similar to the median value for the Intermediate-High scenario from Sweet et al. (2017). This is not the case in 2150, however, where the separation between the scenarios remains similar to Sweet et al. (2017). Because of this, and because the scenarios are defined by the 2100 values, the same scenario naming is used in this report as in Sweet et al. (2017), with the notable exception of the omission of the Extreme (2.5 m) scenario.

In the very long term (over millennia), the magnitude of global mean sea level rise closely relates to the magnitude of global warming; however, over the timescales of decades and centuries, the magnitude of global warming more closely relates to the *rate* of GMSL rise. It is thus not possible to tie specific levels of warming in general to amounts of sea level rise, but it is possible to relate specific levels of warming *at specific points in time* (e.g., at the end of the century) to different levels of sea level rise. Thus, based on the IPCC AR6 (§9.6.3.4 in Fox-Kemper et al., 2021), it is possible to connect the GMSL rise scenarios to different levels

Table 2.3: Global mean sea level and contiguous United States scenarios, in meters, relative to a 2000 baseline.

Global Mean Sea Level				Contiguous United States			
	2050	**2100**	**2150**		**2050**	**2100**	**2150**
Low	0.15	0.3	0.4	Low	0.31	0.6	0.8
Intermediate-Low	0.20	0.5	0.8	Intermediate-Low	0.36	0.7	1.2
Intermediate	0.28	1.0	1.9	Intermediate	0.40	1.2	2.2
Intermediate-High	0.37	1.5	2.7	Intermediate-High	0.46	1.7	2.8
High	0.43	2.0	3.7	High	0.52	2.2	3.9

of future global mean surface air temperature occurring at the end of the century. The median GMSL projection for 2100 for a world with global mean surface air temperature in 2081–2100 averaging 2.0°C above 1850–1900 levels is about 0.5 m (*likely* range of 0.4–0.7 m; Table 2.4), consistent with the Intermediate-Low scenario. The median GMSL projection for a world with global mean surface air temperature in 2081–2100 averaging 4.0°C higher is about 0.7 m (*likely* range of 0.6–0.9 m), between the Intermediate-Low and Intermediate scenarios, with the upper end of the *likely* range approaching the Intermediate scenario. These two scenarios are also consistent with the current observed acceleration, which, if extrapolated, would yield about 0.24 m of GMSL rise by 2050 and 0.69 m by 2100.

However, these projections include only physical processes in which there is at least *medium confidence* in the current scientific understanding. As described in the IPCC AR6 (Box 9.4 in Fox-Kemper et al., 2021), the largest potential contributions to long-term GMSL rise come from ice-sheet processes in which there is currently *low confidence*. Projections that include the magnitudes, rates, and thresholds associated with these ice-sheet processes, particularly under higher emissions futures, could give rise to GMSL rise values well above the *likely* range. Pathways to such unknown-likelihood, high-impact outcomes—"potential surprises" in the words of NCA4 (Kopp et al., 2017)—include

- earlier-than-projected ice-shelf disintegration in Antarctica,
- abrupt, widespread onset of marine ice-sheet instability and/or marine ice-cliff instability in Antarctica, and
- faster-than-projected changes in surface-mass balance on Greenland, potentially associated with changes in atmospheric circulation, cloud processes, or albedo changes.

These outcomes are represented in the IPCC projections (§9.6.3 in Fox-Kemper et al., 2021) through the inclusion of an illustrative very high emissions (SSP5-8.5), *low-confidence* projection range, the 83rd percentile of which for 2100 extends to 1.6 m (modestly above the Intermediate-High scenario) and the 95th percentile of which extends to 2.3 m (above the High scenario). In 2150, the 83rd and 95th percentiles of this *low-confidence* scenario are 4.8 and 5.4 m, respectively. Because these outcomes are based on processes poorly represented in climate and ice-sheet models, the IPCC assessment of these processes incorporates information from a structured expert-judgement study (Bamber et al., 2019) and a single Antarctic ice-sheet modeling study that explicitly incorporates ice-shelf hydrofracturing and ice-cliff collapse mechanisms (DeConto et al., 2021). (See §9.6.3.2, §9.6.3.3, and Box 9.4 of Fox-Kemper et al., 2021, for further discussion.)

To connect this to the scenarios provided here, the Intermediate-High and High scenarios represent potential futures in which these deeply uncertain ice-sheet processes play important roles in the late 21st century and beyond. After 2100, these processes may also play important roles in the Intermediate scenario. These trajectories are highly emissions-dependent. For example, in an illustrative low emissions (SSP1-2.6) future, in which the world achieves net-zero carbon dioxide emissions by the 2070s and net-negative emissions thereafter, the corresponding AR6 l*ow-confidence* ranges in 2100 extend to 0.8 m at the 83rd percentile (between the Intermediate-Low and Intermediate scenarios) and 1.1 m at the 95th percentile (modestly above the Intermediate scenario), reaching 1.3 m (between the Intermediate-Low and Intermediate scenarios) and 1.9 m (consistent with the Intermediate scenario), respectively, in 2150. Thus, in a low emissions future, there is little evidence to support the plausibility of GMSL projections substantially higher than the median Intermediate scenario.

These warming levels are further compared to the five scenarios in this report by assessing the probability that the given GMSL value in 2100 will be exceeded for a particular warming level (Table 2.4). At all warming levels, there is at least a 92% chance of *exceeding* the Low scenario in 2100. The probability for exceeding the Intermediate-Low (0.5 m) scenario drops for all warming levels when compared to the probability for exceeding the Low scenario. For the Intermediate, Intermediate-High, and High scenarios, the probability drops

off at each warming level. Consistent with the framing of the five scenarios in this report, greater warming and higher emissions are generally needed to arrive at the Intermediate through High scenarios in 2100.

Table 2.4: IPCC warming level–based global mean sea level projections. Global mean surface air temperature anomalies are projected for years 2081–2100 relative to the 1850–1900 climatology. Sea level anomalies are relative to a 2005 baseline (adapted from Fox-Kemper et al., 2021). The probabilities are *imprecise probabilities*, representing a consensus among all projection methods applied. For imprecise probabilities >50%, all methods agree that the probability of the outcome stated is at least that value; for imprecise probabilities <50%, all methods agree that the probability of the outcome stated is *less than or equal to* the value stated.

Global Mean Surface Air Temperature 2081–2100	1.5°C	2.0°C	3.0°C	4.0°C	5.0°C	Unknown Likelihood, High Impact – Low Emissions	Unknown Likelihood, High Impact – Very High Emissions
Closest Emissions Scenario–Based GMSL Projection	Low (SSP1-2.6)	Low (SSP1-2.6) to Intermediate (SSP2-4.5)	Intermediate (SSP2-4.5) to High (SSP3-7.0)	High (SSP3-7.0)	Very High (SSP5-8.5)	Low (SSP1-2.6), *Low Confidence* processes	Very High (SSP5-8.5), *Low Confidence* processes
Total (2050)	0.18 (0.16–0.24)	0.20 (0.17–0.26)	0.21 (0.18–0.27)	0.22 (0.19–0.28)	0.25 (0.22–0.31)	0.20 (0.16–0.31)	0.24 (0.20–0.40)
Total (2100)	0.44 (0.34–0.59)	0.51 (0.40–0.69)	0.61 (0.50–0.81)	0.70 (0.58–0.92)	0.81 (0.69–1.05)	0.45 (0.32–0.79)	0.88 (0.63–1.60)
Bounding Median Scenarios in 2100	Low to Intermediate-Low	Intermediate-Low to Intermediate	Intermediate-Low to Intermediate	Intermediate-Low to Intermediate	Intermediate-Low to Intermediate	Low to Intermediate-Low	Intermediate-Low to Intermediate
Probability > Low (0.3 m) in 2100	92%	98%	>99%	>99%	>99%	89%	>99%
Probability > Int.-Low (0.5 m) in 2100	37%	50%	82%	97%	>99%	49%	96%
Probability > Int. (1.0 m) in 2100	<1%	2%	5%	10%	23%	7%	49%
Probability > Int.-High (1.5 m) in 2100	<1%	<1%	<1%	1%	2%	1%	20%
Probability > High (2.0 m) in 2100	<1%	<1%	<1%	<1%	< %	<1%	8%

The median regional scenario values in 2100 and 2150 for the eight coastal regions discussed in Section 2.3 are provided in Table 2.5. The values in 2100 for each region differ from the GMSL value used to define a given scenario due to the combination of regionally relevant factors that are discussed in Section 2.1. Similar to the near term, the highest values across all scenarios are found in the Western Gulf region, followed by the Eastern Gulf. These high values are heavily driven by the high rates of subsidence in the region. For all but two regions (Southwest and Northwest), the projected values exceed the GMSL values associated with a particular scenario. The values for each scenario in the Southwest region correspond closely to the GMSL values, which is consistent with the agreement seen between the observation-based extrapolations in 2050 for the global and regional case discussed in Section 2.3. To further understand the regional variability for a given scenario, Figure 2.5 shows the regional departure from the GMSL value for each scenario in 2100. In other words, the provided maps display the amount that needs to be added to the global value to get the associated regional value for a given scenario. The regional pattern is similar in each case. The Eastern Gulf and Western Gulf regions are consistently much higher than the global value, and the southern coast of Alaska is much lower across all scenarios. In the highest scenarios, the Northeast, Southeast, Northwest, and Southwest regions are near the global values, although there is a larger east–west separation in the lower scenarios. In these lower scenarios, the higher projections for the Northeast, when compared to the Southwest, are a result of both VLM and ocean circulation changes along the U.S. East Coast. In the higher

scenarios, the contributions from the ice sheets dominate and lead to less separation between the U.S. East and West Coasts.

Table 2.5: Scenarios of relative sea level, in meters, for eight coastal regions of the United States in 2100 and 2150 relative to a baseline of 2000. Median values are shown.

Region	Low	Intermediate-Low	Intermediate	Intermediate-High	High
Northeast					
2100	0.6	0.8	1.3	1.6	2.1
2150	0.9	1.3	2.3	2.7	3.7
Southeast					
2100	0.5	0.7	1.1	1.6	2.1
2150	0.7	1.1	2.1	2.7	3.7
Eastern Gulf					
2100	0.6	0.8	1.2	1.7	2.2
2150	0.8	1.2	2.2	2.8	3.9
Western Gulf					
2100	0.9	1.1	1.6	2.1	2.6
2150	1.3	1.7	2.8	3.4	4.5
Southwest					
2100	0.3	0.5	1.0	1.5	2.0
2150	0.4	0.8	1.9	2.6	3.7
Northwest					
2100	0.2	0.4	0.8	1.3	1.8
2150	0.3	0.7	1.6	2.3	3.3
Pacific Islands					
2100	0.4	0.6	1.1	1.7	2.3
2150	0.6	1.0	2.2	2.9	4.2
Caribbean					
2100	0.4	0.6	1.0	1.5	2.1
2150	0.5	0.9	2.0	2.6	3.7

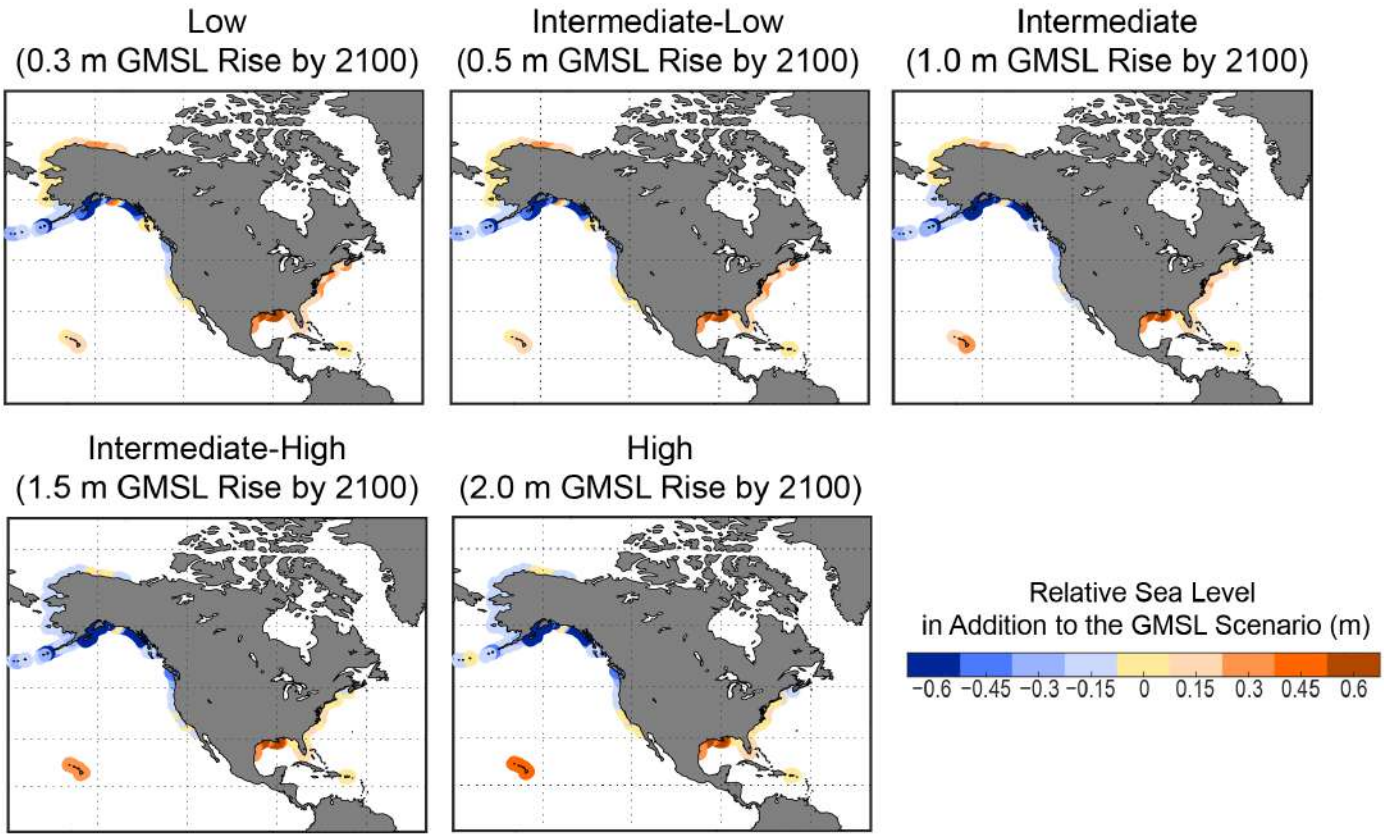

Figure 2.5: Regional deviations of relative sea level from the global mean sea level (GMSL; in meters) value for each scenario in 2100. To obtain the regional projection in 2100 for each scenario, the mapped values must be added to the GMSL value for the associated scenario.

2.5. Scenario Divergence and Tracking

In this report, for the first time, a specific focus is given to the near-term time period (2020–2050). During this window, observations can provide useful information on the trajectory of sea level rise on global and regional scales and serve as a comparison to the model-based GMSL scenarios. Prior to 2050, there is relatively small process uncertainty and little sensitivity to different emissions trajectories, and there is reduced spread between the scenarios in this report compared to Sweet et al. (2017). Connected to this reduced spread, the likely ranges of the revised GMSL scenarios presented here remain overlapping after 2050, whereas the Sweet et al. (2017) scenarios do not overlap after about 2040. In other words, in this report, the process uncertainty continues to exceed the GMSL scenario divergence past the near-term time period. Until the divergence exceeds the range for a given scenario, it will not be possible to determine when higher-end GMSL scenarios will unambiguously emerge from the potential range of the lower-end GMSL scenarios for decades to come. In this report, the time periods (or "gates") when the scenarios become separable are estimated. Different considerations for determining these gates must be made before and after the near-term time period, when the observations are most useful. It should be noted that the gates presented here are based solely on the GMSL differences between scenarios. Regionally, the timing of these gates may be different due to uncertainty in the contributing regional processes. Additionally, other lines of evidence including monitoring of individual processes or emissions trajectories could allow for distinguishing between the scenarios earlier than the gates provided here.

In Figure 2.6, the time pathways of the five GMSL scenarios from 2020 to 2100 are shown, and the gates at which the likely ranges diverge from a particular trajectory or scenario are determined. In Figure 2.6a, the divergence relative to the observation-based GMSL extrapolation is assessed. Note: the GMSL observation-based extrapolation is extended only to 2100 here for the purposes of this divergence assessment. For

the Low and High scenarios, the likely ranges separate prior to 2060, with the Intermediate-High scenario separating after 2060. On the other hand, the Intermediate-Low and Intermediate scenarios do not diverge from the extrapolated observation-based trajectory until after 2080. Consistent with the discussion in Section 2.3, if the processes driving sea level rise are assumed to remain similar for the next three decades, the Intermediate-Low and Intermediate scenarios provide useful bounds on GMSL rise for the near-term time period.

In the decades beyond 2050, however, the more uncertain processes described in Section 2.4 could become a factor and the observation-based trajectory becomes less informative. Instead of assessing the divergence relative to this trajectory, the separation gates relative to the Intermediate scenario are shown in Figure 2.6b. In this case, the Intermediate-High and High scenarios will not diverge from the Intermediate scenario until after 2070 and 2060, respectively. Only the Low scenario diverges from the Intermediate scenario prior to 2050. Although not depicted in Figure 2.6, the higher scenarios also start to overlap again after 2100; for example, GMSL rise consistent with the Intermediate scenario in 2100 (1.0 m) does not rule out GMSL rise consistent with the Intermediate-High scenario by 2150. In tying the two different gate assessments together, even though the Intermediate scenario tracks near the current observation-based trajectory, it will not be possible to statistically distinguish between the Intermediate scenario and the two higher scenarios for decades to come. This also provides important context and caution if attempting to use the observations directly to infer future sea level rise beyond the near-term time period.

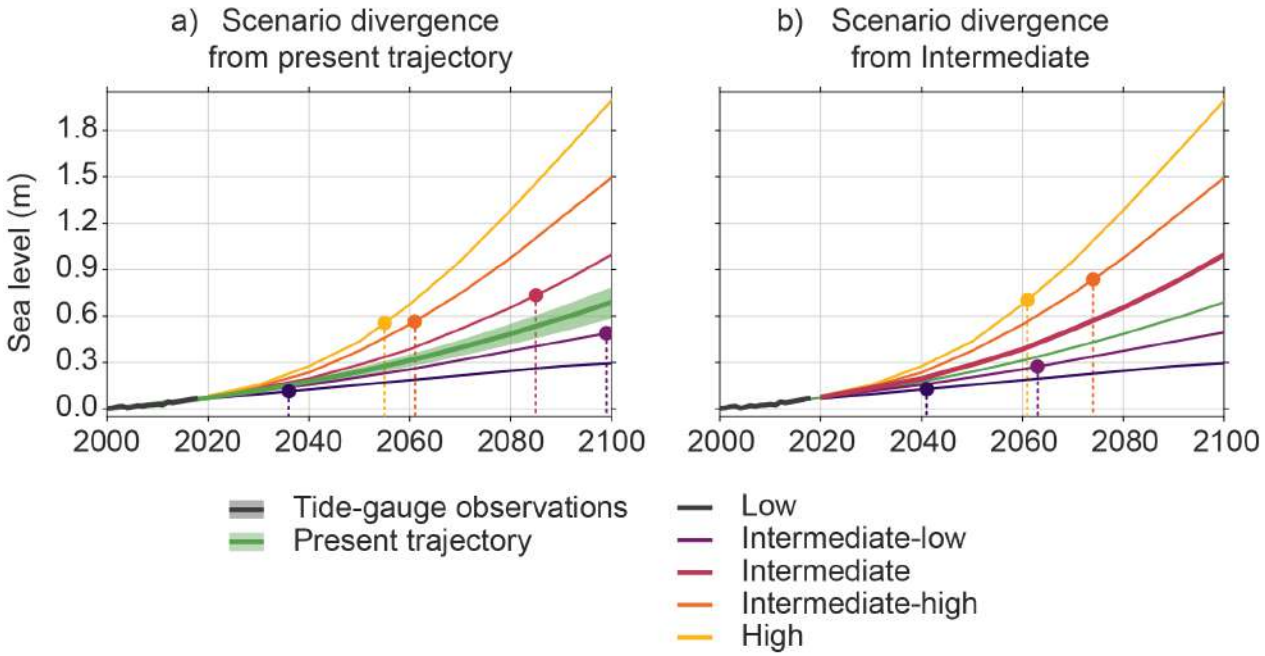

Figure 2.6: Divergence of global mean sea level (GMSL) trajectory and scenarios. The time series shows the observation-based GMSL trajectory and the five GMSL scenarios from 2000 to 2100. The dots denote where each scenario significantly (2 sigma) deviates from the a) observation-based trajectory and from the b) Intermediate scenario.

To explore this further, the proportions of the IPCC AR6 sea level projections contributing to each GMSL rise scenario are shown in Figure 2.7, with contributing emissions pathways specified. As an example interpretation of this figure, the Low scenario generally requires a low emissions pathway, while the Intermediate-Low scenario arises from low, intermediate, and high emissions pathways. Pathways consistent with the Intermediate scenario include low emissions trajectories but are mostly related to high emissions scenarios. In fact, the Intermediate, Intermediate-High, and High scenarios are all heavily driven by high emissions scenarios, and differences between these scenarios are associated predominantly with the possible role and contributions of the low-confidence ice-sheet processes described in section 2.4. The other processes that cause

future sea level change have similar contributions across these scenarios. In other words, sterodynamic sea level change is similar for the Intermediate, Intermediate-High, and High scenarios.

These estimates provide a link between the emissions trajectories in the near term and the possible scenario for GMSL rise in the long term. When coupled with the gating assessment in Figure 2.6, these estimates hold particular relevance for assessing the pathway of sea level rise and determining which long-term scenarios are then possible or even likely. As a way of connecting the elements of the report, the time period where the GMSL scenarios begin to diverge can be put in the context of the analysis done in both the near-term and long-term sections. The likely ranges of the Low and Intermediate-Low versus Intermediate scenarios separate at about 2040 and 2065, respectively. The observation-based extrapolations of global GMSL rise have a relatively narrow range out to this time horizon and can therefore play a role in determining whether a particular low-end trajectory or scenario is more or less likely to be exceeded in the coming decades. As shown in Figure 2.7, the Low scenario depends very heavily on a low emissions pathway on any time horizon. Monitoring using observations of both sea level and emissions can be useful for evaluating the likelihood of the Low scenario, both in the near term and long term.

On the other hand, the separations of the likely ranges for the Intermediate to Intermediate-High and Intermediate to High scenarios do not occur until after 2060 and 2070, respectively. The values at the end of the 21st century and beyond for these scenarios can arise under a variety of different emissions pathways, although higher scenarios are predominantly linked to higher emissions, as expected. To state it another way, the near-term trajectories discussed in Section 2.3 do not currently inform the likelihood of a given scenario occurring in 2100 or 2150. However, the observations can provide useful monitoring as the windows of separation (gates) for a different scenario approach in the future. On these global scales, process-based monitoring of the ice sheets, for example, can play an important role, as the higher scenarios (Intermediate to High) are closely linked to the potential for ice-sheet changes. Additionally, a link between the scenarios in 2100–2150, emissions pathways, and warming levels has been established here. Ongoing and continuous monitoring of both global temperatures[9] and emissions[10] will aid in determining the possible trajectory of future GMSL rise. It should be noted that while the windows provided in Figure 2.6 would be different on the national or regional level, the scenarios for a given location are still closely linked to emissions and warming, and the monitoring discussion above is still relevant.

Finally, regardless of future emissions pathways, GMSL rise will continue past 2150. The amount of "committed" rise can be assessed based on historical comparisons, modeling, and the current process-based understanding of GMSL rise. This committed rise is the amount of total sea level rise that will likely occur for a given warming level. For higher warming levels, the ranges of committed sea level are wide, but the possible values are large in magnitude. Even for a relatively low warming level of 1.5°C, the committed sea level over the next 2000 years still ranges between about 2 m and 3 m. For 2°C, the upper range increases to 6 m (IPCC, 2021a). Although the focus of this report is on the time period between 2020 and 2150, it does reinforce the "when, not if" framing provided in Section 1.

[9] https://climate.nasa.gov/vital-signs/global-temperature/

[10] https://gml.noaa.gov/ccgg/trends/

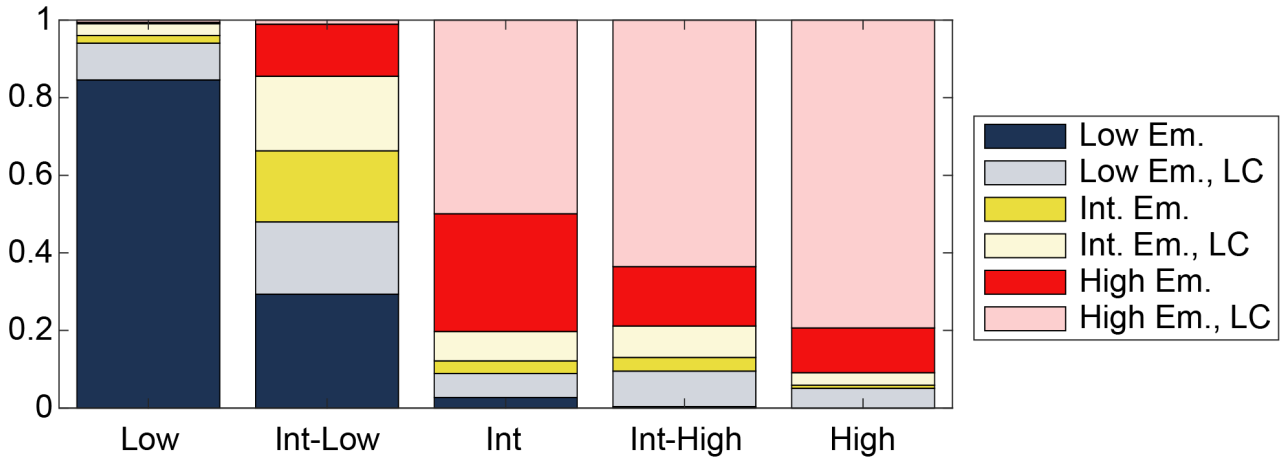

Figure 2.7: Proportions of the contributions from different IPCC AR6 sea level trajectories to each of the five global mean sea level (GMSL) rise scenarios used in this report: Low, Intermediate-Low, Intermediate, Intermediate-High, and High. The IPCC AR6 trajectories are Low Emissions; Low Emissions, LC (where LC indicates inclusion of low-confidence ice-sheet processes); Intermediate Emissions; Intermediate Emissions, LC; High Emissions; and High Emissions LC. The emissions pathways associated with the IPCC AR6 trajectories are as follows: Low Emissions = Shared Socioeconomic Pathway (SSP) 1-1.9 or SSP1-2.6; Intermediate Emissions = SSP 2-4.5; High Emissions = SSP3-7.0 or SSP5-8.5. Shifts between different GMSL rise scenarios approximately reflect the relative odds of being close to a given scenario under different emissions pathways; e.g., the Low scenario is much more plausible under a low emissions pathway, while Intermediate and higher scenarios are much more likely to be associated with high emissions pathways, as well as with low-confidence ice-sheet processes.

Section 3: Extreme Water Levels and Changing Coastal Flood Exposure

Since Sweet et al. (2017), some objectives of the Task Force have been to define and develop for the U.S. coastline 1) a set of coastal-climate flood-resilience standards and 2) a gridded set of extreme water level (EWL) probabilities that span flood frequencies with associated impacts to assess these standards. Together, these sets of information are used to describe how flood exposure within coastal floodplains are slated to change from rising sea levels (i.e., without mitigative action). Specifically for 1), we use a nationally calibrated set of the coastal water-level-impact-severity thresholds from the NOAA National Weather Service (Sweet et al., 2018), which are used in public communications. For 2), a regional frequency analysis (RFA) of tide-gauge observations is developed by adapting methods for exposure assessments within the Pacific Basin (Sweet et al., 2020b) and for the U.S. Department of Defense coastal installations worldwide[11] (Hall et al., 2016). Regional frequency analysis can provide many types of geospatial information based on limited sets of local observations, such as rainfall characteristics published by NOAA[12] (Perica et al., 2018), which are widely used in stormwater design and management within the United States. Both the RFA-based extremes and NOAA flood-threshold information are discussed below.

There are a few important notes about terminology for this section (and the report as a whole). First, "average event frequency" terminology is used throughout (except in Section 4.2 to build off of relevant papers/concepts) to describe extreme water level probabilities instead of the more traditional "return period" terminology. This is done primarily to address best practices (or avoid bad practices), which have been reviewed by the United States Corps of Engineers (USACE; USACE, 1994). Although "frequency" and "period" are related (they are reciprocals), the use of "periods" can be misconstrued; e.g., the so-called 100-year event can be easily confused or communicated (e.g., IPCC, 2021b) as an event that "occurs once per century." Such an interpretation could be assumed to imply a static and permanent water level that happens, on average, 100 years from the last event. In reality, such coastal water levels have and will continue to change with sea level rise, among other potential factors, and can occur (albeit with low probability) several times over the span of a few years. Second, although annual exceedance probability terminology is often used to describe average event frequencies (e.g., 0.1 events/year frequency expressed as the 10% annual chance event), we again stick to events/year frequency terminology, partly due to underlying method but also because events occurring more often than once a year are also being quantified and communicated (a 5 events/year frequency is poorly conveyed as a 500% annual chance event). Finally, the use of the word "occurrence" in this section means "has the probability of equaling or exceeding," as it applies to a particular water level or flood height.

3.1. Overview of Extreme Water Levels and Coastal Flooding

As sea levels continue to rise, coastal water levels—from the mean to the extreme—are growing deeper and reaching farther inland along most U.S. coastlines. Where local relative sea level (RSL) is rising, the wet–dry land delineation (i.e., mean higher high water [MHHW] tidal datum; NOAA, 2003) is encroaching landward, causing more permanent inundation and land loss (e.g., in Louisiana); affecting groundwater levels (Befus et al., 2020), stormwater systems' effectiveness (Habel et al., 2020), and water quality (McKenzie et al., 2021); and altering the intertidal zone and its ecosystems (Kirwan and Gedan, 2019). Where local RSL is falling relative to the land surface, other problems can occur, such as changes in coastal erosion processes, incision of tributaries, decreased draft for waterborne transport, decreased sedimentation in saltwater marshes, and alterations in intertidal zones and estuaries (Larsen et al., 2004; Sweeny and Becker, 2020). Especially problematic for society's coastal footprint is that the entire spectrum of flood exposure is also growing where RSL is rising, from minor high tide flooding (HTF) to more severe major flooding during storms (Sweet and Park, 2014; Fox-Kemper et al., 2021). For example, the national rate of minor HTF is accelerating and is now (circa 2020) more than double what it was in 2000 due to RSL rise (Figure 3.1), with projections suggesting

[11] https://drsl.serdp-estcp.org/

[12] https://www.weather.gov/owp/hdsc

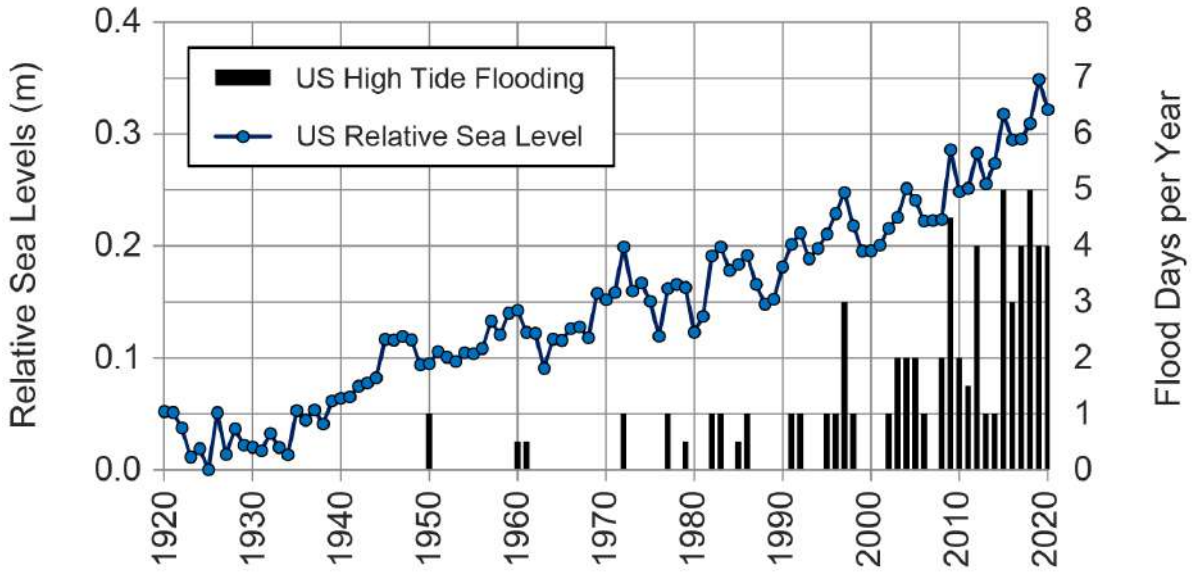

Figure 3.1: National median rate of minor high tide flooding and relative sea level, in meters, from 98 NOAA tide gauges along U.S. coastlines outside of Alaska used to monitor and track flood-frequency changes (from Sweet et al., 2021). Relative sea levels reference the lowest annual (1925) level.

a doubling of its current rate by 2030 (Sweet et al., 2018, 2021; The State of High Tide Flooding and Annual Outlook[13]; Thompson et al., 2021; Flooding Days Projection Tool[14]).

Assessments of current and future changes in minor to major HTF using RSL projections require probabilistic information about local water level variability. Specifically, they require the envelope of variability encapsulating EWLs that define the magnitude and frequency of events capable of causing a range of known or assumed impacts (Tebaldi et al., 2012; Church et al., 2013; Hall et al., 2016; USGCRP, 2017; Oppenheimer et al., 2019; Fox-Kemper et al., 2021). The basis for quantifying EWLs along U.S. coastlines originates with NOAA's tide-gauge network, which measures water level responses from multiple processes operating over a range of frequencies (Table 3.1). However, due to their general placement (e.g., in harbors), protective housings that dampen wave effects, and their multi-minute sampling rates, tide gauges typically do not measure or report values that include higher-frequency wave effects (Sweet et al., 2015; see Box 3.1). Other sources of useful tide level information for the U.S. and globally include USACE inventories (e.g., USACE MRG&P, 2017), the University of Hawaii Sea Level Center,[15] and the Global Extreme Sea Level Analysis database.[16]

Extreme water levels are often used as a proxy for impacts, such as the 0.01 events/year frequency level, better known as the "once per century" event (Oppenheimer et al., 2019), with connotations of the "flood of the century." However, such a probabilistically defined event can be both misleading about its true frequency (USACE, 1994) or might go mostly unnoticed in some locations (Sweet et al., 2020b). High tide flood heights, on the other hand, are absolute heights that are calibrated to the depth-severity impact thresholds of the NOAA National Weather Service and local emergency managers to trigger public notification of impending flood risks (NOAA, 2020). NOAA minor, moderate, and major HTF is defined as a water level reaching or exceeding about (national median values) 0.55 m, 0.85 m, and 1.20 m above current MHHW, respectively (Sweet et al., 2018). Put another way, an EWL is only a "flood" if it actually impacts the public in some manner and is not necessarily a description of a meteorological event.

[13] https://tidesandcurrents.noaa.gov/HighTideFlooding_AnnualOutlook.html

[14] https://sealevel.nasa.gov/data_tools/15

[15] https://uhslc.soest.hawaii.edu/

[16] https://www.gesla.org/

But the NOAA tide-gauge network is relatively sparse compared to the density of coastal communities, and the tide gauges have varying record lengths. From the perspective of a particular coastal community, this may result in either 1) a lack of local data (often data that are simply extrapolated from the closest NOAA tide gauge) or 2) a data record that is biased by lack of or overexposure to regionally significant rare events such as storm surges from landfalling tropical cyclones. Probabilistic assessments using atmospheric/ocean circulation models can increase spatial coverage (Vousdoukas et al., 2018), but they often perform poorly in areas with high tropical storm activity or with complex bathymetries (Muis et al., 2016). Targeted deployments of in situ sensors by communities to monitor changes in sea level, tide heights, and flood exposure (McCallum et al., 2013) can be informative but still lack the necessary longer-term regional perspective.

Table 3.1: Physical processes affecting U.S. coastal water levels and their temporal and spatial scale properties (modification of Sweet et al., 2017). Extreme water levels, which, as measured by tide gauges, generally exclude high-frequency wave effects, include processes between tsunami and ocean-basin variability and, to a lesser extent, low-frequency changes or trends associated with land ice melt/discharge, thermal expansion, and vertical land motion.

Physical Process	Spatial Scale			Temporal Scale	Potential Magnitude (yearly)
	Global	Regional	Local		
Wind Waves Effects	—	—	X	seconds to minutes	<10 m
Tsunami	—	X	X	minutes to hours	<10's of m's
Storm Surge (e.g., tropical and extra-tropical storms)	—	X	X	minutes to days	<10 m
Tides	—	X	X	hours to years	<15 m
Ocean/Atmospheric Variability (e.g., ENSO response)	—	X	X	days to years	<0.5 m
Ocean Gyre and Over-turning Variability	—	X	X	years to decades	<0.5 m
Land Ice Melt/Discharge	X	X	X	years to centuries	mm's to cm's
Thermal Expansion	X	X	X	years to centuries	mm's to cm's
Vertical Land Motion	—	X	X	minutes to centuries	mm's to m's

For the U.S., there are two primary sources of federally provided EWL probabilities. The first comes from the Federal Emergency Management Agency (FEMA, 2016b), which provides sets of regional solutions using a combination of NOAA storm-tide observations, historical high-water marks,[17] synthetic storm simulations (e.g., Nadal-Caraballo et al., 2020; ERDC Coastal Hazards System[18]), and wave effects to estimate the regulatory floodplain and its exposure to the rarest of events (e.g., 1% and 0.2% annual chance events). FEMA provides this information for national flood insurance purposes[19] but does not consider future sea levels. Another set of EWL probabilities is from NOAA's Center for Operational Oceanographic Products and Services (Zervas, 2013), which currently uses a generalized extreme value (GEV) distribution fit to annual highest water levels for tide-gauge records of >30 years).[20] The U.S. Army Corps of Engineers and their Sea Level Change Calculator[21] provide the NOAA EWL probabilities (Zervas, 2013) with several projections of future RSL to help in project planning but only for specific long-term tide-gauge locations.

A primary goal of the following subsections is to introduce a new set of EWL probabilities to support sea level rise and flood-exposure assessments and planning. The EWL set is applicable for most of the U.S. coastline and further resolves (both in physical and probability space) the EWL information currently available from

[17] https://stn.wim.usgs.gov/FEV/

[18] https://chs.erdc.dren.mil/

[19] https://www.fema.gov/flood-maps/national-flood-hazard-layer

[20] https://tidesandcurrents.noaa.gov/est/

[21] https://cwbi-app.sec.usace.army.mil/rccslc/slcc_calc.html

FEMA and NOAA; although again, the EWL data here, which are derived from tide-gauge data, generally do not include wave effects (see Table 3.1 and Figure 1.1). Section 3.2 briefly describes the RFA of NOAA tide-gauge data with pointers to the Appendix for a fuller description. In Section 3.3, data for all NOAA tide gauges with >10 years of record are used to compute EWL probabilities, and these results are compared to NOAA and FEMA datasets. Section 3.4 discusses methods on how local EWL probabilities can be 1) computed using other records, such as those of shorter duration (<10 years) from NOAA or other (user supplied) sources, and 2) estimated approximately every 500 m along the U.S. coastline based on local tide range information from NOAA models (e.g., VDatum[22]). Lastly, Section 3.5 assesses current and future flood exposure within the coastal floodplain using NOAA's height-severity categories of minor, moderate, and major HTF (Sweet et al., 2018), which broadly define water levels where U.S. infrastructure becomes impacted and are used in weather forecasting to trigger emergency responses (NOAA, 2020). Estimates of how flood exposure is projected to change by 2050 (assuming no additional adaptation or risk-deduction measures) are provided using the upper-bounding scenarios of the regional observation-based extrapolations along U.S. coastlines (see Table 2.2).

3.2. Regional Frequency Analysis of Tide-Gauge Data

Extreme water level probabilities and their 95% confidence intervals are provided at a 1-degree spacing along nearly the entire U.S. coastline (Figure 3.2). The EWL information is based on an RFA (Hosking and Wallis, 1997) of NOAA tide gauges within a 400-km radius of the center of each individual 1-degree grid and fit with a Generalized Pareto Distribution (GPD) of threshold exceedances (Coles, 2001). The RFA process not only better assesses EWL exceedance probabilities from a regional perspective as compared to a single-gauge assessment but also can supply information where no tide gauges exist. Furthermore, a GPD fit to exceedances above a high threshold as compared to a GEV fit to annual maxima uses more of the data record (e.g., two or more significant events within a particular year), not just those maxima within a certain (e.g., annual) time block. This approach, using RFA-based GPD fits, better resolves both the low- and high-frequency spectrum with output in this report ranging from 0.01 events/year to 10 events/year frequencies. Combining an RFA with GPD fits to obtain EWL probabilities is unique for U.S. coastlines, although there are other statistical methods such as the joint probability method (Baranes et al., 2020) and Bayesian hierarchical modeling (Calafat and Marcos, 2020), which may also prove useful in assessing rare event probabilities or providing information where no tide gauges exist.

[22] https://vdatum.noaa.gov/

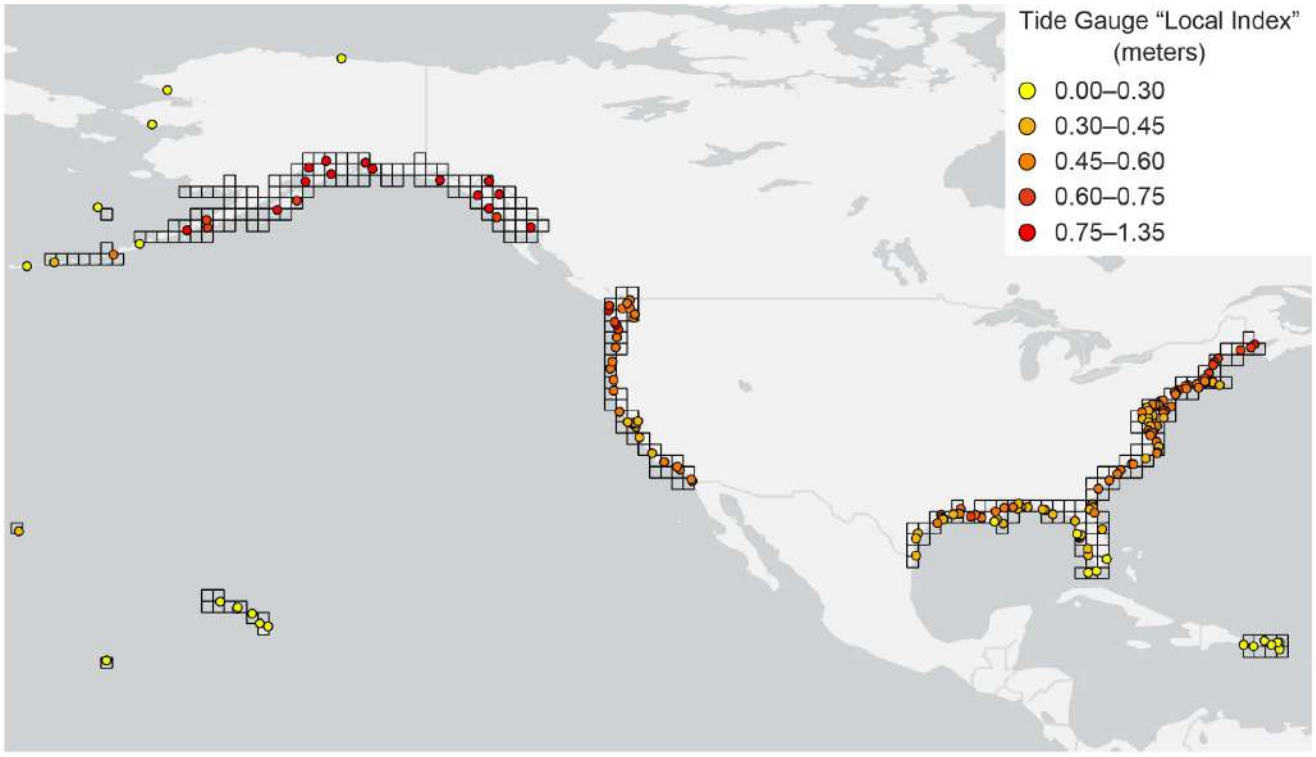

Figure 3.2: Regional Frequency Analysis 1-degree grids and local index values (u) relative to local mean higher high water tidal datum at the NOAA tide gauges used in this study.

To be useful for local decision-making, the gridded EWLs ($EWL_{gridded}$) derived by RFA need to be further localized (EWL_{local}), which is achieved via a "local index" (u) estimated at a particular tide gauge (u values are shown in Figure 3.2) or for a particular location and converted to the vertical control datum on the land surface, normally the North American Vertical Datum of 1988 (NAVD88). The following equation is used to estimate EWL_{local} probabilities (median and 95% confidence intervals):

1) $$EWL_{local} = EWL_{gridded} * u_{local} + u_{local}$$

where $EWL_{gridded}$ is the gridded EWL composed on normalized (unitless) sets of tide-gauge data, and u_{local}, referred to simply as "u," are the same value and represent the height of the 98th percentile of daily highest water levels with a 4-day filter applied and are relative to the 1983–2001 (or 5-year modified epoch; Gill et al., 2014) MHHW tidal datum. For statistical independence when quantifying the EWL probabilities, the filtering process is needed to isolate and only include the peak water level value from a particular storm or "event," rather than including multiple consecutive daily peak levels resulting from the same event (e.g., a multiday storm surge). See Section A2 for more details.

3.3. Average Event Frequencies of Extreme Water Levels

The focus of this analysis is on EWL events and their probabilities that span the frequency space associated with coastal flooding under current sea levels (Sweet et al., 2018). An example for the NOAA tide gauge at The Battery in New York City (NYC) in Figure 3.3a shows the NOAA HTF heights and probability distributions for hourly water levels and also for their daily maxima.[23] Also shown is the local index (u = 0.55 m above MHHW) computed for this tide gauge, which is used to estimate EWL_{local} from the $EWL_{gridded}$ probabilities for this location (Figure 3.3b). See Figure A2.2f for the gridded probabilities applicable for NYC. At higher frequencies, such as those associated with the height of the minor HTF level (0.56 m above MHHW), the EWL_{local} probabilities for "events" (about 4–5 events/year) are close but slightly underestimate flood frequency estimates for "days" (about 11 days/year; not shown), which are based on a multidecadal distribution

[23] https://tidesandcurrents.noaa.gov/stationhome.html?id=8518750

of daily highest water levels (shown in Figure 3.3a) used by NOAA when making projections of minor HTF (Sweet et al., 2018). This difference reflects the 4-day event filter in estimates of the EWL_{local} probabilities discussed above. A similar ratio (about 2 days per event) exists in NOAA's HTF Outlook (about 11 days/year for 2020 at NYC, which is based on an extrapolation of quadratic or linear fits to annual counts of minor HTF days (Sweet et al., 2020a). The ratio of minor HTF "events" to "days" estimated at NOAA tide gauges as a whole is further discussed later in this section. The main point is that, typically, the duration of a minor HTF "event," as in NYC and along U.S. coastlines, spans about 2 days and multiple tide cycles on average.

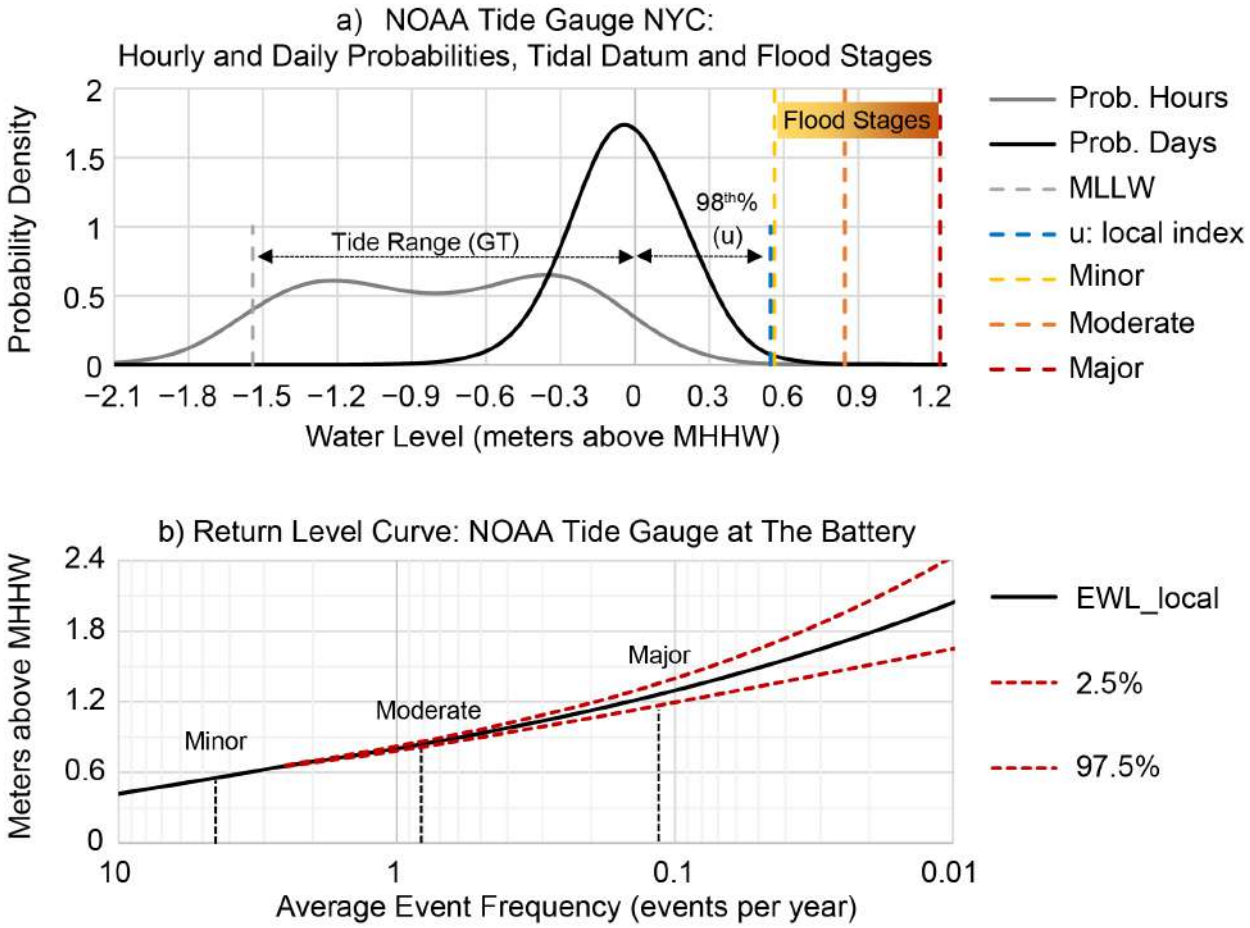

Figure 3.3: a) Empirical probability densities of hourly water levels and their daily maxima measured by the NOAA tide gauge at The Battery (New York City), as well as the tidal datums of mean lower low water (MLLW), great diurnal tide range (GT), local high tide flood (HTF) heights, and the local index (u) used to localize the RFA-gridded EWL for this location (see Figure A2.2f). All values are referenced to the mean higher high water (MHHW) tidal datum and shown in b) as a return interval curve with the 95% confidence interval (2.5% and 97.5% levels) normalized to year 2020 RSLs.

Some general patterns emerge in regional $EWLs_{local}$ with 1 event/year (Figure 3.4a) and 0.01 events/year frequencies (Figure 3.4b). Locations with higher 0.01 events/year EWL_{local} are found adjacent to wide, shallow continental coasts that are exposed to frequent tropical or extratropical storm surges, such as occur along the Eastern and Western Gulf coastal regions at 2.5 ± 1.1 m and 2.8 ± 0.8 m (median ± 1 standard deviation), respectively. In contrast, the U.S. Pacific/Hawaiian Islands and Southwest Pacific coastal regions have lower 0.01 events/year $EWLs_{local}$ due to deep, narrow continental shelves and generally calmer conditions (0.8 ± 0.1 m and 1.0 ± 0.1 m, respectively), although wave effects not inherent to the EWL probabilities are often the primary factor causing flooding, overwash, and erosion along natural landscapes in these locations (Barnard et al., 2019; see Box 3.1). In terms of the 1 event/year heights, tide ranges become influential (correlation of ~0.7 between great diurnal tide range [GT] and u across all locations), as is the case in the Northwest Pacific coastal region and the southern Alaska coasts, where the highest 1-year EWLs occur (0.8 ± 0.1 m and 1.0 ± 0.3 m, respectively) and larger tide ranges are found.

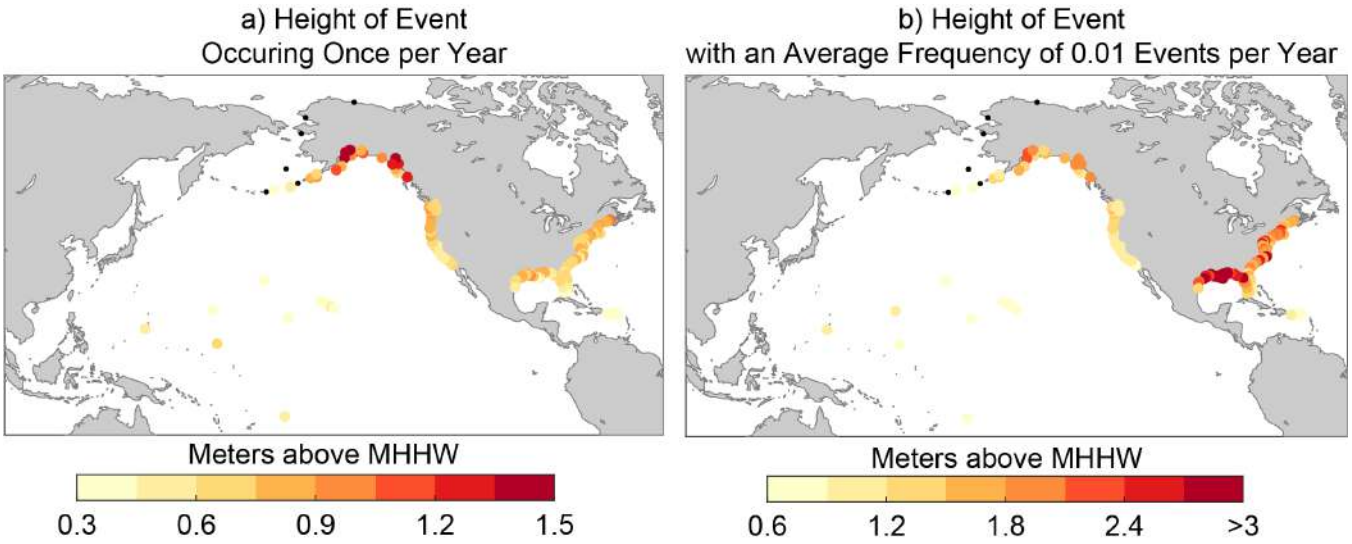

Figure 3.4: Current (circa 2020 relative sea levels) EWL_{local} that a) occur annually on average and b) have a 0.01-year average event frequency. Note: the scales in the two figures are not the same, and to be useful for decision-making, a conversion to land-based heights (e.g., NAVD88) should be made.

There are differences when comparing the RFA-based $EWLs_{local}$ from this study to current FEMA and NOAA governmental datasets. Comparisons to NOAA EWLs (Zervas, 2013) in Figure 3.5a–c show that the RFA-based 0.01, 0.1, and 0.5 events/year levels are about 6%, 9%, and 13% higher across the board based on linear regression, respectively. The bias between datasets is not unexpected, as an RFA typically results in higher EWL probabilities with narrowed confidence intervals due to the regionalization process as compared to a single-gauge analysis (Sweet et al., 2020b). Overall, there is strong correlation between datasets, although less so at the 0.01 events/year EWL_{local} ($R^2 = 0.49$) due in part to the large differences occurring along the Gulf coastlines of Alabama, Mississippi, and Louisiana, where the RFA-based 0.01 events/year EWL_{local} (~4 m above MHHW) values are substantially higher (>1 m) than the NOAA GEV estimates in a few locations.

The RFA-based EWL_{local} probabilities are also compared to the tide-gauge-equivalent "stillwater" component (tides, storm surge, and limited wave set-up, but not wave swash; see Figure 1.1) generated by FEMA and used within their regional Flood Insurance Studies[24] (Figure 3.5d–f). The FEMA EWLs vary in their construction by region, using a combination of singular and RFA tide-gauge analyses, storm-surge modeling, and synthetic tropical storm modeling (for the Northeast, Southeast, and Eastern and Western Gulf coastal regions) via a joint probability method–optimal sampling (JPM–OS) procedure (FEMA, 2016a, 2016b). The 0.01 and 0.1 events/year EWL_{local} are slightly lower (7% and 4%, respectively), with differences again noted along the Eastern and Western Gulf and Caribbean coastal regions. At the 0.5 events/year levels, both sets of EWLs are nearly the same based on linear regression. The goodness-of-fit (R^2) values are about the same as with the NOAA (2013) GEV results, although a little less at the 0.01 events/year levels—likely due to the inclusion of synthetic storm-surge modeling in the FEMA estimates, compared to the NOAA (2013) values, which are based on tide-gauge observations. Thus, it is concluded that the RFA-based EWL provides higher estimates than a single-gauge analysis (Zervas, 2013) but less than those of FEMA stillwater values at lower probabilities, since FEMA's data also include storm-surge modeling, synthetic storms, and high-water marks in addition to tide-gauge data.

[24] https://www.fema.gov/glossary/flood-insurance-study-fis

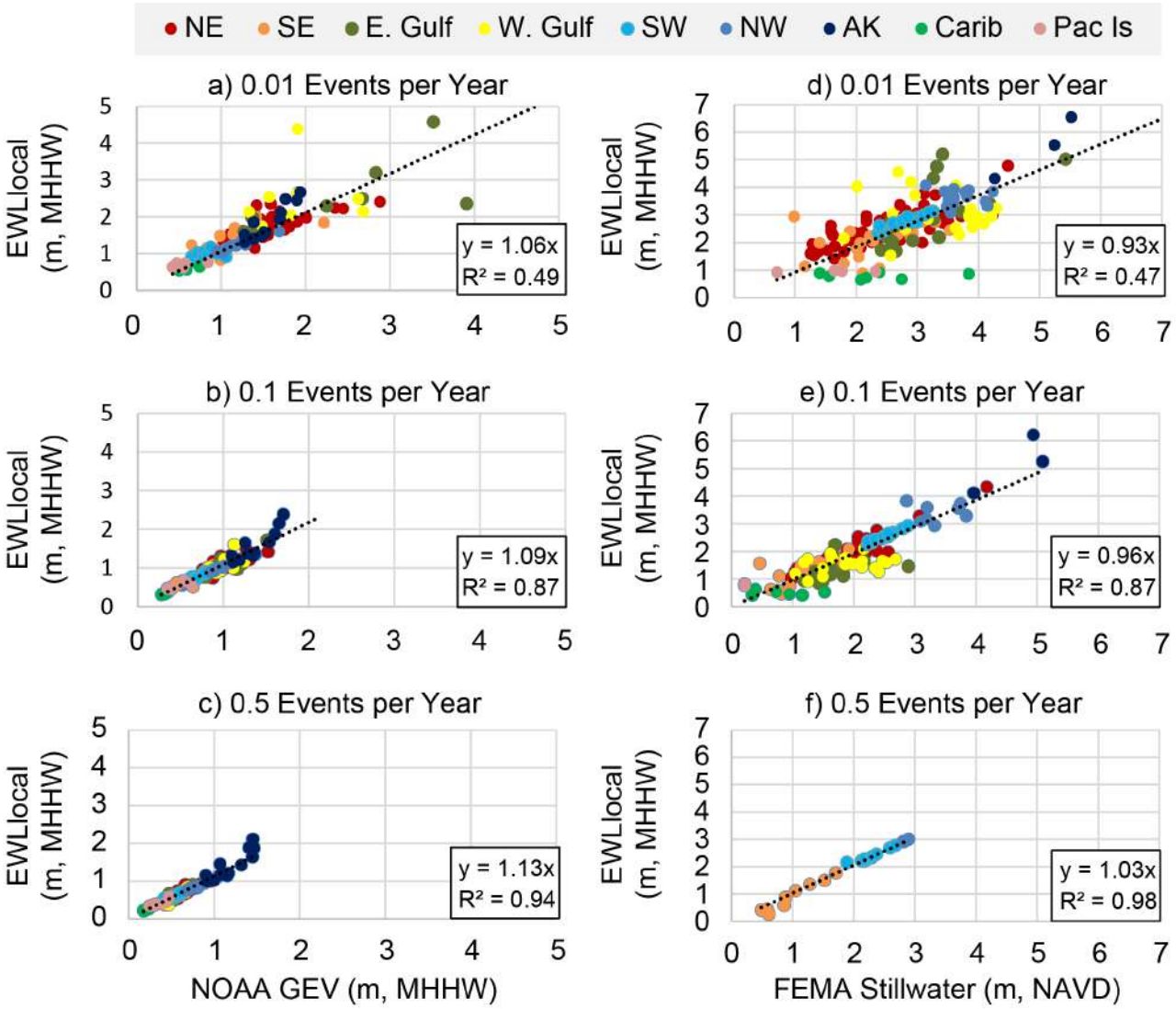

Figure 3.5: Comparison between (a–c) this study's EWL_{local} to those of NOAA (Zervas, 2013) based on a GEV fit of annual highest water levels and to (d–f) the stillwater (storm surge, tides, and wave set-up) components of FEMA used in their Flood Insurance Study at the 0.01-year, 0.1-year, and 0.5-year average event frequency levels.

3.4. Methods to Localize the Gridded Extreme Water Level Event Probabilities

There are several ways to obtain EWL_{local} from the $EWL_{gridded}$. All require a local index (u), which can be obtained from 1) a NOAA tide gauge used in this study (Figure 3.2; Table A1.3); 2) alternative sources of water level/tide-gauge data not used in this study (e.g., see Figure A2.3); or 3) tide range knowledge from measurements or models. When using short-term water level measurements (Figure A2.4), additional uncertainty, dependent on record length, is factored into the 95% confidence interval of the EWL_{local} estimate (see Equation 4 in the Appendix). This additional uncertainty relates to the fact that the local index (u) will vary from year to year akin to how RSL varies through time.[25] On a national scale (and for most regions as well; see Figure A2.4), the root mean square error (RMSE) in local index estimates is about 6–7 cm after 5 years and falls to less than 3 cm at 10 years, which is close to the standard error in tidal datum calculations themselves (see datum errors in Bodnar, 1981).

Where local water level measurements are not available, another option is to estimate a local index (u) and EWL_{local} probabilities based on an underlying relationship between local index values and tide range along U.S. coastlines. Additional uncertainty using this method will need to be factored into the results as well.

[25] https://tidesandcurrents.noaa.gov/sltrends/sltrends.html

This relationship (Figure A2.5) builds off of the findings of Sweet et al. (2020b) within the Pacific Ocean and of Merrifield et al. (2013) globally, who found a strong global correlation between the range of water level variability and average annual highest water level across the globe. Nationally, there exists a strong positive relationship (R^2 = 0.72 in Figure A2.5), although with fairly large uncertainty (RMSE of 0.11 m). But when tide range and local index values are regressed regionally, all the fits' RMSEs are less (see Figure A2.5). Across all U.S. regions, it takes about 6 years of data for the RMSE (see Figure A2.4) in local index (u) estimates to match the RMSE values based on measured tide range (see Figure A2.5). Tide range information can be obtained from NOAA Vertical Datum Transformation (VDatum).[26] Comparison of RMSEs based on multiple years of record versus tide range estimates of a local index (u) will vary by region (see Figures A2.4 and A2.5), and the lesser of the two is considered the better option in estimating an EWL_{local} for any specific location not associated with a tide-gauge location used in the study.

Here we provide an example of how to obtain EWL_{local} probabilities for a location not used in this study. The location for this example is the NOAA National Estuarine Research Reserve in Grand Bay, Mississippi (Figure 3.6a), which has a NOAA tide gauge, but the hourly record is only about 4 years long.[27]

1. The first step is to identify the specific EWL grid where the location resides, which in this case is grid number 42811 (Figure 3.6a), and obtain the $EWL_{gridded}$ probabilities.
2. Next, a local index needs to be estimated for an EWL_{local} to be computed, either by the tide-range-based method (Figure 3.6b) or using the existing short data record (Figure 3.6c) for the specific region, depending on the smaller RMSE of the two methods. The RMSE based on the tide range regression is 0.078 m (Figure 3.6b) and is less than the 0.099 m RMSE based on a 4-year water level record for this region (solving the equation shown in Figure 3.6c).
3. Using the published NOAA tide range value at this location (0.49 m) leads to an estimated local index value of 0.47 m through the regional regression (solving the equation shown in Figure 3.6b).
4. An EWL_{local} return level curve (Figure 3.6d) relative to the 1983–2001 tidal epoch is generated by substituting a local index value of 0.47 m and an RMSE of 0.078 m (with a variance of 0.078^2) into Appendix Equations 1 and 4 (see Section A2), respectively.
5. Finally, to update the curve to current conditions (circa 2020) from the midpoint of the 1983–2001 epoch (1992), 0.12 m is added to the return level curve values. The 0.12 m value represents the regional-median trend in u of 4.3 mm/year multiplied by 28 years (see Table A1.3 and Section A2.3.4 for more information). Alternatively, 0.15 m could be added instead by applying the RSL offsets from the regional observation-based extrapolations for this region (Table A1.2).

The resultant EWL_{local} probabilities estimated for Grand Bay are similar to others at nearby tide gauges that share the same 1-degree $EWL_{gridded}$ (see Figure 3.4). Less noticeable is that the 95th confidence intervals are more inflated (i.e., 0.5 m vs. 0.1 m at the 1 event/year EWL) because of the additional uncertainty from using the tide-range-based method to obtain a local index. Nationally, the spread of the 95% confidence interval at the 1 event/year EWL_{local} using a local index (u) estimated by tide range (Figure 3.6b and Figure A2.5) is 0.32 m as compared to 0.03 m when assessed across all NOAA tide gauges.

[26] https://vdatum.noaa.gov/

[27] https://tidesandcurrents.noaa.gov/stationhome.html?id=8740166

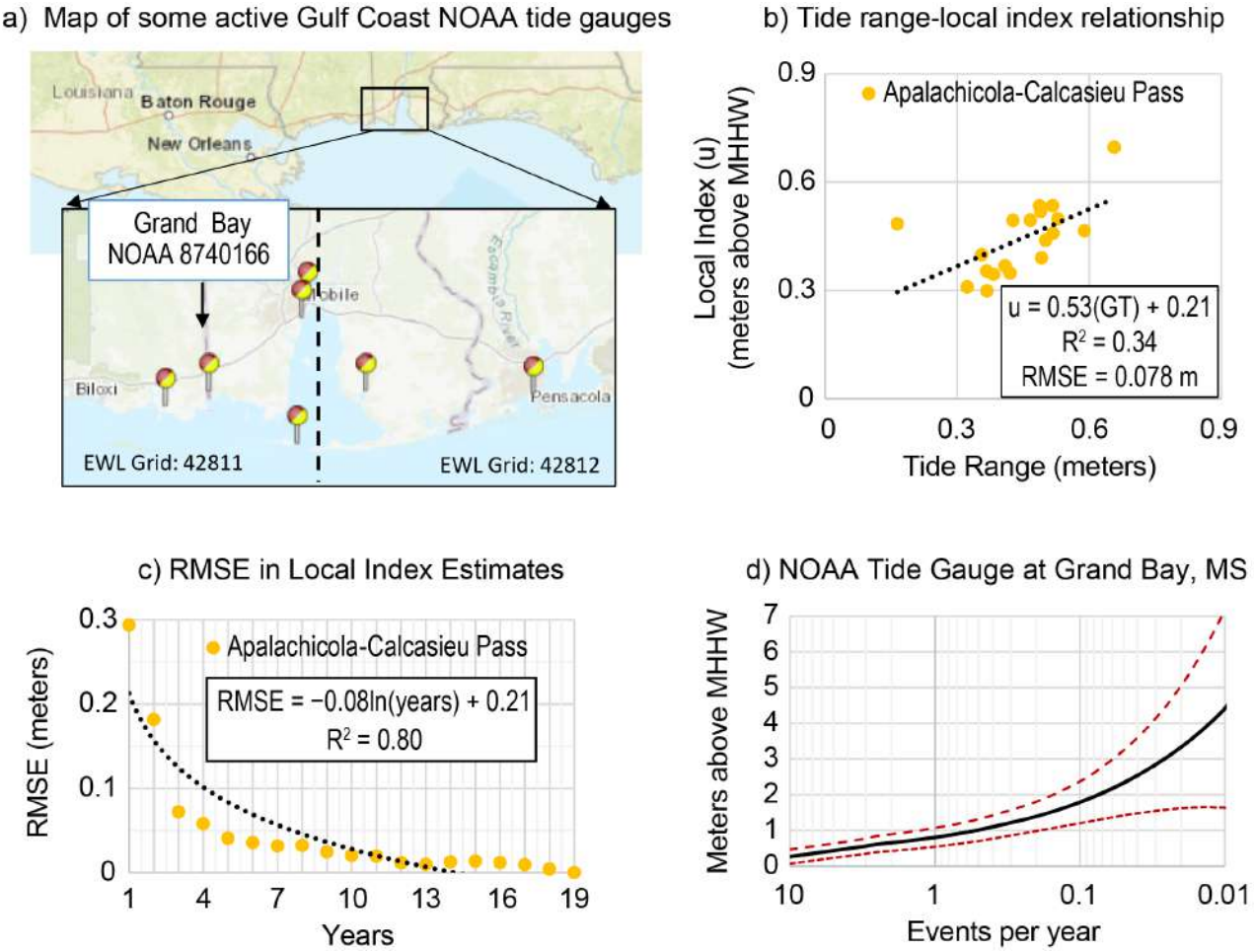

Figure 3.6: a) Map showing active NOAA tide gauges indicating Grand Bay, Mississippi, which has about 4–5 years of hourly data, b) tide range to local index (u) regression relative to the 1983–2001 tidal datum epoch with fit equation, goodness of fit (R^2), and associated root mean square error (RMSE) for the surrounding region, c) RMSE for estimates of u based on 1–19 years of consecutive data over the 2001–2019 period based on the regional tide gauges for the surrounding region; and d) a 2020 EWL_{local} return level curve for Grand Bay using a local index (u) from tide range regression. Note: to be useful for decision-making, a conversion to land-based heights (e.g., NAVD88) should be made.

3.5. The Changing Nature of Coastal Flood Exposure

To assess U.S. coastal flood exposure using the EWL_{local} probabilities, we use the nationally calibrated coastal HTF heights of NOAA (Sweet et al., 2018) and a modification of Sweet et al. (2020b) for Alaska coastlines (see Section A2.4). The NOAA HTF heights include three categories: minor, moderate, and major (national median) starting at about 0.55 m, 0.85 m, and 1.20 m, respectively (Figure A2.6), whose impacts are disruptive, typically damaging, and often destructive, respectively, under current flood defenses. NOAA provides data (e.g., Flood Frequency [MapServer][28]) and maps (Figure 3.7) in its SLR Viewer of exposure to HTF to help communities recognize potential flood exposure associated with weather–water level forecasts and for vulnerability assessments associated with sea level rise.

Currently (with EWL_{local} relative to year 2020 trend levels), minor HTF events occur (median value) about 3 times per year along U.S. coastlines and are most frequent along the Northeast, Western Gulf, and Northwest coastlines (about 4 events/year) and along the Southeast and Eastern Gulf coastlines (about 2 events/year; Figure 3.8a). A similar pattern emerges when comparing the 2020 NOAA minor HTF outlook (Sweet et al., 2020a) for the number of flood "days" at about 100 of the tide gauges (Figure 3.8b). The NOAA outlook for

[28] https://coast.noaa.gov/arcgis/rest/services/dc_slr/Flood_Frequency/MapServer

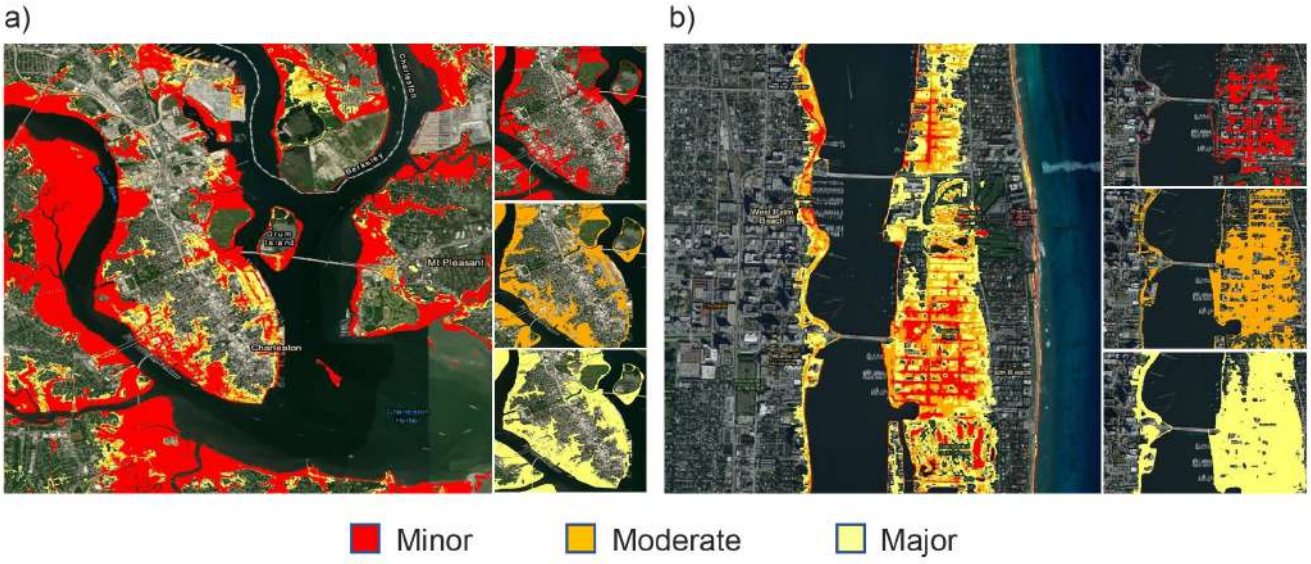

Figure 3.7: NOAA minor (red layer: land between mean higher high water [MHHW] and minor high tide flood [HTF] height above MHHW), moderate (orange layer), and major (yellow layer) HTF maps showing a regional layered map with individual layer panes to the right for a) Charleston, South Carolina, and b) West Palm Beach, Florida. MHHW for 1983–2001 is the shoreline edge. Note: to be useful for decision-making, a conversion to land-based heights (e.g., NAVD88) should be made.

minor HTF days uses extrapolations of linear and/or quadratic fits to days per year with a water level at or above the flood height. As a whole, there are about twice the number of days of minor HTF than the number of discrete events (Figure 3.8b inset), which is largely reflective of typical synoptic-scale (temporal) variability and the 4-day event filtering used in the RFA process and GPD fitting. The national (median) outlook for minor HTF in 2020 was 4–5 days, with about 8–9 days each along the Northeast and Western Gulf coastlines and 3–5 days each along the Southeast and Eastern Gulf coastlines (Sweet et al., 2020a).

Currently, moderate HTF in 2020 (Figure 3.8c) has about a 0.3 events/year frequency (median value) nationally and a similar 0.2–0.4 events/year frequency along the Southeast, Eastern Gulf, and Northwest coastlines. Moderate HTF is most likely along the Western Gulf coastlines (0.6–0.7 events/year). Major HTF (Figure 3.8d) nationally and along the Southeast coastline has about a 0.04 events/year frequency. Major HTF is most likely along the Western Gulf coastline (0.15 events/year) and along the Northeast and Eastern Gulf coastlines (0.08–0.09 events/year). For a more local perspective (see Figure 3.7), 2020 annual frequencies of minor, moderate, and major HTF in Charleston, South Carolina, and West Palm Beach, Florida, were about 2–3 events/year, 0.15–0.25 events/year, and about 0.02–0.04 events/year, respectively, based on the nearest tide gauge (see Table A1.2).

Changes in flood exposure are projected to 2050 considering no additional flood risk reduction or adaptation (e.g., via improved stormwater system functionalities) at NOAA tide gauges (Figure 3.9). The EWL_{local} probabilities are brought to 2050 levels by adding the local RSL projections initiating in year 2005 associated with the upper-bounding sea level scenario identified by the regional observation-based extrapolations (Table 2.2). Other scenarios could be used, but we opted for this particular set because it uses observational evidence—extrapolation of fits over the last 50-years (i.e., 1970–2020) to provide some level of prediction for the next 30 years. For instances where the extrapolations are the same as a particular scenario (e.g., Northeast), the adjacent (higher) scenario is used (e.g., the Intermediate is considered the upper-bounding scenario for the Northeast), which also serves to partially compensate for natural variability that is not reflected in the extrapolations.

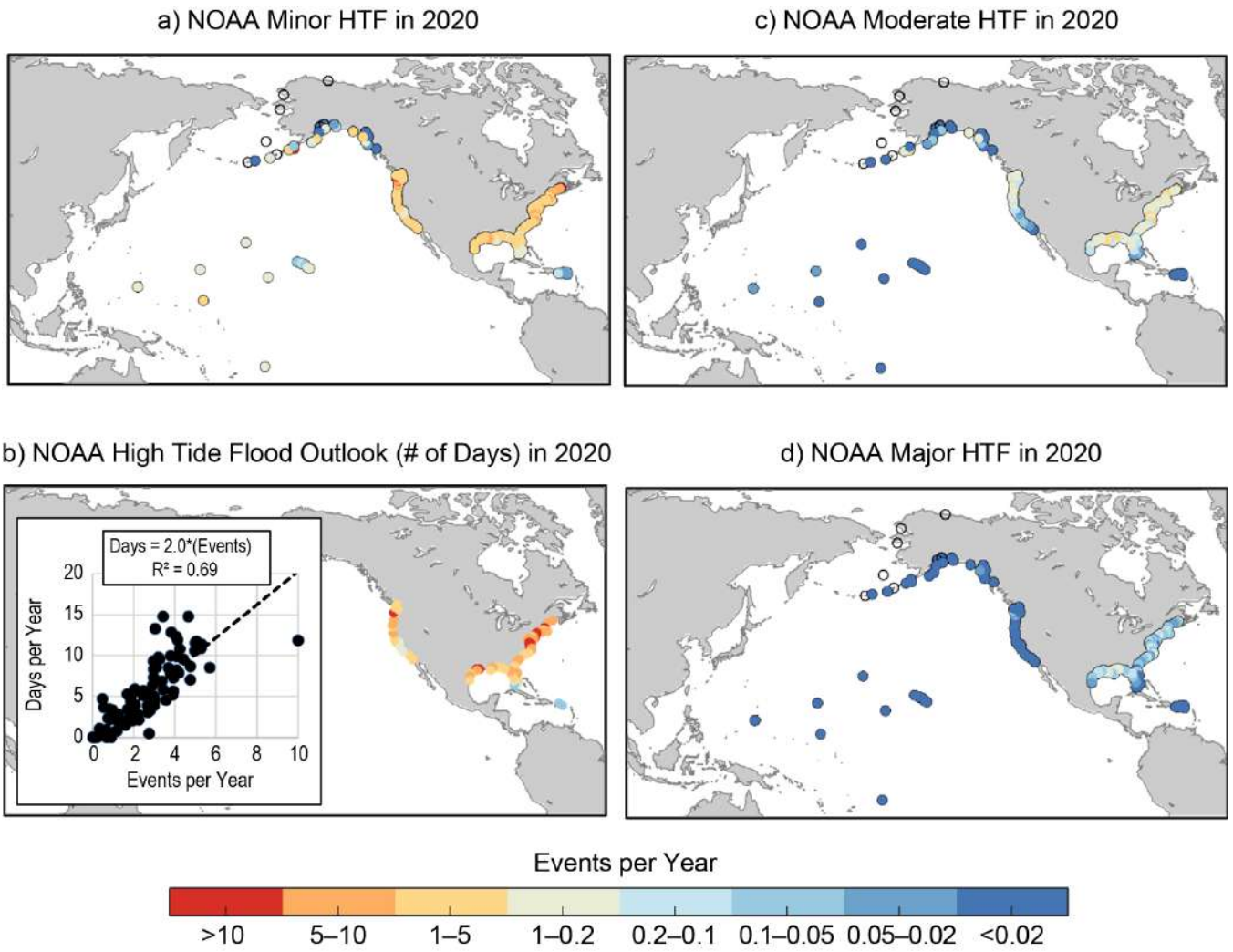

Figure 3.8: Average event frequencies in 2020 of a) minor high tide flooding (HTF); b) number of "days" (as compared to "events") of HTF estimated in NOAA's annual outlook (Sweet et al., 2021) and regression between events and days; c) average event frequencies in 2020 of moderate HTF; and d) average event frequencies in 2020 of major HTF. Flood height-severity definitions are from NOAA (Sweet et al., 2018) and, specifically for Alaska locations, from Sweet et al. (2020b).

Nationally and along all regions except the Hawaiian/Pacific Islands (about 9 events/year), the Caribbean (about 6 events/year), and Alaska (0.7 events/year) coastlines, the median event frequency in minor HTF is projected to increase to >10 events/year (Figure 3.9a). Moderate HTF (median) frequencies (Figure 3.9b) are projected by 2050 to increase nationally to about 4 events/year; >10 events/year along the Western Gulf coastline; 3–6 events/year along the Northeast, Southeast, and Eastern Gulf coastlines; about 1 event/year along the Northwest coastline; and 0.7 events/year along the Southwest coastline. Major HTF frequencies (Figure 3.9c) are projected to increase to about 0.2 events/year nationwide (median), with 1 event/year along the Western Gulf coastline, 0.5 events/year along the Northeast coastline, and 0.2–0.3 events/year along the Southeast Atlantic and Eastern Gulf coastlines. For a local perspective, the 2050 projections of annual frequencies of minor HTF in Charleston and West Palm Beach are >10 events/year, with 4–5 of those events reaching or exceeding moderate HTF and the possibility (0.1–0.2 events/year) of major HTF.

For perspective and a summary assessment by region, Table 3.2 quantifies how minor, moderate, and major HTF frequencies have changed and are projected to change considering the local RSL scenarios associated with the upper-bounding scenario of the regional observation-based extrapolations (Table 2.2) using 1990, 2020, and 2050 time slices. Nationally, minor HTF frequencies nearly tripled between 1990 and 2020, growing from about 1 to 3 events/year. They are projected to more than triple by 2050 to

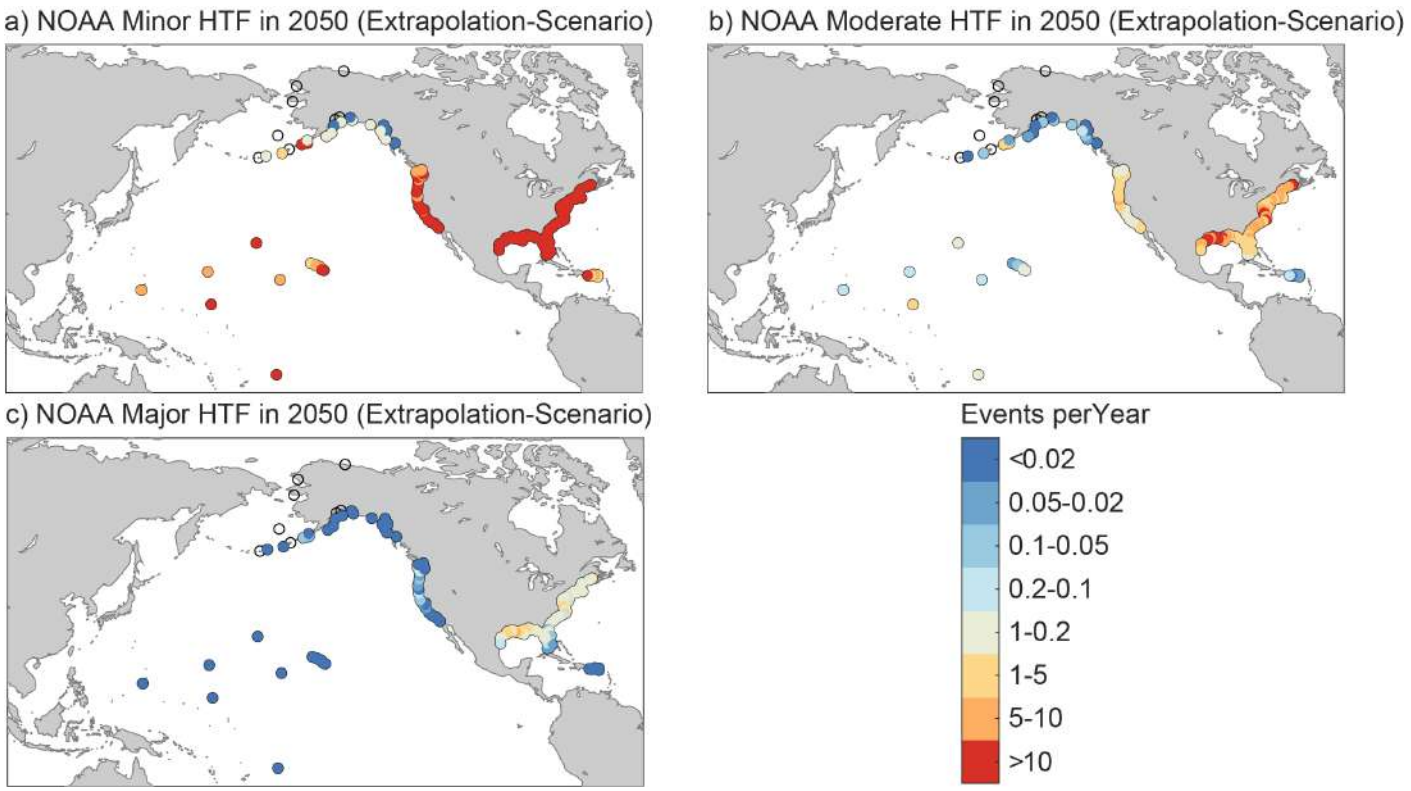

Figure 3.9: Coastal high tide flooding (HTF) frequencies projected at 2050 applying the sea level scenario that upper-bounds the regional observation-based extrapolations for NOAA a) minor, b) moderate, and c) major HTFs.

>10 events/year. Moderate HTF frequencies nationally experienced about a 50% increase (0.2 events/year growing to 0.3 events/year) from 1990 to 2020, which is slightly higher than the frequency increase in major HTF frequencies. By 2050, moderate HTF frequencies nationally are projected to increase by more than a factor of 10, with about a factor of 5 increase in major HTF frequencies. In short, assuming continuation of current trends and summarized at the national level, a flood regime shift is projected by 2050, with moderate HTF occurring a bit more frequently than minor HTF events occur today and major HTF events occurring about as frequently as moderate HTF frequencies occur today.

Table 3.2: Annual average event frequencies for NOAA-defined minor, moderate, and major HTF heights by region that were typical (median values) in 1990, under current (circa 2020) sea levels and projected to occur considering the upper-bounding scenario of the observations-based extrapolations in 2050 (see Table 2.2).

U.S. Region	1990			2020			2050		
	Minor Flood	Moderate Flood	Major Flood	Minor Flood	Moderate Flood	Major Flood	Minor Flood	Moderate Flood	Major Flood
National	1	0.2	0.03	3	0.3	0.04	>10	4	0.2
*Hawaii/Pac Is	0.06	<0.02	<0.02	0.2	<0.02	<0.02	9	0.1	<0.02
NE Atlantic	2	0.3	0.06	4	0.6	0.09	>10	6	0.4
SE Atlantic	0.9	0.1	0.03	2	0.2	0.04	>10	4	0.2
E Gulf	0.7	0.2	0.06	2	0.3	0.08	>10	3	0.3
W Gulf	1	0.3	0.1	4	0.7	0.2	>10	>10	1
SW Pacific	0.8	0.02	<0.02	1	0.04	<0.02	>10	0.7	<0.02
NW Pacific	3	0.3	<0.02	4	0.4	<0.02	>10	1	0.03
**Alaska	0.7	<0.02	<0.02	0.2	<0.02	<0.02	0.7	0.03	<0.02
US Carib	0.02	<0.02	<0.02	0.04	<0.02	<0.02	6	0.04	<0.02

*The Pacific Island locations use the same scenario assigned to the Hawaiian Islands (see Table 2.2); **Alaska locations, which as a whole could not be regionalized due to large differences in VLM, use the lower-bounding scenario per CONUS, which is the Intermediate-Low scenario (see Table 2.1). The lower-bounding scenario for Alaska is used to reflect the significant deviations below the Intermediate scenario (Figure A1.2b).

Box 3.1: Wave Contributions to Extreme Water Levels

Water level heights are a common proxy for coastal flooding (e.g., Sweet et al., 2018) and consist of a variety of components (see Figure 1.1). This report focuses primarily on projections of relative sea level (RSL) rise together with tides and storm surge contributions to extreme water levels (EWLs). However, along exposed coasts, wave-driven water levels can play a significant role in EWLs during storm events and during lesser storm conditions as exacerbated by sea level rise. Here we illustrate the relative influence of wave-driven water levels, broken down into the components of set-up and swash during extreme events across the United States, compared to tide and surge contributions.

Wave set-up is the quasi-static rise in water level at the shoreline due to breaking waves (Longuet-Higgins and Stewart, 1963). Swash is the time-varying elevation of the leading edge of wave uprush, which varies in frequency from seconds (due to incident waves) to minutes (e.g., surf beat; Guza and Thornton, 1982). Wave set-up and swash components, collectively known as wave run-up, are dependent on wave height, period, and beach slope (Stockdon et al., 2006) and are therefore controlled by local beach morphology and transient ocean conditions. To perform regional assessments of present-day or future wave-driven water level contributions, wave conditions are typically determined via global wave models forced by wind-reanalysis studies (e.g., Reguero et al., 2012) or historical/future wind fields produced by global climate models (e.g., Hemer et al., 2013).

Leveraging the global total water level assessment of Vitousek et al. (2017), which combines reanalysis models for waves, surge, and tides ("total water level" implying that all relevant components in Table 3.1 are included), we demonstrate the relative influence of waves on coastal water levels during extreme events (Figure Box 3.1). Even though the coarse resolution of this study (1° x 1° grid cells) cannot fully resolve tropical cyclones, which play a significant role in EWL events for the Southeast, Eastern and Western Gulf, Caribbean, and Hawaiian/Pacific Islands regions, this analysis demonstrates the relevance of waves in contributing to EWLs. Across the United States and its territories, using the 0.1 events/year EWL event as an example, this study estimates that wave set-up ranges from about 20–75 cm (Figure Box 3.1a) and swash from 35–125 cm (Figure Box 3.1b), together accounting for 25%–90% of EWLs (Figure Box 3.1c and based on Vistousek et al., 2017—not this study's RFA-based EWLs) for open-coast beaches (i.e., not for embayments protected from ocean waves). Wave-driven water levels (i.e., wave run-up) represent ~50% or more of the EWL contributions (again, not from this study) in areas with narrow continental shelves (reduces surge potential) and/or small tidal ranges, in particular the Hawaiian and Pacific Islands, the Caribbean, the Outer Banks (North Carolina), most of Florida, the entire U.S. West Coast, and portions of Louisiana, Texas, and Alaska. But swash oscillations only amplify coastal EWLs over short periods (i.e., seconds to minutes), whereas wave set-up represents a relatively sustained

contribution during storm events with about a 10% to 80% contribution to EWLs, with the highest values in the tropics (Figure Box 3.1d). As these examples indicate, when omitting wave-driven processes, coastal flood risk can be significantly underestimated for open-coast beaches, especially along U.S. island coastlines. Including wave-driven processes will be a focus of subsequent Task Force attention leading up to the Sixth National Climate Assessment (NCA6).

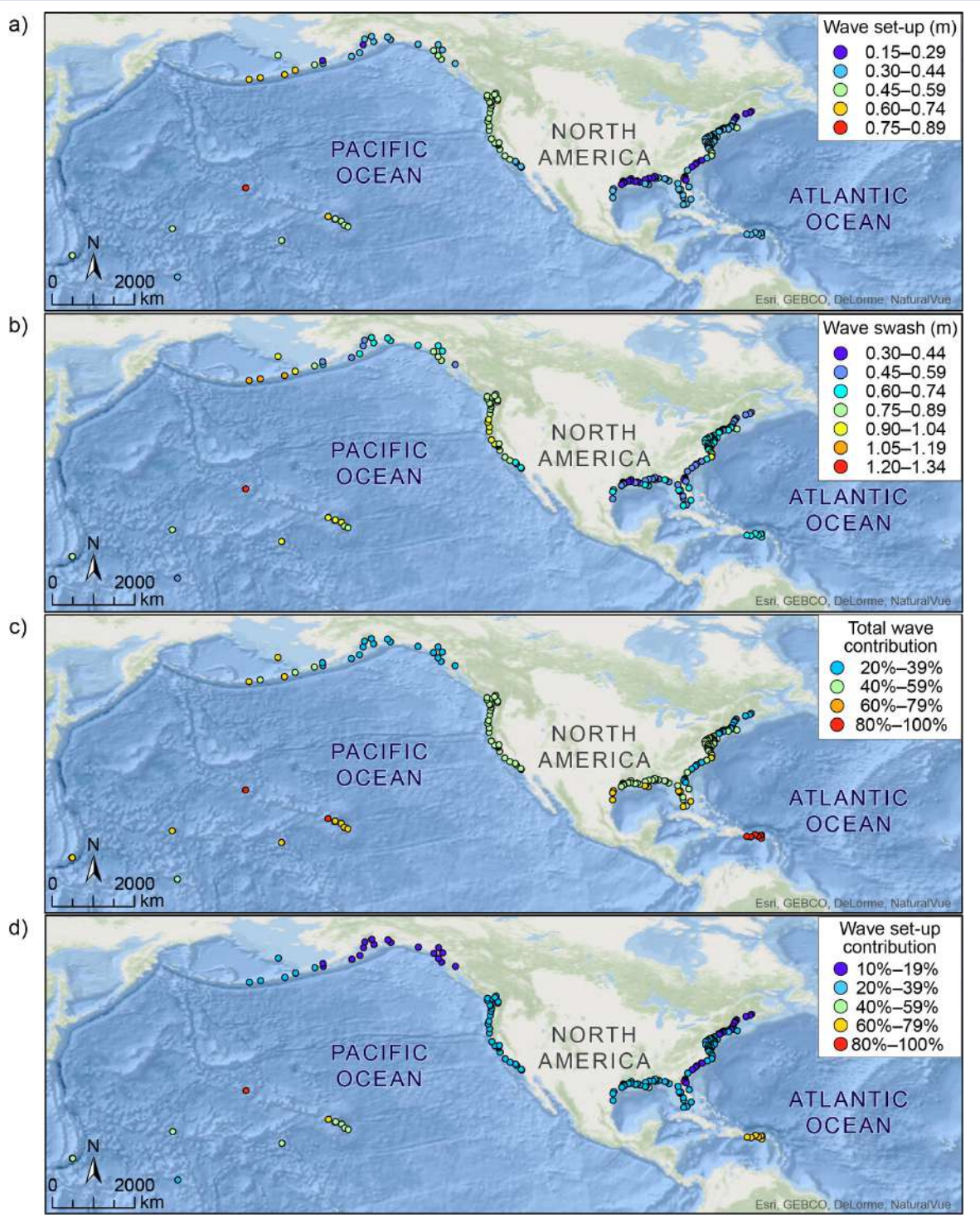

Figure Box 3.1. Water level contribution due to a) wave set-up and b) wave swash; c) percent contribution of wave-driven water levels (i.e., wave run up = wave set-up and swash) relative to all components: tide, storm surge, and waves; and d) percent contribution of wave set-up relative to the sum of tide, storm surge, and wave set-up based on model reanalysis of Vitousek et al. (2017).

Section 4: Use Cases

Below are four use cases, which use

- the (regional frequency analysis) RFA-based extreme water levels (EWLs) to map (at city scales) the annual probabilities/frequencies for the NOAA minor (disruptive), moderate (typically damaging), and major (often destructive) high tide flooding (HTF) layer classifications that are nationally calibrated to those used in weather-warning forecasting by NOAA;
- the relative sea level (RSL) projections and the RFA-based EWLs to incorporate trends (e.g., sea level rise projections) into design engineering criteria for risk management and adaptive planning;
- the RSL projections and RFA-based EWL probabilities with maps of NOAA minor, moderate, and major HTF layers to assess current and future vulnerabilities to combined storm and wastewater systems; and
- vertical land motion (VLM) rates inherent to the RSL projections are compared to rates from new satellite technologies at very high spatial resolution to showcase possibilities to monitor current rates from space and further localize the RSL projections.

The goal is to contextualize how the emerging science and this report's datasets can assist in developing products suitable for approaching (mapping, designing, or bounding) important problems in coastal risk assessment and management.

4.1. Mapping of NOAA High Tide Flood Thresholds and Flood Frequencies

High tide flooding[29] is increasingly common due to years of RSL rise. NOAA has been 1) documenting changes in minor HTF patterns since 2015, with about 100 NOAA tide gauges along the U.S. coastlines, and 2) providing a yearly coastal HTF outlook for these locations for the coming year,[30] as well as projections for the next several decades based on RSL projections from NCA4/Sweet et al., 2017. NOAA has also mapped the three HTF depth-severity (minor, moderate, and major) categories based on the relationship with tide range (Sweet et al., 2018) to show the spatial extent of associated impacts (see Figure 3.7). The minor HTF maps are provided in the NOAA SLR Viewer,[31] and all three map layers are accessible through NOAA map services.[32]

In an effort to provide better flood exposure information, NOAA is developing a product with input from partners (e.g., the Federal Emergency Management Agency [FEMA]) to assign exceedance probabilities using the RFA-based EWLs to the minor, moderate, and major HTF categories as shown for Charleston, South Carolina, and West Palm Beach, Florida (Figure 4.1). The annual event frequency shown for each NOAA HTF "zone" is assigned to the particular flood height. For example, the moderate HTF zone in Charleston is shown as the orange-brown layer in Figure 4.1a, which includes all land elevations between the minor HTF height threshold (0.570 m above mean higher high water [MHHW]; see Table A1.2) and the moderate HTF threshold (0.853 m above MHHW). This moderate HTF zone is expected to be completely (up to 0.853 m above MHHW) at risk of flooding, with an average event frequency between about 1 event/year and 0.2 events/year. A frequency range is provided to partially address the 95% confidence intervals in both the EWL statistics and the mapping data. In the case of local maps, like Charleston and West Palm Beach, the average event frequency for each NOAA HTF layer is a constant across the area shown.

These types of products can help inform the probability of higher-frequency, lower-impact events. As agencies (e.g., FEMA) start to develop products that provide more comprehensive hazard and risk information

[29] https://oceanservice.noaa.gov/facts/high-tide-flooding.html

[30] https://tidesandcurrents.noaa.gov/HighTideFlooding_AnnualOutlook.html

[31] https://coast.noaa.gov/slr/

[32] https://coast.noaa.gov/arcgis/rest/services/dc_slr/Flood_Frequency/MapServer

(e.g., graduated flood risk; see The Future of Flood Risk Data[33]), there is a need to better define and resolve the probabilities of these more frequent flood conditions. In addition, considering today's height-severity flood thresholds in the face of sea level rise (see Figure 1.3), understanding the event probabilities in this more frequent space is critical. Such information would help graduate the flood probabilities more comprehensively than FEMA's binary 1% annual chance floodplain definition and allow for a more comprehensive picture of structure-level risk.

How Can This Be Done?

The process to spatially assign probabilities again relies on a relationship to tide range (see Figure A2.5), with tide range values obtained by subtracting VDatum's MHHW and mean lower low water [MLLW] modeled tidal surfaces.[34] Using VDatum's tide range and the regional regression equations (Figure A2.5) to obtain a local index (u), the EWL return level (or rather, average event frequency) curves for the associated grid are downscaled to individual VDatum grid cells (~100 m) using Equation 1 in Section 3.2. With these downscaled curves, the HTF levels at each VDatum cell—also based on VDatum's tide range (i.e., great diurnal tide range [GT] tide datum) relationships (Sweet et al., 2018)—are intersected with the localized frequency curve (expected values) for the cell in order to determine event frequencies on a cell-by-cell basis. The average event frequencies are then associated with their respective mapped inundation footprints (3–5 m horizontal resolution). To refine the data, they were clipped to the coastal HUC (hydrologic unit code) 12 watersheds[35] that overlapped VDatum model data. This was done in order to provide a probability in watersheds that contained source VDatum data only.

The value of these data is that we can now provide not only the mapped inundation extent of each of the three HTF levels (see Figure 3.7) but also the probability, or event frequencies, for each level on high-resolution inundation data (Figure 4.1). By leveraging the relationship between the local indices (u) to GT on a regional basis, the EWL statistics can provide event frequencies for 1) most water levels or flood heights of interest and 2) most locations, even if there is not a local tide gauge nearby to assist coastal managers when planning for potential impacts to their communities. In terms of the mapped product and inherent uncertainties, it should be recognized that the VDatum model's standard error is on the order of 15 cm,[36] which is similar to that of the LIDAR elevation data.[37] The associated 95% confidence intervals from both VDatum and the LIDAR used in the mapping is then (standard error x 1.96) about 30 cm and similar to that of the EWL at the 1 event/year frequency (0.3 m median) using tide range to spatially derive EWL_{local} (Figure A2.5), although it increases to about 0.9 m at the 0.01 events/year frequency. Thus, it is recommended that these maps be used cautiously in any type of application.

Both NOAA and FEMA are currently exploring methods to further localize the $EWL_{gridded}$ probabilities, such as using NOAA short-term gauges (e.g., Section 3.4) and multidecadal hindcast modeling to develop a higher resolution set of local indices (u). FEMA is working to merge the higher-frequency portion of the EWL distributions (e.g., > 0.05 events/year) with the FEMA EWL stillwater datasets (some of which are shown in Figure 3.5). These efforts will serve, in general, to refine coastal exposure by today's standards and, specifically, minor to major HTF probabilities to better understand and communicate the Nation's coastal flood risk through products such as FEMA's National Risk Index.[38]

[33] https://www.fema.gov/fact-sheet/future-flood-risk-data-ffrd

[34] https://vdatum.noaa.gov/

[35] https://www.usgs.gov/core-science-systems/ngp/national-hydrography/watershed-boundary-dataset?qt-science_support_page_related_con=4 - qt-science_support_page_related_con

[36] https://vdatum.noaa.gov/docs/est_uncertainties.html

[37] https://www.usgs.gov/ngp-standards-and-specifications/lidar-base-specification-online

[38] https://hazards.fema.gov/nri/

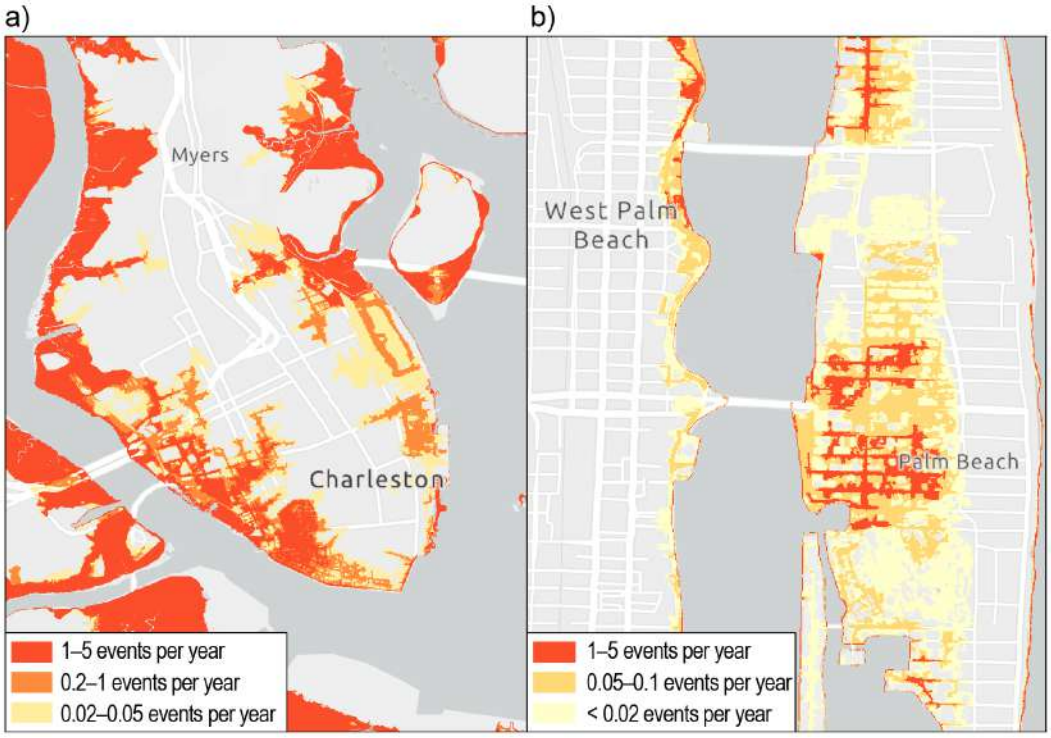

Figure 4.1: Maps of the NOAA minor, moderate, and major high tide flooding layers for a) Charleston, South Carolina, and b) West Palm Beach, Florida (as in Figure 3.7 but providing average event frequencies for each layer). Note: the shoreline on these maps is mean higher high water, but to be useful for decision-making, a conversion to land-based heights (e.g., NAVD88) should be made.

4.2. Application of Scenarios, Observation-Based Extrapolations, and Extreme Water Levels

Because future sea level rise amounts are inherently uncertain, planners and engineers who engage in addressing adaptation to future sea level rise in coastal communities often adopt a scenario approach. Based on several national and regional sea level projections (Hall et al., 2019; Parris et al., 2012; USACE, 2014; Hall et al., 2016; Sweet et al., 2017), many communities have developed their own specific scenario sets and guidelines for how to use them. In this section, the application of the regional sea level scenarios (see Section 2) that leverage the newly developed observation-based extrapolations (see Section 2.3) and the EWL probabilities produced using the RFA (see Section 3) are illustrated for representative locations around the United States.

This use case is not meant to provide standardized planning guidance for using information on sea level rise projections; rather, it is provided as an example of applying concepts of time-varying extreme value probabilities due to sea level rise, risk reduction, and adaptive planning that may be used in practice (Salas and Obeysekera, 2014; Salas et al., 2018). One of the primary tasks in coastal infrastructure projects is to determine the design elevation (also known as the return level) of a particular structure (e.g., seawall or building) for a desired level of risk or probability. Such design problems typically require the knowledge of advanced statistical methods associated with extreme values such as those illustrated in the commonly referenced textbook by Coles (2001).

The use case is illustrated for 10 tide gauges around the United States (Figure 4.2). For reference, the upper-bounding scenarios of the observation-based extrapolations for 2050 (see Table 2.2) and the RFA-based EWL distribution parameters (Section 3) are provided in Table 4.1. The EWL probability parameters are necessary to replicate this use case, and they are specifically from a Generalized Pareto Distribution (GPD) peaks-

over-threshold approach (Coles 2001): a) the local Index, u; b) rate of exceedances above the local index, λ; c) scale, σ_{RFA}; and d) shape, ξ (see Section A2 for more details). In the examples below, the upper-bounding scenario is used (Figure 4.3a) with the corresponding return level curves for the selected tide-gauge locations (Figure 4.3b).

Figure 4.2: Tide gauges selected for the application of sea level scenarios and extreme water level methods.

Table 4.1: Tide-gauge locations, scenarios bounding the observation-based extrapolations, and the extreme value distribution Generalized Pareto Distribution (GPD) model parameters estimated using the regional frequency analysis (RFA).

Tide-gauge location details			Upper-bounding scenarios circa 2050 of the observation-based extrapolations	RFA-based GPD parameters			
NOAA ID	Location	Region	Upper Bound	Local Index u	λ	σ_{RFA}	ξ
1612340	Honolulu, HI	Haw.	Int	0.248	3.19	0.218	0.066
8518750	The Battery, NY	NE	Int	0.546	2.98	0.261	0.179
8638610	Sewells Point, VA	NE	Int	0.502	2.95	0.332	0.067
8723214	Virginia Key, FL	SE	Int-High	0.284	3.00	0.152	0.251
8726520	St. Petersburg, FL	E. Gulf	High	0.337	2.99	0.266	0.354
8729840	Pensacola, FL	E. Gulf	High	0.345	2.85	0.212	0.456
8771450	Galveston Pier 21, TX	W. Gulf	Int-High	0.366	2.75	0.289	0.340
9410660	Los Angeles, CA	SW	Int-High	0.472	3.21	0.150	−0.063
9414290	San Francisco, CA	SW	Int-High	0.375	3.15	0.211	0.038
9447130	Seattle, WA	NW	Int	0.541	3.07	0.233	−0.110

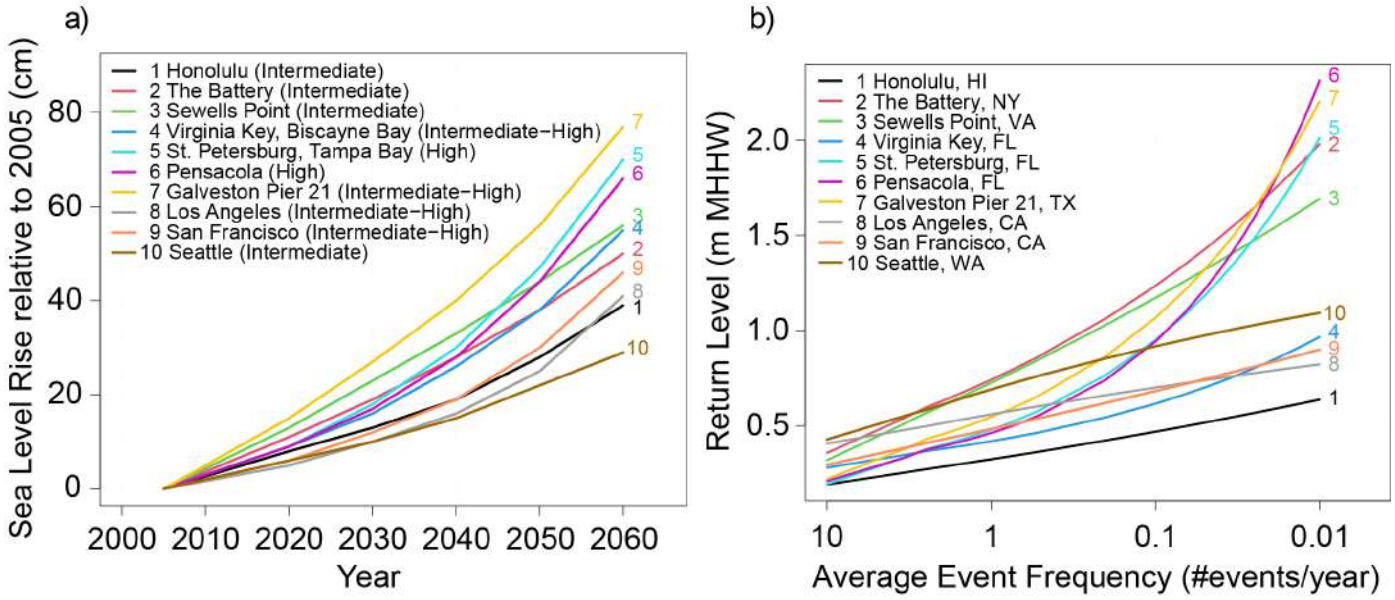

Figure 4.3: a) RSL projections for the scenarios providing the upper bound to observation-based extrapolations to 2060 for the selected tide gauges. The corresponding scenario for each tide gauge is shown in parentheses in the legend. b) RFA-based EWL (see Section 3) return level curves relative to the 1983–2001 MHHW tidal datum. Notes: (1) to be useful for decision-making, a conversion to land-based heights (e.g., geodetic datum such as NAVD88) should be made. (2) Average event frequency (x-axis label) is the reciprocal of average recurrence interval, which is also known as return period.

As shown in Figure 4.3a, 2005 is the reference year for the projection scenarios. However, the return level curves shown in Figure 4.3b are referenced to the year 2000. The return level curves are first adjusted to the year 2005 by raising the curves by an amount equivalent to the local trend in the flood index (u) from 2000 to 2005 (see Table A1.3). Alternatively, the RSL offsets (see Table A1.2) could be applied, with differences between the two insignificant to the results here.

Accounting for Time-Varying Relative Sea Level Rise

A particular scenario depicts the changes in RSL at a selected location. A common assumption is that as RSL rises, the EWLs also increase, and that must be accounted for in the changing behavior of the probability distribution of the EWLs. One approach for developing a time-varying extreme value distribution is to assume that one or more parameters (location, scale, and shape) are functions of time or some other covariate (e.g., El Niño–Southern Oscillation index; Coles, 2001; Menendez and Woodworth, 2010). When two or more parameters evolve with time (i.e., strong nonstationarity), the paradigm shifts from a "stationary" approach, typically used for planning infrastructure until recently, to one reflecting significant temporal change in the probability distribution. A common practice is to remove the trend in the extreme dataset and then to assume the distribution of the detrended extremes to be stationary. This approach is similar to the case when only the location parameter is varying with time and the other parameters are constant.

In the ensuing sections, it is assumed that only the location parameter (i.e., local index, u, in GPD) changes as a function of RSL (i.e., per the specified sea level scenario). This may be expressed as

$$F(z) = GPD(\mathrm{u}(RSL), \tilde{\sigma}, \xi)$$

where u is the RFA/GPD local index that is a function of RSL, and $\tilde{\sigma}$ and ξ are scale and shape parameters, respectively, which are assumed to be constant over time. However, this assumption does not preclude the analysis of using a higher degree of temporal variability (e.g., both u and $\tilde{\sigma}$ are functions of RSL or some other covariate). As a consequence of the above assumption, the local index u is adjusted by a magnitude δ (i.e., the regional mean sea level change from the reference year) obtained from a selected scenario.

For planning infrastructure using the scenario's RSL projections and the EWL probabilities, two approaches are illustrated: 1) recurrent flood frequency and 2) time-varying average recurrence interval (ARI; which is the reciprocal of average event frequency [AEF]) and risk.[39] While the infrastructure designs are based on a variety of factors, one or both of these approaches may be used to support that process (e.g., height of a seawall or base-flood elevation). In this use case, the term "flood" could pertain to a particular NOAA HTF level or an arbitrary probabilistic EWL level, although not necessarily to imply a meteorological (e.g., storm) event.

Designs Based on Recurrent Flood Frequency

In many U.S. coastal locations, the frequency of flooding is increasing, mostly due to rising sea levels (Sweet et al., 2021). A community may tolerate infrequent flooding initially, but at some point, when the sea level rise is significant, the flooding frequency will increase, which in turn may exceed that community's risk tolerance for flooding. Using the extreme value distributions and the sea level scenarios, it is possible to predict the time-varying change in frequency (e.g., as in Figure 3.9). In case of the GPD, the recurrent flood frequency (number of exceedances above a return level [z]) may be computed as (Buchanan et al., 2017)

$$N(z,\delta) = \lambda\left(1 + \frac{\xi(z-[u+\delta])}{\tilde{\sigma}}\right)^{\frac{-1}{\xi}} \text{ for } \xi \neq 0$$

where δ is the change in RSL (relative to the project construction year) obtained from Figure 4.3a.

In the example used here, the planning problem may be stated as follows: What should the initial return level (used for the design) be to ensure that the recurrent flood frequency is limited to a specified number of events at the end of the design life? It is now possible to lay this out graphically, as shown in Figure 4.4 for two tide gauges (Sewells Points, Virginia, and Galveston Pier 21, Texas).

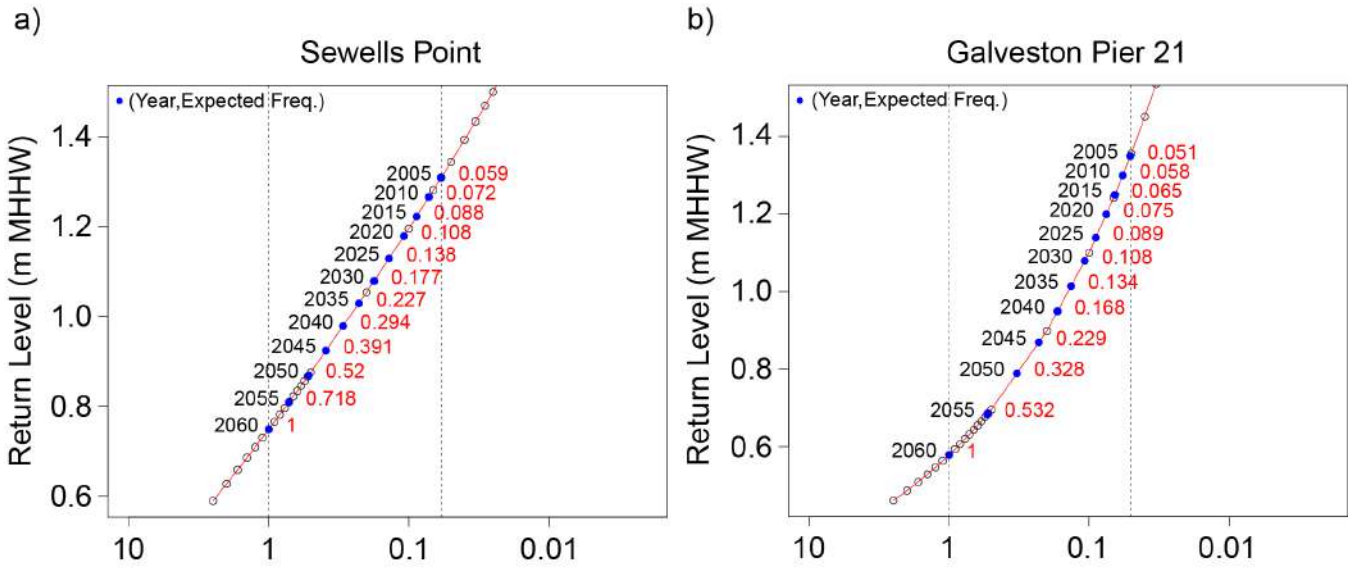

Figure 4.4: Recurrent flood frequency estimates for a) Sewells Point (Norfolk), Virginia, and b) Galveston Pier 21, Texas. For both, the relative sea level projection for the scenarios and the return level are the same as in Table 4.1. Note: to be useful for decision-making, a conversion of the return level to land-based heights (e.g., geodetic datum such as NAVD88) should be made.

In Figure 4.4, the number to the right of each point along the curve shows the recurrent flood frequency, N, corresponding to the year indicated on the left. For this example, it was assumed that by 2060, the desired value of N = 1, and the design AEF necessary for this criterion, is indicated in Figure 4.4 (AEF = 0.06 events/year for Sewells Point and AEF = 0.05 events/year for Galveston Pier 21). The corresponding design return levels are 1.31 m and 1.35 m, respectively, relative to MHHW datum. A summary of results for all 10 tide

[39] In the context of Section 4.2, risk is defined as the probability of one or more events exceeding a given height threshold over the life of a project.

gauges is shown in Table 4.2. The design average event frequency required in 2005 to meet the flood frequency criteria shows significant variability across the sites. The design return level depends on two factors: 1) the magnitude of the sea level rise from 2005 to 2060 (end of the design life); and 2) the slope (a function of the scale and shape parameters) of the return level curve (Figure 4.3b).

Table 4.2: Summary of design parameters to constrain the average event frequency, N, to 1 per year by 2060 (end-year of the design life). The 2005–2060 RSL projections are the local values associated with the scenarios providing the upper bound to the regional observation-based extrapolations shown in Table 2.2. Note: to be useful for decision-making, a conversion of the return level to land-based heights (e.g., geodetic datum such as NAVD88) should be made.

NOAA ID	Location	Relative Sea level rise (in meters from 2005 to 2060)	Return level (m above 1983–2001 MHHW) corresponding to AEF = 1 year	Return level (m above 1983–2001 MHHW) required in 2005 to ensure N = 1 by 2060	Design average event frequency (events/year) required in 2005 to achieve N = 1 by 2060
1612340	Honolulu, HI	0.39	0.33	0.72	<0.01
8518750	The Battery, NY	0.50	0.76	1.26	0.10
8638610	Sewells Point, VA	0.56	0.75	1.31	0.06
8723214	Virginia Key, FL	0.55	0.44	0.99	0.01
8726520	St. Petersburg, FL	0.70	0.49	1.19	0.05
8729840	Pensacola, FL	0.66	0.47	1.13	0.06
8771450	Galveston Pier 21, TX	0.77	0.58	1.35	0.05
9410660	Los Angeles, CA	0.41	0.57	0.98	<0.01
9414290	San Francisco, CA	0.46	0.49	0.95	<0.01
9447130	Seattle, WA	0.29	0.70	0.99	0.05

Design Based on Time-Varying Exceedance Probabilities

Average recurrence interval is used to describe EWL probabilities in the following examples to directly relate to and build off of a couple of recent, relevant focused studies on the topic. Interpretation of the results should follow guidelines of the U.S Army Corps of Engineers (USACE, 1994).

In current practice, the projects with a longer design life (> 25 years) typically use a low average event frequency (<0.1 events/year) or, equivalently, a high/long ARI (> 10 years or more). At high recurrence intervals, the peaks-over-threshold and the annual maxima recurrence intervals converge (Langbein, 1949), although not necessarily where tropical storm surges are present (Wahl et al., 2017). Revisiting the concepts of traditional ARI and risk concepts for annual maxima in time-varying frameworks has been addressed recently (e.g., Salas and Obeysekera, 2014). The application of time-varying ARI and risk concepts is illustrated by converting the GPD model to an equivalent annual maxima model, which in this case is the GEV distribution. The equivalent annual-maxima modeling approach, as used here, will also facilitate the direct application of emerging risk and recurrent interval concepts already developed for situations of time-varying extreme probabilities (Salas and Obeysekera, 2014; Salas et al., 2018; Obeysekera and Salas, 2020).

The cumulative distribution function (CDF) of the GEV model of annual maxima is expressed as

$$F(z) = exp\left\{-\left[1+\xi\left(\frac{z-\mu}{\sigma}\right)\right]^{-\frac{1}{\xi}}\right\}$$

where μ, σ, ξ are the location, scale, and shape parameters of the GEV (Coles 2001).

For computing u, the local index is further adjusted to reflect the translation of the return level curve from 2000 to the reference year (i.e., 2005). The GEV scale parameter, $\sigma = \tilde{\sigma}\lambda^{\xi}$, where the at-site scale parameter $\tilde{\sigma}$, is computed as $\tilde{\sigma} = \sigma_{RFA} * u$. For this use case, the adjusted local index is computed as $u_{adj} = u * s\,(2005–2000)$, where s is the trend of the local index u at the site (see Table A1.3). If desirable, other adjustment procedures may be used. Finally, the time-varying GEV model assumes that only the location parameter, μ, changes with sea level change, δ and the time varying annual extreme value distribution is given by

$$F^t(z,\delta) = exp\left\{-\left[1+\xi\left(\frac{z-(\mu+\delta)}{\sigma}\right)\right]^{-\frac{1}{\xi}}\right\}$$

The exceedance probability, p_t, which corresponds to an initial return level (z_{q0}, initial design), changes with time because of the rising RSL, δ (Figure 4.5). Consequently, the ARI is not a fixed measure but decreases with increasing sea level.

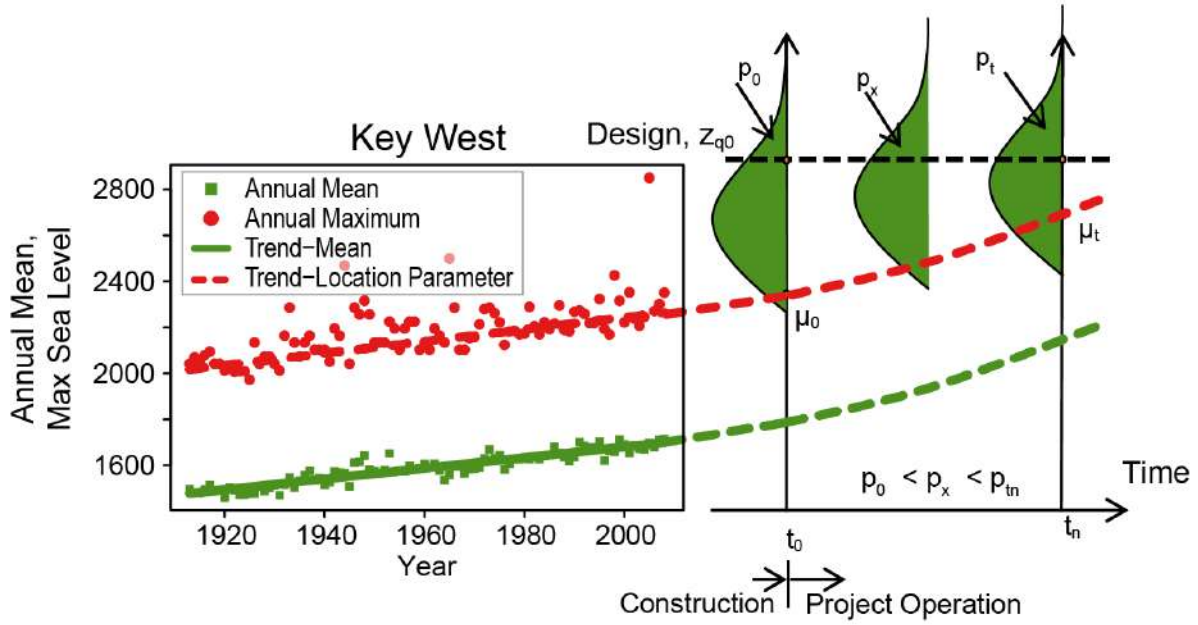

Figure 4.5: Conceptual illustration of increasing exceedance probability (hence decreasing average recurrence interval) that assumes that the location parameter is a function of the magnitude of the relative sea level rise.

The traditional concept of the ARI is the average waiting time for between two successive exceedances of the return level. Using the same definition but in a time-varying exceedance probability framework (Figure 4.5), an equivalent measure of ARI (T) may be derived as (Cooley, 2013; Salas and Obeysekera, 2014)

$$T = 1 + \sum_{x=1}^{\infty}\prod_{t=1}^{x}(1-p_t)$$

where $p_t = 1 - F^t(z, \delta)$ i is the time-varying exceedance probability. If a project is designed for a return period, $T_0[t = t_0]$, then $T < T_0$ implies that the actual recurrence interval due to rising RSL will be less.

The methods described in the preceding paragraphs are applied to the 10 tide-gauge locations shown in Figure 4.2. For illustration, it was assumed that the projection scenario for each tide gauge would continue beyond 2060. However, the methodology described above can be used with any other scenario. The derived GEV parameters for each gauge are shown in Table 4.3.

Table 4.3: The parameters of generalized extreme value computed using the peaks-over-threshold Generalized Pareto Distribution model (Coles 2001).

NOAA ID	Location	At-site scale parameter	Local index adjustment from 2000–2005 (m)	GEV location parameter	GEV scale parameter	GEV shape parameter
1612340	Honolulu, HI	0.054	0.007	0.330	0.058	0.066
8518750	The Battery, NY	0.142	0.016	0.757	0.173	0.179
8638610	Sewells Point, VA	0.167	0.023	0.748	0.179	0.067
8723214	Virginia Key, FL	0.048	0.026	0.444	0.063	0.251
8726520	St. Petersburg, FL	0.090	0.014	0.494	0.132	0.354
8729840	Pensacola, FL	0.073	0.012	0.474	0.118	0.456
8771450	Galveston Pier 21, TX	0.106	0.033	0.579	0.149	0.340
9410660	Los Angeles, CA	0.071	0.005	0.565	0.066	−0.063
9414290	San Francisco, CA	0.079	0.010	0.492	0.083	0.038
9447130	Seattle, WA	0.126	0.010	0.701	0.111	−0.110

The ARI curves, T, as a function of T_0, for all 10 tide gauge locations are shown in Figure 4.6a. This figure demonstrates that, in all cases, the actual ARI is less than the design recurrence interval. For instance, for a location near Pensacola, Florida, if a project is designed for T_0 = 100 years, the actual ARI, due to future RSL rise (Table 4.1, "Upper Bound" column), is only about 50 years. As another example, for a location near The Battery, New York City, a project may need to be designed for T_0 = 90 years if the desired ARI under its associated (Table 4.1, "Upper Bound" column) RSL rise scenario is 40 years.

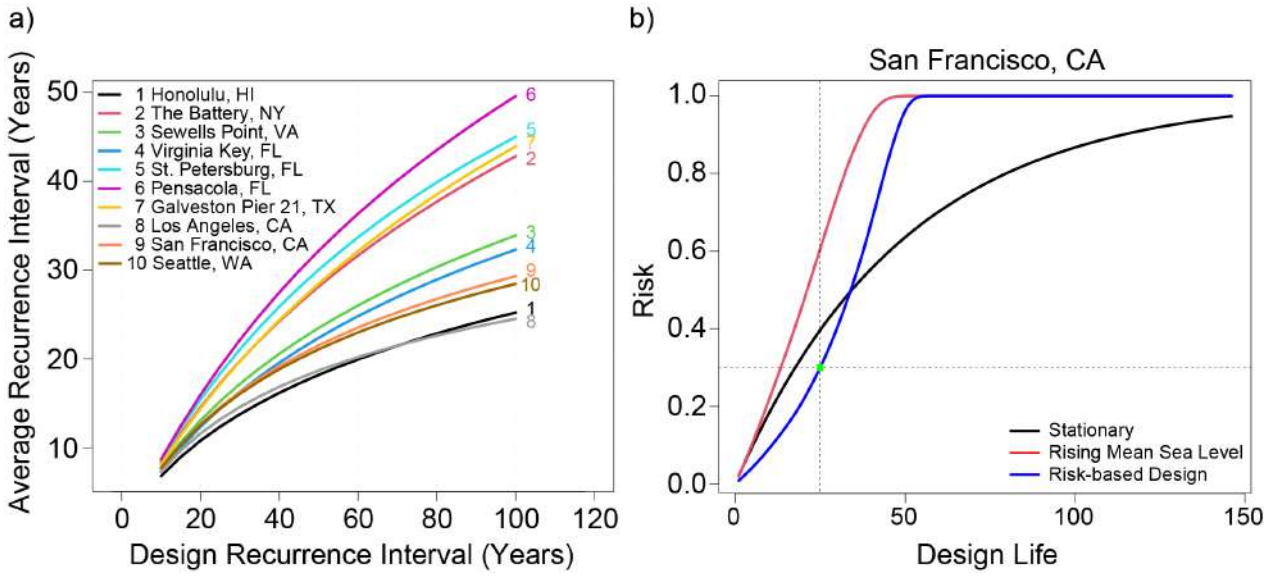

Figure 4.6: a) Average recurrence interval (due to rising RSL) curves (T versus T_0) at each tide gauge using the selected scenario's RSL projection (see Table 4.1). b) Risk curves as a function of design life: stationary (black curve), actual risk resulting from incorporating the site's RSL scenario projection (red curve), and risk curve for a specific risk (blue curve).

Risk-Based Design

Under stationary conditions, the risk (defined as the probability of one or more exceedances above the design elevation) is a function of the life of the project, n. The risk formula under stationarity is given by $R = 1 - (1 - 1/T_0)^n$. For example, there is about a (R = 0.26) 26% chance of experiencing an event with an ARI of (T_0) 100 years over the course of (n) 30 years under a non-changing (stationary statistical) environment. As the length of the design life increases, risk also increases. Under conditions of time-varying exceedance probability, p_t, the risk (R) formula is (Salas and Obeysekera, 2014)

$$R = 1 - \prod_{t=1}^{n}(1 - p_t)$$

With rising relative sea levels, p_t increases, and the risk is higher than that under stationarity. This increase in risk is illustrated for the San Francisco, California, tide gauge in Figure 4.6b when the initial design, T_0 = 50 years (the event level with a 50-year ARI). The black curve in Figure 4.6b shows the increasing risk as the design life becomes longer even under stationarity. For instance, if the design life, equals 25 years, this risk is about 0.4 (40%). However, when the local sea level rise scenario is incorporated, the risk over a given life of the project increases more rapidly, exceeding the corresponding risk under stationarity (see red curve in Figure 4.6b). In the above example, when n = 25 years, the risk will increase to about 60% due to the RSL scenario projection. Moreover, the RSL rise causes the risk to approach 100% (R = 1) when the design life is about 50 years or more. In the risk-based design approach, one can specify the tolerable risk and determine the initial design period (or return level).

One option is to design a project in such a way that the resulting increasing risk profile due to application of the scenario's RSL projection is at or below that under stationarity. While the risk-reduction approach described below is illustrated for a selected RSL scenario for the future, it can be implemented for multiple scenarios, leading to a variety of risk-reduction options depending on the future RSL scenarios. In such a broader application, a risk-based framing founded on risk tolerance may be adopted.

Considering uncertainty in the sea level rise projections, one may wish to approach the problem using concepts of dynamically adaptive planning. In the example shown in Figure 4.6b (blue curve), two parameters are specified to illustrate this concept. First, it is assumed that the project will be constructed in, for example, two or more phases. Considering such a planning assumption, phase I is 25 years long (i.e., n = 25 years), and the maximum tolerable risk during this phase is 0.3 (30%), as opposed to the 60% risk mentioned above. The blue curve shows the risk profile for such a design. This curve was computed by constraining R = 0.3 when n = 25, as shown by the green dot in Figure 4.6b. The implication of this adaptive approach is that the initial return level will need to increase from 0.84 m MHHW to 0.93 m MHHW (Table 4.4), and the corresponding initial ARI has to increase from 50 years to 125 years. In this approach, one must also assume that the project will be expanded after that initial period, and measures must be adopted to prevent locking in the design and preempting the planners from expanding it into a bigger project after the initial 25-year period. For example, the foundation design of the project may need to assume the eventual capacity expansion and allow for it in the initial design. This approach of dynamically adaptive planning is becoming increasingly popular as a way to deal with deep uncertainties associated with sea level rise.

Table 4.4 shows that with a relatively small increase in initial design elevation, the risk can be managed to a desirable level. In this example, however, the ultimate design (at the end of the full design life; e.g., 50 or 100 years) needs to be assessed to ensure that resources (e.g., land) that may be needed for the build-out are considered.

Table 4.4: Results of the risk-based design for all tide gauges shown in Figure 4.2. Average recurrence interval (ARI) is listed and is the reciprocal of average event frequency. Values in the last column have been rounded to the closest 5-year interval. Note: to be useful for decision-making, a conversion of the return level to land-based heights (e.g., geodetic datum such as NAVD88) should be made.

NOAA ID	Location	Design return level for T_0 = 50 years (m above MHHW)	Design return level to constrain risk to 30% over a 25-year period (m MHHW)	Average recurrence interval (ARI) of the design to constrain probability (risk) to 30% over a 25-year period
1612340	Honolulu, HI	0.59	0.69	>100
8518750	The Battery, NY	1.74	1.95	90
8638610	Sewells Point, VA	1.55	1.75	>100
8723214	Virginia Key, FL	0.78	1.00	>100
8726520	St. Petersburg, FL	1.61	1.88	80
8729840	Pensacola, FL	1.75	2.09	75
8771450	Galveston Pier 21, TX	1.79	2.13	85
9410660	Los Angeles, CA	0.79	0.86	>100
9414290	San Francisco, CA	0.84	0.93	>100
9447130	Seattle, WA	1.05	1.13	>100

4.3. Growing Risk to Combined Storm and Wastewater Systems from Sea Level Rise

Sea level rise is causing HTF to become more severe—more frequent, deeper, and more widespread—in terms of its impacts (Sweet et al., 2021). Coastal areas that are not exposed to HTF now may become so in the coming decades. As the footprint of flooding expands, water from adjacent estuaries and bays will flood into communities and encounter previously unaffected urban infrastructure.

Many places already see backflow from tidal waters through stormwater pipes that spill out of catch basins into neighborhood streets. Cities with combined sewer systems often have backflow preventers on their vulnerable outfall pipes (EPA, 1995a, 1995b). However, combined sewers will be open to inflow from surface flooding. If floodwater in the streets encounters a catch basin that connects to a combined sewer system, then high tide waters will enter the sewer. At best, the tide waters will be on their way to the sewage treatment plant; at worst, a combined sewer outflow would be triggered if the sewer pipes cannot handle the volume of water.

While Camden, New Jersey, has taken action to prevent runoff from entering its system,[40] tidal inflow is a novel problem. Identification of risks like this can provide lead time to take adaptation actions. Still, in some combined sewer communities, such as Camden, the onset of risk can arrive well before midcentury. Mapping shows that minor HTF at a height of 0.58 m above current MHHW tidal datum (Table A1.3) begins to have a footprint in Camden neighborhoods served by combined sewers (red shade in Figure 4.7, spanning from MHHW to 0.58 m [1.9 feet] above MHHW; locations are provided by the New Jersey Department of Environmental Protection[41]). By the time the tide reaches the moderate (0.86 m above MHHW) and major

[40] https://www.epa.gov/arc-x/camden-new-jersey-uses-green-infrastructure-manage-stormwater

[41] https://njdep.maps.arcgis.com/apps/Viewer/index.html?appid=70dd49de342949ca933e840d0c530fc7

(1.25 m above MHHW) HTF levels, the extent of flooding increases dramatically, and many intersections will be flooded.

The Camden region currently (circa 2020) experiences

- about 2 events/year (or about 4 days/year per Figure 3.8b) of minor HTF;
- 0.2 events/year of moderate HTF; and
- 0.03 events/year of major HTF,

based on the EWL_{local} directly across the Delaware River at the NOAA tide gauge in Philadelphia. The EWL-based probabilities support actual observations in 2020, when the Camden/Philadelphia region experienced 4 days of minor HTF, with 4–8 days projected to occur in 2021 (Sweet et al., 2021).

Considering the Intermediate scenario, which is the upper-bounding scenario for this region's RSL observation-based extrapolations (see Table 2.2), a rise of 0.19 m by 2030 (measured since 2005) is projected to result in

- 5–10 events/year (on the order of 10–20 days/year) of minor HTF,
- 0.6 events/year of moderate HTF, and
- 0.07 events/year of major HTF.

By 2050, a 0.38 m RSL rise is projected (above 2005 levels) for this area, resulting in

- >10 events/year (perhaps >20 days/year) of minor HTF,
- about 3 events/year (6 days/year) of moderate HTF, and
- 0.3 events/year of major HTF.

So, within about the next 30 years (by 2050), a surface flood regime shift with subsurface impacts is projected to occur in Camden, considering current RSL rise trajectories. By then, moderate and major HTF (flooding upwards of 0.9 m and 1.2 m above MHHW, respectively) is projected to occur with similar frequencies/probabilities as minor (about 0.6 m above MHHW) and moderate HTF occur today. With nearly 4 high tides per event (1 event lasts about 2 days; 2 high tides occur almost every day), this implies that by 2050, upwards of 80 tides per year or more at the minor HTF level are projected, with about 12 of those tides per year exceeding the moderate HTF level and a 0.3 events/year frequency of major HTF flooding. Any time street intersections are underwater, tidal waters could flow down catch basins into the combined system (Figure 4.7). Beyond 2050, HTF frequency, depth, and extent will continue to grow. It is unclear how this increased flood frequency will affect the combined sewer system's functionality and surrounding water quality.

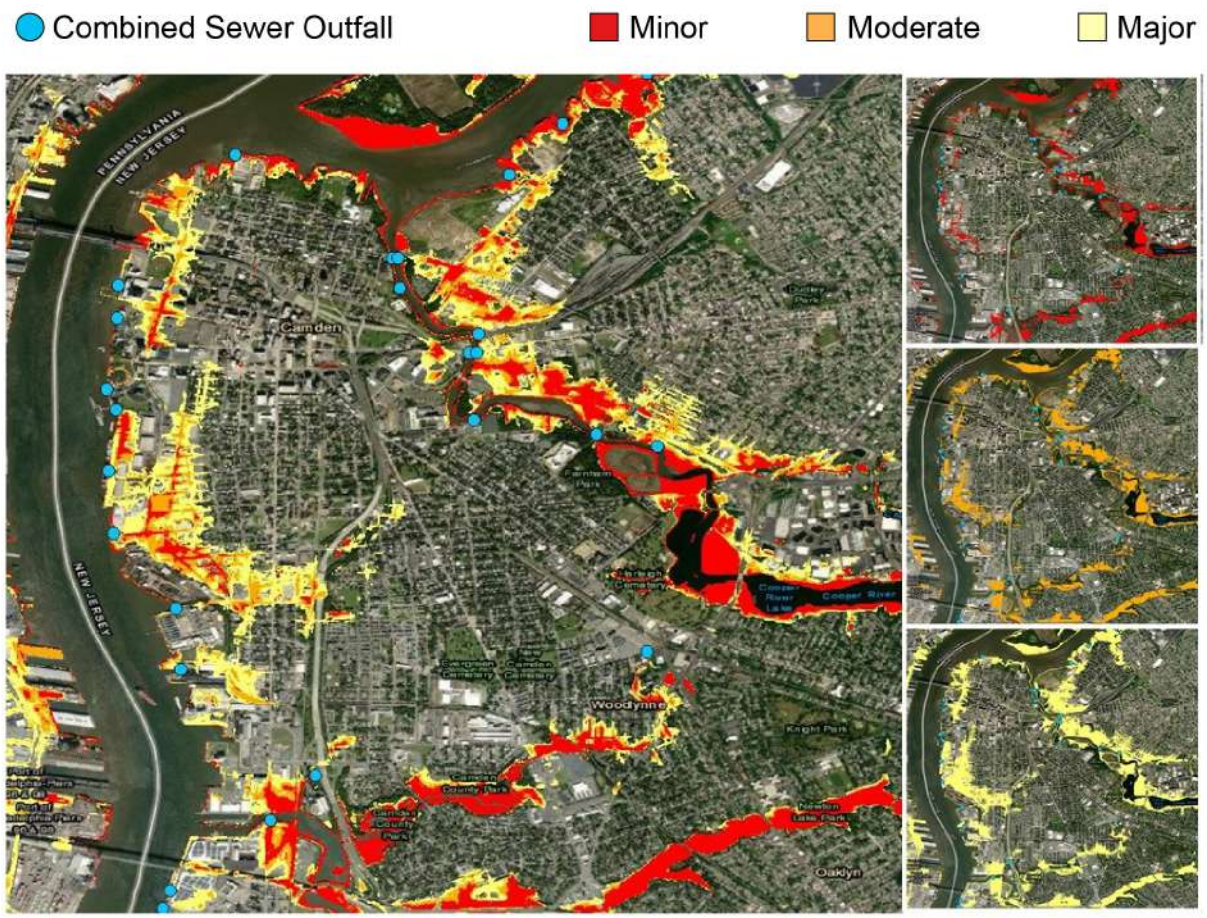

Figure 4.7: Location of combined stormwater and sewer system outfalls that are likely draining regions exposed to HTF within the Camden, New Jersey, region, with the minor (red: MHHW to 0.58 m [1.9 feet] above MHHW), moderate (orange: MHHW to 0.86 m [2.8 feet] above MHHW), and major (yellow: MHHW to 1.25 m [4.1 feet] above MHHW) HTF layers stacked in the enlarged map and individual layers mapped to the right. Note: heights are relative to the 1983–2001 tidal epoch, and to be useful for decision-making, a conversion to land-based heights (e.g., NAVD88) should be made.

4.4: Use of InSAR Technology for Determining Regional Vertical Land Motion and Its Suitability for Computing Long-Term Sea Level Rise Projections

Vertical land motion is an important component of RSL rise, leading to changes in the height of the ocean relative to land. Vertical land motion is not a singular phenomenon but instead results from various processes that display different patterns in space and time. These patterns have different impacts from place to place, especially in coastal settings where many of them operate at the same time and can serve to either increase RSL (subsidence) or decrease RSL (uplift). For much of the coastal United States, subsidence is driven on local scales by both natural processes, such as compaction of river sediments, and unnatural, human-caused reasons, such as groundwater and fossil fuel withdrawal; on larger scales, subsidence is driven by glacial isostatic adjustment (GIA). On the other hand, in some regions, such as southern Alaska, GIA leads to high rates of uplift in coastal regions. For example, Grand Isle, Louisiana, has experienced more than 0.9 m (3 feet) of RSL rise, whereas Juneau, Alaska, has experienced more than 1.2 m (4 feet) of RSL fall based on a 100-year historical linear rate value,[42] in large part due to VLM. For perspective, the national median RSL rise along U.S. coastlines during this 100-year period was about 0.25–0.30 m (see Figure 1.2b).

[42] https://tidesandcurrents.noaa.gov/sltrends/

Accurate future projections of VLM require an understanding of and accounting for the underlying processes and the time and space scales on which they vary. In this report, VLM projections are based in part on analysis of past observations. Vertical land motion rates are estimated at tide-gauge locations as well as at 1-degree grids using a statistical model of tide-gauge observations (Kopp et al., 2014; Sweet et al., 2017; Fox-Kemper et al., 2021; Garner et al., 2021). The model assesses RSL change across the global tide-gauge network[43] with data through about 2019 and separates the tide-gauge observations into 3 modes: 1) a global rise signal (Dangendorf et al., 2019), 2) a long-term linear—but regionally varying—rate, and 3) local effects that vary in time and by region. It is the second mode that defines this report's linear VLM rates, which have been incorporated into the RSL projections for each GMSL rise scenario. These rates are assumed to be linear over the past record and to persist linearly into the future over the length of the projected record. Assumed persistence may not necessarily be valid over the long term (e.g., if groundwater pumping ceases) but may be necessary due to a lack of data. As shown in Figure 4.8a, high rates of subsidence are estimated along the entire Gulf Coast, and moderate rates of subsidence are assessed along the entire East Coast. On the other hand, high rates of uplift are estimated for the southern coast of Alaska.

Over the past couple of decades, GPS stations have provided estimates of VLM in coastal areas across the United States. These GPS-based VLM estimates provide a comparison to the VLM rates in this report, albeit with a couple of caveats. First, the record lengths over which the GPS-based estimates are computed are significantly shorter than the tide-gauge data records used to infer the VLM rates in this report. Second, many tide-gauge locations do not have a co-located GPS station. While it is not possible to extend the record lengths of the available GPS measurements, the second challenge has been addressed using the GPS-imaging technique discussed in Hammond et al. (2021), which leverages the GPS network in coastal areas of the United States to generate VLM estimates at all tide-gauge locations (Figure 4.8b). Note that negative values of VLM reflect subsidence while positive values reflect uplift. To determine the VLM contribution to RSL at the coast, the negative and positive direction would be reversed. Broadly, the GPS-based estimates are consistent with the VLM estimates contained in this report. However, when subtracting the VLM rates in this report from the GPS-derived rates, differences become apparent (Figure 4.8c). The largest differences are found along the Southern Alaska coastlines, where rates of uplift are very large, and along the entire Gulf Coast, where subsidence rates are large. The rates are further compared in Figure 4.8d, which again reflects general agreement between the two sets of estimates, although at roughly 75% of the gauges, the tide-gauge-based VLM estimate in this report is greater (less negative in the case of subsidence) than that from GPS. In other words, there are generally higher rates of subsidence indicated in the GPS rates when compared to the VLM estimates in this report.

This comparison with the GPS is not intended to be an assessment of the accuracy of VLM rates and associated projections included in this report. Instead, it highlights some of the challenges associated with both estimating VLM rates at the coast and then projecting these into the future, particularly away from the tide-gauge and GPS stations. The spatial variability and local drivers of VLM are clear in Figure 4.8, and extending the tide-gauge-centered estimates to fill in spatial gaps either through the projection framework in this report or with GPS imaging is challenging to validate, particularly as these methods are not intended to capture VLM varying on small spatial scales. An opportunity is provided, however, by new technologies using satellite-based advanced Interferometric Synthetic Aperture Radar (InSAR) analysis, which can provide higher spatial resolution measurements of VLM rates. Calibrated to land GPS station estimates, measurements of land elevations over time by InSAR are producing VLM rates for large swaths or the U.S. coastal plain (e.g., Bekaert et al., 2017; Buzzanga et al., 2020; Bekaert et al., 2019; all InSAR VLM estimates are publicly available through references). Having a higher-resolution assessment of VLM rates can in turn help communities understand where VLM is now occurring at very fine scales (e.g., street block level) and help make informed decisions of how continued VLM will contribute to future RSL projections. Furthermore, InSAR provides an

[43] https://www.psmsl.org/data/

additional component to the coastal VLM observing network. Integrated assessments across tide gauges, GPS, and InSAR are likely to be most useful for inferring VLM rates and projecting these rates forward at the spatial scales key to coastal communities. Following is a case study of how the InSAR VLM connects to this VLM-observing network. In general, as there is the possibility of using a user-defined VLM rate within the RSL projections, we examine other sources of VLM that may offer options.

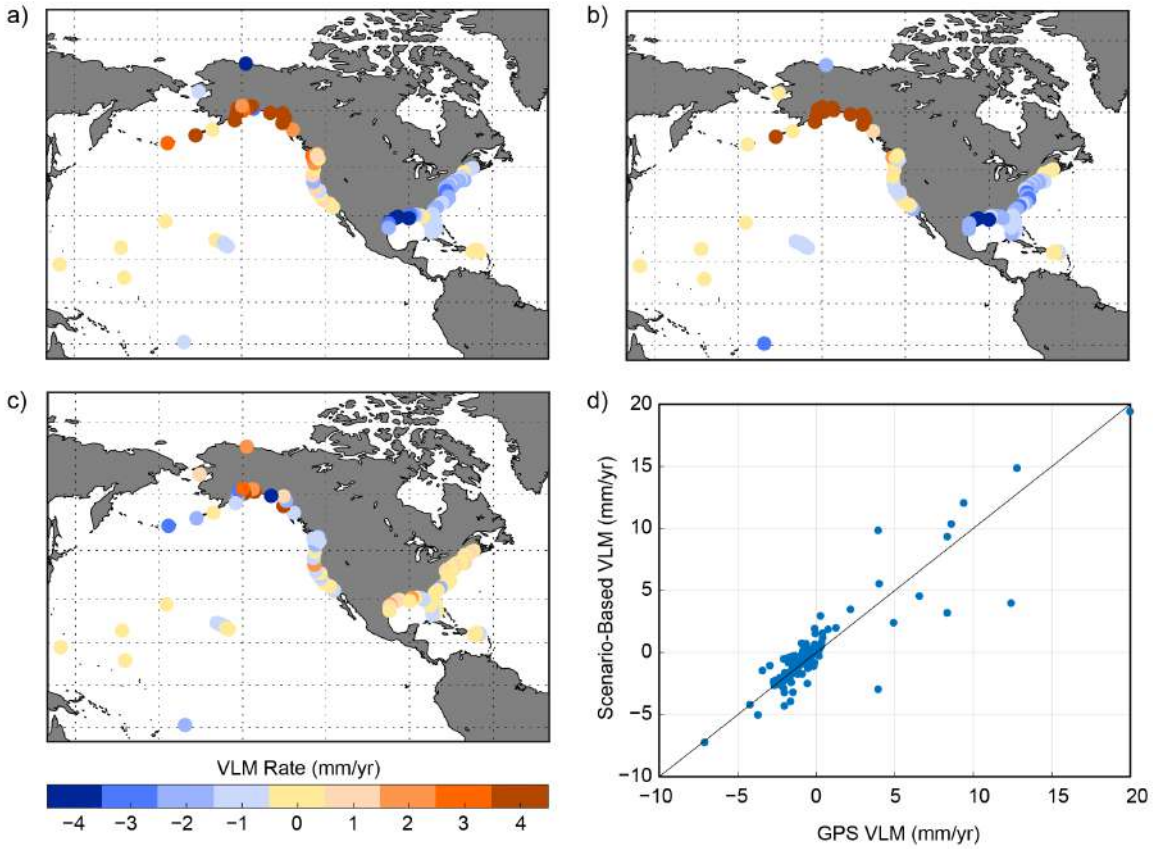

Figure 4.8: Comparison of vertical land motion (VLM) rate estimates (mm/year) from a) the scenario-based framework used in this report, and b) GPS-imaging estimates from Hammond et al. (2021). c) The difference between GPS-derived rates and scenario-derived rates and d) a comparison of the VLM estimates at the U.S. tide-gauge locations are also shown. Negative values of VLM reflect subsidence, while positive values reflect uplift.

Hampton Roads, Virginia

The historical long-term linear RSL rise rate at the Sewells Point, Virginia, tide gauge[44] is about 4.7 mm/year. More than half of this rate is estimated to be from downward VLM or subsidence with a rate of about 2.9 mm/year, which is close to previous estimates (Zervas, 2013; Kopp et al., 2014; Sweet et al., 2017). This subsidence is driven by both GIA and more localized groundwater withdrawal. If assumed to be linear and persistent into the future, VLM will contribute about 0.29 m to projections of RSL over the next 100 years. For example, by 2050 under the Intermediate-Low and Intermediate scenarios, the amount of RSL rise is projected to be between about 0.4 m and 0.45 m, respectively, with about 35% and 30% of that rise amount, respectively, from VLM.

However, VLM rates across the Hampton Roads region are not uniform. A past study (Eggleston and Pope, 2013) leveraged a variety of in situ observations to find a spatially varying pattern of subsidence ranging from 1.8 to 4.4 mm/year in the region from 1940 to 1971. The variations were connected to groundwater withdrawal in the region, which was captured via this assessment even with an effective spatial resolution on the order of tens of kilometers. More recently, InSAR rate maps have shown a range of subsidence from

[44] https://tidesandcurrents.noaa.gov/stationhome.html?id=8638610

about 1 mm to 5 mm/year in the region over the time period from 2014 to present, with locally higher rates (Figure 4.9; Buzzanga et al., 2020). Importantly, the satellite-based assessment revealed spatial variations on sub-kilometer scales, with some of the most prominent features in the spatial map connected to specific construction projects and land-use changes. With an average rate of subsidence around 3 mm/year over the course of the 21st century, VLM could contribute about 0.3 m to projected RSL, with locally higher amounts elsewhere in the region. Furthermore, comparing the InSAR-derived spatial pattern of VLM to that in either Eggleston and Pope (2013) or the gridded rates in this report provides important information about the linearity of VLM and the timescales on which VLM varies. There are considerable differences between the different assessments, indicating a shift in rates over the time periods considered. While it is necessary to consider the uncertainty in the VLM rate estimates and differences in measurement type, users of VLM information should assess land-use changes over the time periods considered along with the relevant processes driving VLM in the region. InSAR-derived VLM maps will play an increasingly key role in this assessment due to the spatial coverage and resolution provided by the satellites.

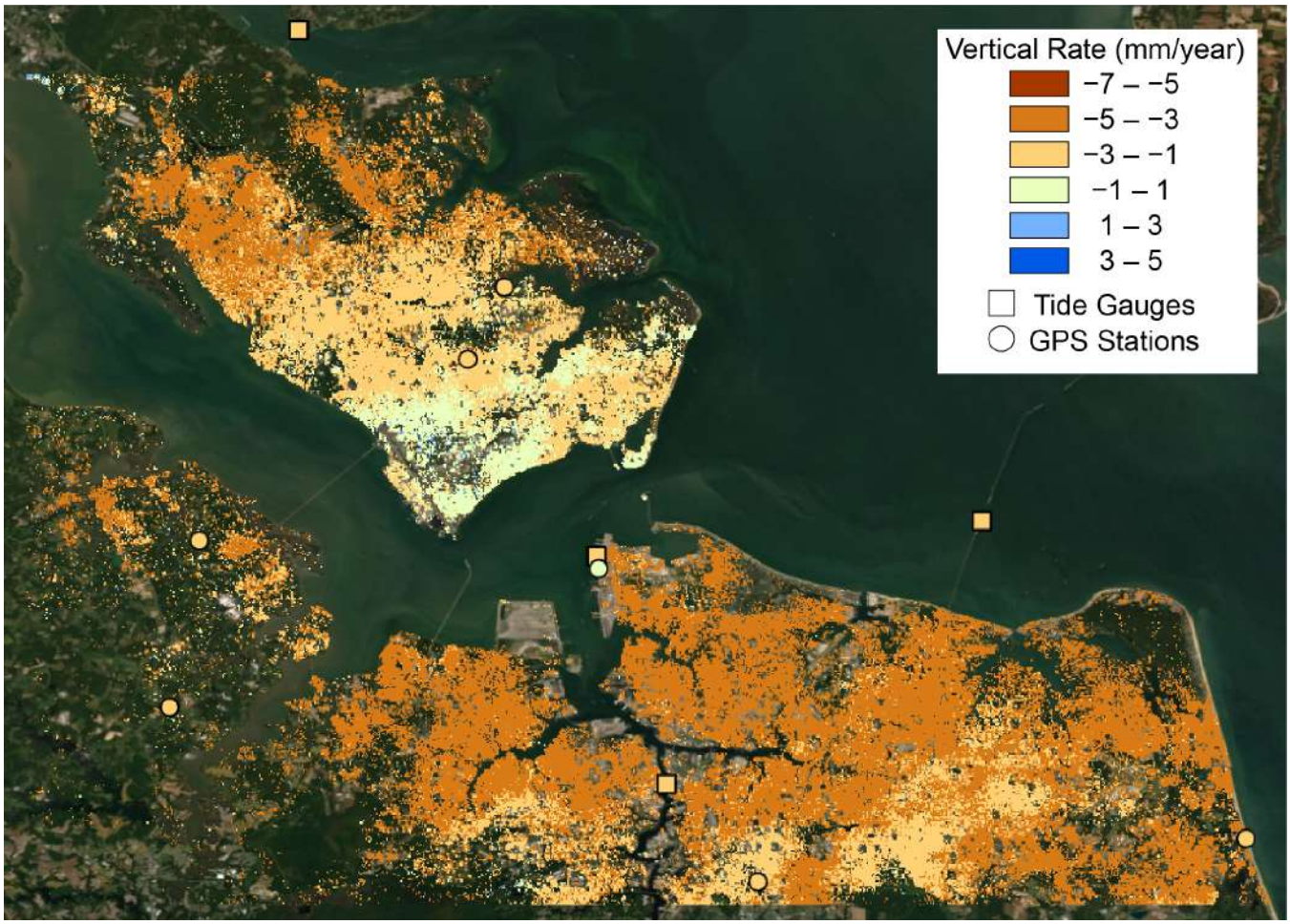

Figure 4.9: Map showing VLM rates (mm/year) for the Hampton Roads region displayed on top of satellite imagery. Higher rates of subsidence are indicated by darker orange colors. Of particular interest is the range of rates in such a small region (e.g., on the order of up to 5 mm/year difference in places). Based on Buzzanga et al. (2020).

Observing and Projecting Coastal Vertical Land Motion

While InSAR-measured VLM provides advantages over other measurement platforms in terms of spatial coverage and resolution, it should be considered in the context of the larger observing network when assessing VLM at the coast. In particular, InSAR serves two potential roles. First, InSAR can be used to provide ongoing monitoring of VLM at high spatial resolutions. InSAR has the potential to generate time series of VLM on a fine spatial scale. Subsidence "hotspots" can be identified along with abrupt shifts in VLM, which can assist in planning and executing adaptation efforts. For coastal communities attempting to alleviate subsidence in their region through efforts such as groundwater reinjection, InSAR provides a potentially better alternative to in situ monitoring to assess the effectiveness of these efforts. Second, InSAR can serve to assess spatial variability in VLM, filling in the gaps between tide gauges and GPS stations in coastal regions. The observations can then be combined in a statistical framework to provide more accurate projections of VLM with better estimates of uncertainty.

Assessing VLM with InSAR is not without challenges, however, although many of these are being addressed in ongoing and planned efforts. First, to be useful for assessing long-term VLM rates with the still relatively short satellite records, the shorter-term VLM rates can be calibrated and tied into the existing National Spatial Reference System (NSRS)[45] to improve accuracy and representativeness of long-term changes. Second, the availability and coverage of GPS in coastal regions impact the accuracy of VLM by InSAR. To provide a measurement of absolute VLM, InSAR needs to be tied to available GPS measurements. In areas with large gaps between GPS stations, this can lead to reduced accuracy of the InSAR estimates. Ideally, analysis would be conducted to determine optimal GPS station spacing for maintaining integrity of the InSAR-derived velocity field in various environments, including, but not limited to, regions of coastal subsidence, landslide/earthquake/volcanic activity, high plains aquifer depletion, and aquifer depletion in a tectonic area. Finally, InSAR VLM estimates are computationally expensive to perform over large regions, making national coverage a challenge. Efforts are underway, however, to generate a consistent surface displacement product (a preliminary step to estimating VLM) for the United States. A generalized approach for generating absolute VLM estimates from this product could then be created, paving the way for ongoing monitoring of VLM along the U.S. coastlines at high spatial resolutions.

To improve projections of VLM, InSAR alone is not sufficient. Instead, InSAR should be analyzed in tandem with available tide-gauge, GPS, and any other available in situ observations to assess both the spatial variability of VLM rates and potential non-linearities in the VLM rates estimated over these records. These non-linearities are critical for determining the future contribution of VLM to RSL. For example, the long-term rate assessed at a tide gauge as done in this report could differ significantly from the rate of VLM over the past decade because of a sustained land-use change. The comparison between the two types of VLM estimates in Figure 4.9 indicate that these shifts may be present at some locations along the U.S. coastlines and need to be assessed to improve projections of VLM.

[45] https://oceanservice.noaa.gov/education/tutorial_geodesy/geo08_spatref.html

Section 5: Conclusions

Sea level rise driven by global climate change is a clear and present risk to the United States, now and for the foreseeable future. It is the goal of the Sea Level Rise and Coastal Flood Hazard Scenarios and Tools Interagency Task Force to continue to provide projections and future scenarios to assist decision-makers for both planning and risk-bounding purposes. This report builds upon the progress made in Sweet et al. (2017), updating the GMSL scenarios and the associated local and regional RSL projections to reflect recent advances in sea level science, as well as expanding the types of scenario information provided to better serve stakeholder needs for coastal risk management and adaptation planning.

The major findings of this report are as follows:

Multiple lines of evidence provide increased confidence, regardless of the emissions pathway, in a narrower range of projected global, national, and regional sea level rise at 2050 than previously reported (Sweet et al., 2017).

Both trajectories assessed by extrapolating rates and accelerations estimated from historical tide-gauge observations, and model projections, fall within the same range in all cases, giving higher confidence in these relative sea level (RSL; land and ocean height changes) rise amounts by 2050. Specifically, RSL along the contiguous U.S. (CONUS) coastline is expected to rise, on average, as much over the next 30 years (0.25–0.30 m over 2020–2050) as it has over the last 100 years (1920–2020). Due to processes driving regional changes in sea level, the report found regional differences in both the modeled scenarios and observation-based extrapolations, with higher RSL rise along the East (0–5 cm higher on average than CONUS) and Gulf Coasts (10–15 cm higher) as compared to the West (10–15 cm lower) and Hawaiian/Caribbean (5–10 cm lower) Coasts.

For coastlines outside CONUS, and for individual regions and locations within CONUS, the projections can differ from the aforementioned mean values. In addition, it is important to note that the projections do not include natural year-to-year sea level variability that occurs along U.S. coastlines in response to climatic modes such as the El Niño–Southern Oscillation. Nevertheless, if we assume that regional sea level will keep following its present trajectory for the coming three decades, most U.S. regions are mostly tracking between the Intermediate-Low and Intermediate-High scenarios. Although the near-term observation-based extrapolations will continue to evolve over time with new observations and analyses, this updated information should help inform both near-term decisions and projects that may require decades' worth of planning prior to actual implementation.

By 2050, the expected relative sea level (RSL) will cause tide and storm surge heights to increase and will lead to a shift in U.S. coastal flood regimes, with major and moderate high tide flood events occurring as frequently as moderate and minor high tide flood events occur today. Without additional risk-reduction measures, U.S. coastal infrastructure, communities, and ecosystems will face significant consequences.

Minor/disruptive high tide flooding (HTF; about 0.55 m above mean higher high water [MHHW]) is projected to increase from a U.S average frequency of about 3 events/year in 2020 to >10 events/year by 2050. The projected increases for moderate/typically damaging (about 0.85 m above MHHW) and major/often destructive (about 1.20 m above MHHW) HTF are 0.3 events/year in 2020 to about 4 events/year in 2050 and 0.04 events/year in 2020 to 0.2 events/year by 2050, respectively. Across all severities (minor, moderate, major), HTF along the U.S. East and Gulf Coasts will largely continue to occur at or above the national average frequency.

In other words, much of the coastline is already close to a flood regime shift with respect to flood frequency and, consequently, damages. Only a small height difference (0.3–0.7 m) currently separates infrequent, damaging, or destructive HTF from the current regime of more frequent, so-called nuisance, flooding (whose impacts are in fact already remarkable throughout dozens of densely populated coastal cities). Decades ago, powerful storms were what typically caused coastal flooding, but due to RSL rise, even today's common wind events and seasonal high tides are already regularly flooding communities, and they will do so to an ever greater extent in the next few decades, affecting homes and businesses, overloading stormwater and wastewater systems, infiltrating coastal groundwater aquifers with saltwater, and stressing coastal wetlands and estuarine ecosystems.

Higher global temperatures increase the chances of higher sea level by the end of the century and beyond. The scenario projections of relative sea level (RSL) along the contiguous U.S. (CONUS) coastline are about 0.6–2.2 m in 2100 and 0.8–3.9 m in 2150 (relative to sea level in 2000); these ranges are driven by uncertainty in future emissions pathways and the response of the underlying physical processes.

With an increase in average global temperature of 2°C above preindustrial levels, and not considering the potential contributions from ice-sheet processes with limited agreement (low confidence) among modeling approaches, the probability of exceeding 0.5 m rise globally (0.7 m along the CONUS coastline) by 2100 is about 50%. With 3°–5°C of warming under high emissions pathways, this probability rises to >80% to >99%. The probability of exceeding 1 m globally (1.2 m CONUS) by 2100 rises from <5% with 3°C warming to almost 25% with 5°C warming. Considering low-confidence ice-sheet processes and high emissions pathways with warming approaching 5°C, these probabilities rise to about 50%, 20%, and 10% of exceeding 1.0 m, 1.5 m, or 2.0 m of global rise by 2100, respectively. While these low-confidence ice-sheet processes are unlikely to make significant contributions with 2°C of warming, how much warming might be required to trigger them is currently unknown.

In addition, as a result of improved understanding of the timing of possible large future contributions from ice-sheet loss, the "Extreme" scenario from the 2017 report (2.5 m GMSL rise by 2100) is now viewed as less plausible and has been removed from consideration. Nevertheless, the increased acceleration in the late 21st century and beyond means that the other high-end scenarios provide pathways that potentially reach this threshold in the decades immediately following 2100 (and continue rising). Regionally, the projections are near or higher than the global average in 2100 and 2150 for almost all U.S. coastlines due to vertical land motion (VLM); gravitational, rotational, and deformational effects due to land ice loss; and ocean circulation changes. Largely due to VLM, RSL projections are lower than the global amounts along the southern Alaska coast and are higher along the Eastern and Western Gulf coastlines.

Monitoring the sources of ongoing sea level rise and the processes driving changes in sea level is critical for assessing scenario divergence and tracking the trajectory of observed sea level rise, particularly during the time period when future emissions pathways lead to increased ranges in projected sea level rise.

Efforts are currently under way to narrow the uncertainties in ice-sheet dynamics and future sea level rise amounts in response to increasing greenhouse gas forcing and associated global warming. Early indicators of changes in sea level rise trajectories can serve to trigger adaptive management plans and are identified through continuous monitoring and assessment of changes in sea level (on global and local scales) and of the key drivers of sea level change that most affect U.S. coastlines, such as ocean heat content, ice-mass loss from Greenland and Antarctica, vertical land motion, and Gulf Stream system changes.

As emphasized in the summary findings above, beyond 2050 the amount of sea level rise is strongly affected by future global warming. By reducing greenhouse gas (GHG) emissions, severe and transformative

impacts occurring later this century or early next century along U.S. coastlines are more likely to be avoided. As GHG emissions and global temperatures continue to rise, the likelihood of very high U.S. sea level rise does too. If global warming reaches 2°C (warming levels are already >1°C), corresponding to a 50% chance that U.S. sea level as a whole will rise at least 0.7 m by 2100 and 1.2 m by 2150 (measured since 2000), major HTF by 2100 would occur more often than minor HTF occurs today in many coastal communities if risk-reduction action is not taken. If global mean temperatures were to rise as high as about 3°–5°C, much larger amounts of sea level rise would become increasingly possible, as instabilities in ice-sheet dynamics would potentially come into play. Constant monitoring of global to local sea levels and their source contributions by Federal agencies, such as NOAA and NASA, will be key to help assess potential trajectory divergence for triggering adaptive management plans.

The updated sea level scenarios and the EWL probability datasets in this study are being delivered or planned via numerous agency data servers, tools, and associated guidance products. Additionally, this report is a key technical input to the Fifth National Climate Assessment (NCA5 currently under way), and the datasets and derived information are being delivered to the NCA5 author teams. In terms of next steps, the Task Force will continue to refine these sea level projections and extreme (e.g., high tides, storms) water level probabilities while working to improve understanding of the implications of these projections for coastal hazards (e.g., flooding, erosion, and rising water tables), societal exposure and risk, infrastructure vulnerability, ecosystem health (including habitat transformation/loss), and cascading societal impacts. In order to do so, additional and improved observations and more sophisticated modeling approaches that incorporate the relevant physical processes (e.g., waves; see Box 3.1) will be needed at the regional scale, with local granularity to assess the impacts of these coastal hazards. Such information is expected to ultimately feed into the next generation of interagency reports and assessments to enable informed climate adaptation planning.

Section 6: Acknowledgments

The authors appreciate the review and constructive comments from the following external reviewers*: Dr. Mark Merrifield (Scripps Institution of Oceanography), Dr. Gary Mitchum (University of South Florida), Dr. Claudia Tebaldi (Lawrence Berkeley National Laboratory), Dr. Thomas Wahl (University of Central Florida), Dr. Steve Nerem (University of Colorado), Abby Sullivan (Philadelphia Water Department), and David Behar (San Francisco Public Utilities Commission).

We also thank the following agencies and/or their personnel for the reviews provided: Dr. Davina Passeri (U.S. Geological Survey [USGS]), Dr. Erika Lentz (USGS), Dr. Rebecca Beavers (National Park Service), Heidi Stiller (NOAA), Jamie Carter (National Oceanic and Atmospheric Administration [NOAA]), Lisa Auermuller (Rutgers University), Dr. Renee Collini (Mississippi State University), Laura Engeman (Scripps Institution of Oceanography), Dr. Ian Miller, (University of Washington), Katy Hintzen (University of Hawai'i), Jill Gambill (University of Georgia), Carey Schafer (EcoAdapt), and Rachel Johnson (NOAA). We would like to thank Sean Vitousek (model output) and Amy Foxgrover (figure illustration) of the USGS for Wave Call-out box support.

The contributions of Robert Kopp and Greg Garner were supported by the National Science Foundation (ICER-1663807, ICER-2103754) and the National Aeronautics and Space Administration (award 80NSSC20K1724 and JPL task 105393.509496.02.08.13.31). Contributions of John Marra, William Sweet, Jayantha Obeysekera, and Ayesha Genz were supported by the U.S. Department of Defense Strategic Environmental Research and Development Program through work carried out under Project RC-2644. The contributions of Benjamin Hamlington, Thomas Frederikse, Eric Larour, and David Bekaert were carried out in part at the Jet Propulsion Laboratory, California Institute of Technology, under a contract with the National Aeronautics and Space Administration (80NM0018D0004). The contributions of Patrick Barnard were supported by the USGS Coastal and Marine Hazards and Resources Program.

Production Team

Brooke C. Stewart,
Science Editor, NC State University

Andrea L. McCarrick,
Technical Editor, NC State University

Jessicca Allen,
Lead Graphic Designer, NC State University

S. Elizabeth Love-Brotak,
Graphic Designer, NOAA

Deborah Misch,
Lead Graphic Designer, Innovative Consulting & Management Services, LLC

Sara W. Veasey,
Visual Communications Team Lead, NOAA

Jacquelyn Crossman,
Librarian, ZAI-MPF

**The identification of the external reviewers does not imply that they agreed with all of the content of this report.*

Section 7: References

Bamber, J.L. and W.P. Aspinall, 2013: An expert judgement assessment of future sea level rise from the ice sheets. *Nature Climate Change*, 3 (4), 424–427. https://doi.org/10.1038/nclimate1778

Bamber, J.L., M. Oppenheimer, R.E. Kopp, W.P. Aspinall, and R.M. Cooke, 2019: Ice sheet contributions to future sea-level rise from structured expert judgment. *Proceedings of the National Academy of Sciences of the United States of America*, 116 (23), 11195–11200. https://doi.org/10.1073/pnas.1817205116

Baranes, H.E., J.D. Woodruff, S.A. Talke, R.E. Kopp, R.D. Ray, and R.M. DeConto, 2020: Tidally driven interannual variation in extreme sea level frequencies in the Gulf of Maine. *Journal of Geophysical Research: Oceans*, 125 (10), e2020JC016291. http://dx.doi.org/10.1029/2020JC016291

Barnard, P.L., L.H. Erikson, A.C. Foxgrover, J.A. Finzi Hart, P. Limber, A.C. O'Neill, M. van Ormondt, S. Vitousek, N. Wood, M.K. Hayden, and J.M. Jones, 2019: Dynamic flood modeling essential to assess the coastal impacts of climate change. Scientific reports, 9 (1), 1–13. https://doi.org/10.1038/s41598-019-40742-z

Befus, K.M., P.L. Barnard, D.J. Hoover, J.A. Finzi Hart, and C.I. Voss, 2020: Increasing threat of coastal groundwater hazards from sea-level rise in California. *Nature Climate Change*, 10 (10), 946–952. https://doi.org/10.1038/s41558-020-0874-1

Bekaert, D.P.S., B.D. Hamlington, B. Buzzanga, and C.E. Jones, 2017: Spaceborne synthetic aperture radar survey of subsidence in Hampton Roads, Virginia (USA). Scientific Reports, 7 (1), 1–9. https://doi.org/10.1038/s41598-017-15309-5

Bekaert, D.P.S., C.E. Jones, K. An, and M.-H. Huang, 2019: Exploiting UAVSAR for a comprehensive analysis of subsidence in the Sacramento Delta. *Remote Sensing of Environment*, 220, 124–134. https://doi.org/10.1016/j.rse.2018.10.023

Bloemen, P., T. Reeder, C. Zevenbergen, J. Rijke, and A. Kingsborough, 2018: Lessons learned from applying adaptation pathways in flood risk management and challenges for the further development of this approach. *Mitigation and Adaptation Strategies for Global Change*, 23 (7), 1083–1108. https://doi.org/10.1007/s11027-017-9773-9

Bodnar, A.N., 1981: Estimating Accuracies of Tidal Datums from Short Term Observations. Technical Report NOS CO-OPS 077. National Oceanic and Atmospheric Administration, National Ocean Service, Center for Operational Oceanographic Products and Services, Silver Spring, MD, 40 pp. https://tidesandcurrents.noaa.gov/publications/NOAA_Technical_Report_NOS_COOPS_077.pdf

Boening, C., J.K. Willis, F.W. Landerer, R.S. Nerem, and J. Fasullo, 2012: The 2011 La Niña: So strong, the oceans fell. *Geophysical Research Letters*, 39 (19). https://doi.org/10.1029/2012GL053055

Bos, M.S., R.M.S. Fernandes, S.D.P. Williams, and L. Bastos, 2013: Fast error analysis of continuous GNSS observations with missing data. *Journal of Geodesy*, 87 (4), 351–360. http://dx.doi.org/10.1007/s00190-012-0605-0

Bos, M.S., S.D.P. Williams, I.B. Araújo, and L. Bastos, 2014: The effect of temporal correlated noise on the sea level rate and acceleration uncertainty. *Geophysical Journal International*, 196 (3), 1423–1430. http://dx.doi.org/10.1093/gji/ggt481

Bromirski, P.D., A.J. Miller, R.E. Flick, and G. Auad, 2011: Dynamical suppression of sea level rise along the Pacific coast of North America: Indications for imminent acceleration. *Journal of Geophysical Research*, 116, C07005. https://doi.org/10.1029/2010jc006759

Buchanan, M.K., M. Oppenheimer, and R.E. Kopp, 2017: Amplification of flood frequencies with local sea level rise and emerging flood regimes. *Environmental Research Letters*, 12 (6), 064009. https://doi.org/10.1088/1748-9326/aa6cb3

Buzzanga, B., D.P.S. Bekaert, B.D. Hamlington, and S.S. Sangha, 2020: Toward sustained monitoring of subsidence at the coast using InSAR and GPS: An application in Hampton Roads, Virginia. *Geophysical Research Letters*, 47 (18), e2020GL090013. https://doi.org/10.1029/2020GL090013

Calafat, F.M., D.P. Chambers, and M.N. Tsimplis, 2012: Mechanisms of decadal sea level variability in the eastern North Atlantic and the Mediterranean Sea. *Journal of Geophysical Research: Oceans*, 117, C09022. https://doi.org/10.1029/2012JC008285

Calafat, F.M. and M. Marcos, 2020: Probabilistic reanalysis of storm surge extremes in Europe. *Proceedings of the National Academy of Sciences*, 117 (4), 1877–1883. http://dx.doi.org/10.1073/pnas.1913049117

CCRM, 2019: Recommendations for Sea Level Rise Projections: A Report for the Governor's Coastal Climate Resiliency Plan. Center for Coastal Resources Management, Virginia institute of Marine Science, Gloucester Point, VA, 6 pp. https://www.naturalresources.virginia.gov/media/governorvirginiagov/secretary-of-natural-resources/images/1c.-Sea-level-rise-projections-for-Virginia-planning-purposes-(2)-FINAL-10_31.pdf

Chao, B.F., Y.-H. Wu, and Y.S. Li, 2008: Impact of artificial reservoir water impoundment on global sea level. *Science*, 320 (5873), 212–214. https://doi.org/10.1126/science.1154580

Church, J.A., P.U. Clark, A. Cazenave, J.M. Gregory, S. Jevrejeva, A. Levermann, M.A. Merrifield, G.A. Milne, R.S. Nerem, P.D. Nunn, A.J. Payne, W.T. Pfeffer, D. Stammer and A.S. Unnikrishnan, 2013: Sea Level Change. In: *Climate Change 2013: The Physical Science Basis. Contribution of Working Group I to the Fifth Assessment Report of the Intergovernmental Panel on Climate Change* [Stocker, T.F., D. Qin, G.-K. Plattner, M. Tignor, S.K. Allen, J. Boschung, A. Nauels, Y. Xia, V. Bex and P.M. Midgley (eds.)]. Cambridge University Press, Cambridge, United Kingdom and New York, NY, USA https://www.ipcc.ch/site/assets/uploads/2018/02/WG1AR5_Chapter13_FINAL.pdf

Coles, S., 2001: *An Introduction to Statistical Modeling of Extreme Values*. Springer-Verlag, London, 224 pp.

Coles, S.G., and M.J. Dixon, 1999: Likelihood-based inference for extreme value models. *Extremes*, 2, 5–23. https://doi.org/10.1023/A:1009905222644

Cooley, D., 2013: Return periods and return levels under climate change. In: *Extremes in a Changing Climate*. AghaKouchak, A., D. Easterling, K. Hsu, S. Schubert, and S. Sorooshian, Eds. Springer, Dordrecht, Netherlands, 97–114.

Dalrymple, T. (1960). Flood Frequency Analyses, Manual of Hydrology: Part 3. U.S. Geological Survey Water-Supply Paper 1543-A. U.S. Geological Survey, Reston, VA, 86 pp. https://doi.org/10.3133/wsp1543A

Dangendorf, S., C. Hay, F.M. Calafat, M. Marcos, C.G. Piecuch, K. Berk, and J. Jensen, 2019: Persistent acceleration in global sea-level rise since the 1960s. *Nature Climate Change*, 9 (9), 705–710. https://doi.org/10.1038/s41558-019-0531-8

DeConto, R.M., D. Pollard, R.B. Alley, I. Velicogna, E. Gasson, N. Gomez, S. Sadai, A. Condron, D.M. Gilford, E.L. Ashe, R.E. Kopp, D. Li, and A. Dutton, 2021: The Paris Climate Agreement and future sea-level rise from Antarctica. *Nature*, 593 (7857), 83–89. https://doi.org/10.1038/s41586-021-03427-0

Dokka, R.K., 2011: The role of deep processes in late 20th century subsidence of New Orleans and coastal areas of southern Louisiana and Mississippi. *Journal of Geophysical Research*, 116, B06403. https://doi.org/10.1029/2010JB008008

Edwards, T.L., S. Nowicki, B. Marzeion, R. Hock, H. Goelzer, H. Seroussi, N.C. Jourdain,D.A. Slater, F.E. Turner, C.J. Smith, C.M. McKenna, E. Simon, A. Abe-Ouchi, J.M. Gregory, E. Larour, W.H. Lipscomb, A.J. Payne, A. Shepherd, C. Agosta, P. Alexander, T. Albrecht, B. Anderson, X. Asay-Davis, A. Aschwanden, A. Barthel, A. Bliss, R. Calov, C. Chambers, N. Champollion, Y. Choi, R. Cullather, J. Cuzzone, C. Dumas, D. Felikson, X. Fettweis, K. Fujita, B.K. Galton-Fenzi, R. Gladstone, N.R. Golledge, R. Greve, T. Hattermann, M.J. Hoffman, A. Humbert, M. Huss, P. Huybrechts, W. Immerzeel, T. Kleiner, P. Kraaijenbrink, S. Le clec'h, V. Lee, G.R. Leguy, C.M. Little, D.P. Lowry, J.-H. Malles, D.F. Martin, F. Maussion, M. Morlighem, J.F. O'Neill, I. Nias, F. Pattyn, T. Pelle, S.F. Price, A. Quiquet, V. Radić, R. Reese, D.R. Rounce, M. Rückamp, A. Sakai, C. Shafer, N.-J. Schlegel, S. Shannon, R.S. Smith, F. Straneo, S. Sun, L. Tarasov, L.D. Trusel, J. Van Breedam, R. van de Wal, M. van den Broeke, R. Winkelmann, H. Zekollari, C. Zhao, T. Zhang, and T. Zwinger, 2021: Projected land ice contributions to twenty-first-century sea level rise. *Nature*, 593 (7857), 74–82. https://doi.org/10.1038/s41586-021-03302-y

Eggleston, J. and J. Pope, 2013: Land Subsidence and Relative Sea-Level Rise in the Southern Chesapeake Bay Region. Circular 1392. U.S. Geological Survey, Reston, VA, 30 pp., http://dx.doi.org/10.3133/cir1392

EPA, 1995a: Combined Sewer Overflows: Guidance for Long-Term Control Plan. EPA/832-B-95-002. U.S. Environmental Protection Agency, Office of Wastewater Management, Washington, DC, 201 pp. https://www.epa.gov/sites/default/files/2015-10/documents/owm0272_0.pdf

EPA, 1995b: Combined Sewer Overflows: Guidance for Nine Minimum Controls. EPA 832-B-95-003. U.S. Environmental Protection Agency, Office of Wastewater Management, Washington, DC, 69 pp. https://www.epa.gov/sites/default/files/2015-10/documents/owm0030_2.pdf

Farrell, W.E. and J.A. Clark, 1976: On postglacial sea level. *Geophysical Journal International*, 46 (3), 647–667. https://doi.org/10.1111/j.1365-246X.1976.tb01252.x.

Fasullo, J. T., Boening, C., Landerer, F. W., & Nerem, R. S. (2013). Australia's unique influence on global sea level in 2010–2011. Geophysical Research Letters, 40 (16), 4368–4373. https://doi.org/10.1002/grl.50834

Fasullo, J.T. and R.S. Nerem, 2018: Altimeter-era emergence of the patterns of forced sea-level rise in climate models and implications for the future. *Proceedings of the National Academy of Sciences*, 115 (51), 12944–12949. https://doi.org/10.1073/pnas.1813233115

FEMA, 2016a: Guidance for Flood Risk Analysis Mapping: Coastal Flood Frequency and Extreme Value Analysis. Guidance Document 76. Federal Emergency Management Agency, Hyattsville, MD, 22 pp. https://www.fema.gov/sites/default/files/2020-02/Coastal_Flood_Frequency_and_Extreme_Value_Analysis_Guidance_Nov_2016.pdf

FEMA, 2016b: Guidance for Flood Risk Analysis Mapping: Statistical Simulation Methods. Guidance Document 77. Federal Emergency Management Agency, Hyattsville, MD, 37 pp. https://www.fema.gov/sites/default/files/documents/fema_coastal-statistical-simulation-methods_nov-2016.pdf

Fox-Kemper, B., H.T. Hewitt, C. Xiao, G. Aðalgeirsdóttir, S.S. Drijfhout, T.L. Edwards, N.R. Golledge, M. Hemer, R.E. Kopp, G. Krinner, A. Mix, D. Notz, S. Nowicki, I.S. Nurhati, L. Ruiz, J.-B. Sallée, A.B.A. Slangen, and Y. Yu, 2021: Ocean, Cryosphere and Sea Level Change. In: *Climate Change 2021: The Physical Science Basis. Contribution of Working Group I to the Sixth Assessment Report of the Intergovernmental Panel on Climate Change* [MassonDelmotte, V., P. Zhai, A. Pirani, S.L. Connors, C. Péan, S. Berger, N. Caud, Y. Chen, L. Goldfarb, M.I. Gomis, M. Huang, K. Leitzell, E. Lonnoy, J.B.R. Matthews, T.K. Maycock, T. Waterfield, O. Yelekçi, R. Yu, and B. Zhou (eds.)]. Cambridge University Press. In Press. https://www.ipcc.ch/report/ar6/wg1/

Frau, R., M. Andreewsky, and P. Bernardara, 2018: The use of historical information for regional frequency analysis of extreme skew surge. *Natural Hazards and Earth System Sciences*, 18 (3), 949–962. https://doi.org/10.5194/nhess-18-949-2018

Frederikse, T., K. Simon, C.A. Katsman, and R. Riva, 2017: The sea-level budget along the Northwest Atlantic coast: GIA, mass changes, and large-scale ocean dynamics. *Journal of Geophysical Research: Oceans*, 122, 5486–5501. https://doi.org/10.1002/2017JC012699

Frederikse, T., F. Landerer, L. Caron, S. Adhikari, D. Parkes, V.W. Humphrey, S. Dangendorf, P. Hogarth, L. Zanna, L. Cheng, and Y.-H. Wu, 2020: The causes of sea-level rise since 1900. *Nature*, 584 (7821), 393–397. https://doi.org/10.1038/s41586-020-2591-3

Fu, X., 2020: Measuring local sea-level rise adaptation and adaptive capacity: A national survey in the United States. *Cities*, 102, 102717. https://doi.org/10.1016/j.cities.2020.102717.

Garner, G.G., T. Hermans, R.E. Kopp, A.B.A. Slangen, T.L. Edwards, A. Levermann, S. Nowikci, M.D. Palmer, C. Smith, B. Fox-Kemper, H.T. Hewitt, C. Xiao, G. Aðalgeirsdóttir, S.S. Drijfhout, T.L. Edwards, N.R. Golledge, M. Hemer, R.E. Kopp, G. Krinner, A. Mix, D. Notz, S. Nowicki, I. S. Nurhati, L. Ruiz, J-B. Sallée, Y. Yu, L. Hua, T. Palmer, and B. Pearson, 2021. IPCC AR6 Sea-Level Rise Projections. Version 20210809. PO.DAAC, CA, USA. Dataset accessed [2021-09-01]. https://podaac.jpl.nasa.gov/announcements/2021-08-09-Sea-level-projections-from-the-IPCC-6th

Gill, S., G. Hovis, K. Kriner, and M. Michalski, 2014: Implementation of Procedures for Computation of Tidal Datums in Areas with Anomalous Trends of Relative Mean Sea Level. NOAA Technical Report NOS CO-OPS 068. National Oceanic and Atmospheric Administration, National Ocean Service, Silver Spring, MD, 58 pp. https://tidesandcurrents.noaa.gov/publications/NOAA_Technical_Report_NOS_COOPS_68.pdf

Guza, R.T. and E.B. Thornton, 1982: Swash oscillations on a natural beach. *Journal of Geophysical Research*, 87 (C1), 483–491. https://doi.org/10.1029/JC087iC01p00483

Haasnoot, M., J.H. Kwakkel, W.E. Walker, and J. ter Maat, 2013: Dynamic adaptive policy pathways: A method for crafting robust decisions for a deeply uncertain world. *Global Environmental Change*, 23 (2), 485–498. https://doi.org/10.1016/j.gloenvcha.2012.12.006

Haasnoot, M., S. Brown, P. Scussolini, J.A. Jimenez, A.T. Vafeidis, and R.J. Nicholls, 2019: Generic adaptation pathways for coastal archetypes under uncertain sea-level rise. *Environmental Research Communications*, 1 (7), 071006. https://doi.org/10.1088/2515-7620/ab1871

Habel, S., C.H. Fletcher, T.R. Anderson, and P.R. Thompson, 2020: Sea-level rise induced multi-mechanism flooding and contribution to urban infrastructure failure. *Scientific Reports*, 10 (1), 3796. http://dx.doi.org/10.1038/s41598-020-60762-4

Hall, J.A., S. Gill, J. Obeysekera, W. Sweet, K. Knuuti, and J. Marburger, 2016: Regional Sea Level Scenarios for Coastal Risk Management: Managing the Uncertainty of Future Sea Level Change and Extreme Water Levels for Department of Defense Coastal Sites Worldwide. U.S. Department of Defense, Strategic Environmental Research and Development Program, Alexandria, VA, 224 pp. https://climateandsecurity.files.wordpress.com/2014/01/regional-sea-level-scenarios-for-coastal-risk-management_managing-uncertainty-of-future-sea-level-change-and-extreme-water-levels-for-department-of-defense.pdf

Hall, J.W., H. Harvey, and L.J. Manning, 2019: Adaptation thresholds and pathways for tidal flood risk management in London. *Climate Risk Management*, 24, 42–58. https://doi.org/10.1016/j.crm.2019.04.001

Hamlington, B.D., A.S. Gardner, E. Ivins, J.T.M. Lenaerts, J.T. Reager, D.S. Trossman, E.D. Zaron, S. Adhikari, A. Arendt, A. Aschwanden, B.D. Beckley, D.P.S. Bekaert, G. Blewitt, L. Caron, D.P. Chambers, H.A. Chandanpurkar, K. Christianson, B. Csatho, R.I. Cullather, R.M. DeConto, J.T. Fasullo, T. Frederikse, J.T. Freymueller, D.M. Gilford, M. Girotto, W.C. Hammond, R. Hock, N. Holschuh, R.E. Kopp, F. Landerer, E. Larour, D. Menemenlis, M. Merrifield, J.X. Mitrovica, R.S. Nerem, I.J. Nias, V. Nieves, S. Nowicki, K. Pangaluru, C.G. Piecuch, R.D. Ray, D.R. Rounce, N.-J. Schlegel, H. Seroussi, M. Shirzaei, W.V. Sweet, I. Velicogna, N. Vinogradova, T. Wahl, D.N. Wiese, and M.J. Willis, 2020a: Understanding of contemporary regional sea-level change and the implications for the future. *Reviews of Geophysics*, 58 (3), e2019RG000672. https://doi.org/10.1029/2019RG000672

Hamlington, B.D., C.G. Piecuch, J.T. Reager, H. Chandanpurkar, T. Frederikse, R.S. Nerem, J.T. Fasullo, and S.-H. Cheon, 2020b: Origin of interannual variability in global mean sea level. *Proceedings of the National Academy of Sciences*, 117 (25), 13983. http://dx.doi.org/10.1073/pnas.1922190117

Hamlington, B.D., T. Frederikse, P.R. Thompson, J.K. Willis, R.S. Nerem, and J.T. Fasullo, 2021: Past, present, and future Pacific sea-level change. *Earth's Future*, 9 (4), e2020EF001839. https://doi.org/10.1029/2020EF001839

Hammond, W.C., G. Blewitt, C. Kreemer, and R.S. Nerem, 2021: GPS imaging of global vertical land motion for studies of sea level rise. *Journal of Geophysical Research: Solid Earth*, 126 (7), e2021JB022355. https://doi.org/10.1029/2021JB022355

Hawley, W.B., C.C. Hay, J.X. Mitrovica, and R.E. Kopp., 2020: A spatially variable time series of sea level change due to artificial water impoundment. *Earth's Future*, 8 (7), e2020EF001497. https://doi.org/10.1029/2020EF001497

Hemer, Mark A., Y. Fan, N. Mori, A. Semedo, and X.L. Wang, 2013: Projected changes in wave climate from a multi-model ensemble. *Nature Climate Change*, 3 (5), 471–476. https://doi.org/10.1038/nclimate1791

Hinkel, J., J.C.J.H. Aerts, S. Brown, J.A. Jiménez, D. Lincke, R.J. Nicholls, P. Scussolini, A. Sanchez-Arcilla, A. Vafeidis, and K.A. Addo, 2018: The ability of societies to adapt to twenty-first-century sea-level rise. *Nature Climate Change*, 8 (7), 570–578. https://doi.org/10.1038/s41558-018-0176-z

Hosking, J.R.M. and J. R. Wallis, 1997: *Regional Frequency Analysis: An Approach Based on L-Moments*. Cambridge University Press, Cambridge, U.K, 224 pp.

IPCC, 2021a: Climate Change 2021: *The Physical Science Basis. Contribution of Working Group I to the Sixth Assessment Report of the Intergovernmental Panel on Climate Change* [Masson-Delmotte, V., P. Zhai, A. Pirani, S.L. Connors, C. Péan, S. Berger, N. Caud, Y. Chen, L. Goldfarb, M.I. Gomis, M. Huang, K. Leitzell, E. Lonnoy, J.B.R. Matthews, T.K. Maycock, T. Waterfield, O. Yelekçi, R. Yu, and B. Zhou (eds.)]. Cambridge University Press. In Press. https://www.ipcc.ch/report/ar6/wg1/

IPCC, 2021b: *Summary for Policymakers. In: Climate Change 2021: The Physical Science Basis. Contribution of Working Group I to the Sixth Assessment Report of the Intergovernmental Panel on Climate Change* [MassonDelmotte, V., P. Zhai, A. Pirani, S.L. Connors, C. Péan, S. Berger, N. Caud, Y. Chen, L. Goldfarb, M.I. Gomis, M. Huang, K. Leitzell, E. Lonnoy, J.B.R. Matthews, T.K. Maycock, T. Waterfield, O. Yelekçi, R. Yu, and B. Zhou (eds.)]. Cambridge University Press. In Press. https://www.ipcc.ch/report/ar6/wg1/

Karegar, M.A., T.H. Dixon, and S.E. Engelhart, 2016: Subsidence along the Atlantic Coast of North America: Insights from GPS and late Holocene relative sea level data. *Geophysical Research Letters*, 43, 3126–3133. https://doi.org/10.1002/2016GL068015

King, D., D. Schrag, Z. Dadi, Q. Ye, and A. Gosh, 2015: Climate Change: A Risk Assessment. Hynard, J. and T. Rodger, Eds. Centre for Science and Policy, Cambridge, UK, 154 pp. www.csap.cam.ac.uk/projects/climate-change-risk-assessment/

Kirwan, M.L. and K.B. Gedan, 2019: Sea-level driven land conversion and the formation of ghost forests. *Nature Climate Change*, 9 (6), 450–457. https://doi.org/10.1038/s41558-019-0488-7

Konikow, L.F., 2011: Contribution of global groundwater depletion since 1900 to sea-level rise. *Geophysical Research Letters*, 38 (17). https://doi.org/10.1029/2011GL048604

Kopp, R.E., R.M. Horton, C.M. Little, J.X. Mitrovica, M. Oppenheimer, D.J. Rasmussen, B.H. Strauss, and C. Tebaldi, 2014: Probabilistic 21st and 22nd century sea-level projections at a global network of tide-gauge sites. *Earth's Future*, 2 (8), 383–406. https://doi.org/10.1002/2014EF000239

Kopp, R.E., R.M. DeConto, D.A. Bader, C.C. Hay, R.M. Horton, S. Kulp, M. Oppenheimer, D. Pollard, and B.H. Strauss, 2017: Evolving understanding of Antarctic ice-sheet physics and ambiguity in probabilistic sea-level projections." *Earth's Future*, 5 (12), 1217–1233. https://doi.org/10.1002/2017EF000663

Kopp, R.E., E.A. Gilmore, C.M. Little, J. Lorenzo-Trueba, V.C. Ramenzoni, and W.V. Sweet, 2019: Usable science for managing the risks of sea-level rise. *Earth's Future*, 7, 1235–1269. https://doi.org/10.1029/2018EF001145

Krasting, J.P., J.P. Dunne, R.J. Stouffer, and R.W. Hallberg, 2016: Enhanced Atlantic sea-level rise relative to the Pacific under high carbon emission rates. *Nature Geoscience*, 9 (3), 210–214. http://dx.doi.org/10.1038/ngeo2641

Langbein W.B., 1949: Annual floods and the partial-duration flood series. *Eos, Transactions American Geophysical Union*, 30 (6), 879–881. https://doi.org/10.1029/TR030i006p00879

Larsen, C.F., R.J. Motyka, J.T. Freymueller, K.A. Echelmeyer, and E.R. Ivins, 2004: Rapid uplift of southern Alaska caused by recent ice loss. *Geophysical Journal International*, 158 (3), 1118–1133. http://dx.doi.org/10.1111/j.1365-246X.2004.02356.

Levermann, A., R. Winkelmann, T. Albrecht, H. Goelzer, N.R. Golledge, R. Greve, P. Huybrechts J. Jordan, G. Leguy, D. Martin, M. Morlighem, F. Pattyn, D. Pollard, A. Quiquet, C. Rodehacke, H. Seroussi, J. Sutter, T. Zhang, J. Van Breedam, R. Calov, R. DeConto, C. Dumas, J. Garbe, G.H. Gudmundsson, M.J. Hoffman, A. Humbert, T. Kleiner, W.H. Lipscomb, M. Meinshausen, E. Ng, S.M.J. Nowicki, M. Perego, S.F. Price, F. Saito, N.J. Schlegel, S. Sun, and R.S.W. van de Wal, 2020: Projecting Antarctica's contribution to future sea level rise from basal ice shelf melt using linear response functions of 16 ice sheet models (LARMIP-2). *Earth System Dynamics*, 11 (1), 35–76. https://doi.org/10.5194/esd-11-35-2020

Longuet-Higgins, M.S. and R.W. Stewart, 1963: A note on wave set-up. *Journal of Marine Research*, 21 (4), 4–10. https://images.peabody.yale.edu/publications/jmr/jmr21-01-01.pdf

Lyu, K., X. Zhang, J.A. Church, A.B.A. Slangen, and J. Hu. 2014: Time of emergence for regional sea-level change. *Nature Climate Change*, 4 (11), 1006–1010. https://doi.org/10.1038/nclimate2397

Marzeion, B., A.H. Jarosch, and M. Hofer, 2012: Past and future sea-level change from the surface mass balance of glaciers. *The Cryosphere*, 6 (6), 1295–1322. https://doi.org/10.5194/tc-6-1295-2012

Marzeion, B., R. Hock, B. Anderson, A. Bliss, N. Champollion, K. Fujita, M. Huss, W.W. Immerzeel, P. Kraaijenbrink, J.-H. Malles, F. Maussion, V. Radić, D.R. Rounce, A. Sakai, S. Shannon, R. van de Wal, and H. Zekollari, 2020: Partitioning the uncertainty of ensemble projections of global glacier mass change. *Earth's Future*, 8 (7), e2019EF001470. https://doi.org/10.1029/2019EF001470

McCallum, B.E., S.M. Wicklein, R.G. Reiser, R. Busciolano, J. Morrison, R.J. Verdi, J.A. Painter, E.R. Frantz, and A.J. Gotvald, 2013: Monitoring Storm Tide and Flooding from Hurricane Sandy along the Atlantic Coast of the United States, October 2012. Open File Report 2013-1043. U.S. Geological Survey, Reston, VA, 42 pp. http://dx.doi.org/10.3133/ofr20131043

McKenzie, T., S. Habel, and H. Dulai, 2021: Sea-level rise drives wastewater leakage to coastal waters and storm drains. *Limnology and Oceanography Letters*, 6, 154–163. https://doi.org/10.1002/lol2.10186

Menéndez, M., and P.L. Woodworth, 2010: Changes in extreme high water levels based on a quasi-global tide-gauge data set. *Journal of Geophysical Research: Oceans*, 115, C10011. https://doi.org/10.1029/2009JC005997

Merrifield, M.A., A.S. Genz, C.P. Kontoes, and J.J. Marra, 2013: Annual maximum water levels from tide gauges: Contributing factors and geographic patterns. *Journal of Geophysical Research: Oceans*, 118 (5), 2535–2546. https://doi.org/10.1002/jgrc.20173

Milne, G.A. and J.X. Mitrovica, 1998: Postglacial sea-level change on a rotating Earth. *Geophysical Journal International*, 133 (1), 1–19. https://doi.org/10.1046/j.1365-246X.1998.1331455.x

Mitrovica, J.X., M.E. Tamisiea, J.L. Davis, and G.A. Milne, 2001: Recent mass balance of polar ice sheets inferred from patterns of global sea-level change. *Nature*, 409 (6823), 1026–1029. https://doi.org/10.1038/35059054

Moftakhari, H. R., Jay, D. A., & Talke, S. A. (2016). Estimating river discharge using multiple-tide gauges distributed along a channel. *Journal of Geophysical Research: Oceans*, 121 (4), 2078–2097. https://doi.org/10.1002/2015JC010983

Moore, F.C. and N. Obradovich, 2020: Using remarkability to define coastal flooding thresholds. *Nature Communications*, 11 (1), 1–8. https://doi.org/10.1038/s41467-019-13935-3

Muis, S., M. Verlaan, H.C. Winsemius, J.C.J.H. Aerts, and P.J. Ward, 2016: A global reanalysis of storm surges and extreme sea levels. *Nature Communications*, 7 (1), 11969. http://dx.doi.org/10.1038/ncomms11969

Nadal-Caraballo, N.C., M.O. Campbell, V.M. Gonzalez, M.J. Torres, J.A. Melby, and A.A. Taflanidis, 2020: Coastal Hazards System: A probabilistic coastal hazard analysis framework. *Journal of Coastal* Research, 95 (SI), 1211–1216. http://dx.doi.org/10.2112/SI95-235.1

NGS, 2001: Geodetic Program Needs of Louisiana and Wisconsin: Report to Congress. National Oceanic and Atmospheric Administration, National Ocean Service, National Geodetic Survey, Silver Spring, MD, 38 pp. https://www.ngs.noaa.gov/PUBS_LIB/NGSreport_823.pdf

NOAA, 2003: Computational Techniques for Tidal Datums Handbook. NOAA Special Publication NOS CO-OPS 2. National Oceanic and Atmospheric Administration, National Ocean Service, Center for Operational Oceanographic Products and Services, Silver Spring, MD, 113 pp. https://tidesandcurrents.noaa.gov/publications/Computational_Techniques_for_Tidal_Datums_handbook.pdf

NOAA, 2020: Surf Zone Forecast and Coastal/Lakeshore Hazard Services. National Weather Service Instruction 10-320. National Oceanic and Atmospheric Administration, National Weather Service, 38 pp. http://www.nws.noaa.gov/directives/sym/pd01003020curr.pdf

NOAA NOS and U.S. Census Bureau, 2013: National Coastal Population Report: Population Trends from 1970 to 2020. National Oceanic and Atmospheric Administration, National Ocean Service, and U.S. Census Bureau, Silver Spring, MD, 22 pp. https://aambpublicoceanservice.blob.core.windows.net/oceanserviceprod/facts/coastal-population-report.pdf

Obeysekera, J. and J. Salas, 2020: Hydrologic designs for extreme events under nonstationarity. In: *Engineering Methods for Precipitation under a Changing Climate*. Olsen, J.R. and K.T. Adamec, Eds. American Society of Civil Engineers, 63–82. http://dx.doi.org/10.1061/9780784415528.ch04

One Climate Future, 2019: One Climate Future Climate Change Vulnerability Assessment. One Climate Future, Cities of Portland and South Portland, 181 pp. https://www.oneclimatefuture.org/wp-content/uploads/2020/12/OneClimateFuture_VulnerabilityAssessment_Final.pdf

Oppenheimer, M., B.C. Glavovic , J. Hinkel, R. van de Wal, A.K. Magnan, A. Abd-Elgawad, R. Cai, M. Cifuentes-Jara, R.M. DeConto, T. Ghosh, J. Hay, F. Isla, B. Marzeion, B. Meyssignac, and Z. Sebesvari, 2019: Sea Level Rise and Implications for Low-Lying Islands, Coasts and Communities. In: *IPCC Special Report on the Ocean and Cryosphere in a Changing Climate* [H.-O. Pörtner, D.C. Roberts, V. Masson-Delmotte, P. Zhai, M. Tignor, E. Poloczanska, K. Mintenbeck, A. Alegría, M. Nicolai, A. Okem, J. Petzold, B. Rama, N.M. Weyer (eds.)]. In Press. https://www.ipcc.ch/site/assets/uploads/sites/3/2019/11/08_SROCC_Ch04_FINAL.pdf

Parris, A., P. Bromirski, V. Burkett, D. Cayan, M. Culver, J. Hall, R. Horton, K. Knuuti, R. Moss, J. Obeysekera, A. Sallenger, and J. Weiss, 2012: Global Sea Level Rise Scenarios for the US National Climate Assessment. NOAA Tech Report OAR CPO-1. National Oceanic and Atmospheric Administration, Climate Program Office, 37 pp. https://repository.library.noaa.gov/view/noaa/11124

Perica, S., S. Pavlovic, M. St. Laurent, C. Trypaluk, D. Unruh, and O. Wilhite, 2018: Precipitation-Frequency Atlas of the United States. Volume 11, Version 2.0 Texas. National Oceanic and Atmospheric Administration, National Weather Service, Silver Spring, MD. https://repository.library.noaa.gov/view/noaa/22619

Piecuch, C. G. and, & Quinn, K. J. 2016: El Niño, La Niña, and the global sea level budget. *Ocean Science*, 12 (6), 1165–1177. https://doi.org/10.5194/os-12-1165-2016

Reguero, B.G., M. Menéndez, F.J. Méndez, R. Mínguez, and I.J. Losada. 2012: A Global Ocean Wave (GOW) calibrated reanalysis from 1948 onwards. *Coastal Engineering*. 65, 38–55. https://doi.org/10.1016/j.coastaleng.2012.03.003

Richter, K., B. Meyssignac, A.B.A. Slangen, A. Melet, J.A. Church, X. Fettweis, B. Marzeion, C. Agosta, S.R.M. Ligtenberg, G. Spada, M.D. Palmer, C.D. Roberts, and N. Champollion, 2020: Detecting a forced signal in satellite-era sea-level change. *Environmental Research Letters*, 15 (9), 094079. https://doi.org/10.1088/1748-9326/ab986e

Rydlund, P. H. Jr., B. J. Densmore (2012). Methods of practice and guidelines for using survey-grade Global Navigation Satellite Systems (GNSS) to establish vertical datum in the United States Geological Survey. Chapter 1 of Section D, Field Survey Methods, Book 11, *Collection and Delineation of Spatial Data*. U.S. Geological Survey, Reston, Virginia, 102 pp. with appendixes. http://pubs.usgs.gov/tm/11d1/

Salas, J.D., and J. Obeysekera, 2014: Revisiting the concepts of return period and risk for nonstationary hydrologic extreme events. *Journal of Hydrologic Engineering*, 19 (3) 554–568. https://doi.org/10.1061/(ASCE)HE.1943-5584.0000820

Salas, J.D., J. Obeysekera, and R. Vogel, 2018: Techniques for assessing water infrastructure for nonstationary extreme events: A review. *Hydrologic Science Journal*, 63 (3), 325–352. https://doi.org/10.1080/02626667.2018.1426858

Salas, J.D. and J. Obeysekera, 2019: Probability distribution and risk of the first occurrence of k extreme hydrologic events. *Journal of Hydrologic Engineering*, 24 (10), 04019032. https://doi.org/10.1061/(ASCE)HE.1943-5584.0001809

Slangen, A.B.A., M. Carson, C.A. Katsman, R.S.W. van de Wal, A. Köhl, L.L.A. Vermeersen, and D. Stammer, 2014: Projecting twenty-first century regional sea-level changes. *Climatic Change*, 124 (1), 317–332. http://dx.doi.org/10.1007/s10584-014-1080-9

Stockdon H.F., R.A. Holman, P.A. Howd, and A.H. Sallenger, Jr., 2006: Empirical parameterization of setup, swash, and runup. *Coastal Engineering*, 53 (7), 573–588. https://doi.org/10.1016/j.coastaleng.2005.12.005

Sutton, R.T., 2019: Climate science needs to take risk assessment much more seriously. *Bulletin of the* American *Meteorological Society*, 100 (9), 1637–1642. https://doi.org/10.1175/BAMS-D-18-0280.1

Sweeney, B. and A. Becker, 2020: Considering future sea level change in maritime infrastructure design: A survey of US Engineers. *Journal of Waterway, Port, Coastal, and Ocean Engineering*, 146 (4), 04020019. http://dx.doi.org/10.1061/(ASCE)WW.1943-5460.0000583

Sweet, W.V. and J. Park, 2014: From the extreme to the mean: Acceleration and tipping points of coastal inundation from sea level rise. *Earth's Future*, 2 (12), 579–600. https://doi.org/10.1002/2014EF000272

Sweet, W.V., J. Park, S. Gill, and J. Marra, 2015: New ways to measure waves and their effects at NOAA tide gauges: A Hawaiian-network perspective. *Geophysical Research Letters*, 42 (21), 9355–9361. https://doi.org/10.1002/2015GL066030

Sweet, W.V., R.E. Kopp, C.P. Weaver, J. Obeysekera, R.M. Horton, E.R. Thieler, and C. Zervas, 2017: Global and Regional Sea Level Rise Scenarios for the United States. NOAA Technical Report NOS CO-OPS 083. National Oceanic and Atmospheric Administration, National Ocean Service, Center for Operational Oceanographic Products and Services, Silver Spring, MD, 75 pp. https://tidesandcurrents.noaa.gov/publications/techrpt83_Global_and_Regional_SLR_Scenarios_for_the_US_final.pdf

Sweet, W.V., G. Dusek, J. Obeysekera, and J.J. Marra, 2018: Patterns and Projections of High Tide Flooding Along the U.S. Coastline Using a Common Impact Threshold. NOAA Technical Report NOS CO-OPS 086. National Oceanic and Atmospheric Administration, National Ocean Service, Silver Spring, MD, 44 pp. https://tidesandcurrents.noaa.gov/publications/techrpt86_PaP_of_HTFlooding.pdf

Sweet, W.V., G. Dusek, G. Carbin, J.J. Marra, D. Marcy, and S. Simon, 2020a: 2019 State of U.S. High Tide Flooding with a 2020 Outlook. NOAA Technical Report NOS CO-OPS 092. National Oceanic and Atmospheric Administration, National Ocean Service, Silver Spring, MD, 24 pp. https://tidesandcurrents.noaa.gov/publications/Techrpt_092_2019_State_of_US_High_Tide_Flooding_with_a_2020_Outlook_30June2020.pdf

Sweet, W.V., A.S. Genz, J. Obeysekera, and J.J. Marra. 2020b: A regional frequency analysis of tide gauges to assess Pacific coast flood risk. *Frontiers in Marine Science*, 7, 883. https://doi.org/10.3389/fmars.2020.581769

Sweet, W.V., S. Simon, G. Dusek, D. Marcy, W. Brooks, M. Pendleton, and J. Marra, 2021: 2021 State of High Tide Flooding and Annual Outlook. NOAA High Tide Flooding Report. National Oceanic and Atmospheric Administration, National Ocean Service, Silver Spring, MD, 28 pp. https://tidesandcurrents.noaa.gov/publications/2021_State_of_High_Tide_Flooding_and_Annual_Outlook_Final.pdf

Tebaldi, C., B.H. Strauss, and C.E. Zervas, 2012: Modelling sea level rise impacts on storm surges along US coasts. *Environmental Research Letters*, 7 (1), 014032. https://doi.org/10.1088/1748-9326/7/1/014032

Thompson, P.R., M.J. Widlansky, B.D. Hamlington, M.A. Merrifield, J.J. Marra, G.T. Mitchum, and W. Sweet, 2021: Rapid increases and extreme months in projections of United States high-tide flooding. *Nature Climate Change*, 1–7. https://doi.org/10.1038/s41558-021-01077-8

USACE, 1994: Engineering and Design: Hydrologic Frequency Estimates. ER 1110-2-1450. U.S. Army Corps of Engineers, Washington, DC, 8 pp. https://www.publications.usace.army.mil/Portals/76/Publications/EngineerRegulations/ER_1110-2-1450.pdf

USACE. 2014. Procedures to Evaluate Sea Level Change: Impacts, Responses, and Adaptation. Technical Letter 1100-2-1. U.S. Army Corps of Engineers, Washington, DC, 254 pp. https://www.publications.usace.army.mil/portals/76/publications/engineertechnicalletters/etl_1100-2-1.pdf

USACE MRG&P, 2017: 2015 Updated Atlas of U.S. Army Corps of Engineers Historic Daily Tide Data in Coastal Louisiana. MRG&P Report No. 14. U.S. Army Corps of Engineers, Mississippi River Geomorphology and Potamology Program, New Orleans, LA, 41 pp. https://erdc-library.erdc.dren.mil/jspui/bitstream/11681/25484/1/MRG%26P%20Report%20No%2014.pdf

USGCRP, 2017: *Climate Science Special Report: Fourth National Climate Assessment, Volume I* [Wuebbles, D.J., D.W. Fahey, K.A. Hibbard, D.J. Dokken, B.C. Stewart, and T.K. Maycock (eds.)]. U.S. Global Change Research Program, Washington, DC, USA, 470 pp. doi:10.7930/J0J964J6

USGCRP, 2018: *Impacts, Risks, and Adaptation in the United States: Fourth National Climate Assessment, Volume II* [Reidmiller, D.R., C.W. Avery, D.R. Easterling, K.E. Kunkel, K.L.M. Lewis, T.K. Maycock, and B.C. Stewart (eds.)]. U.S. Global Change Research Program, Washington, DC, USA, 1515 pp. doi:10.7930/NCA4.2018

Vitousek, S., P.L. Barnard, C.H. Fletcher, N. Frazer, L. Erikson, and C.D. Storlazzi, 2017: Doubling of coastal flooding frequency within decades due to sea-level rise. *Scientific Reports*, 7 (1), 1–9. http://dx.doi.org/10.1038/s41598-017-01362-7

Vousdoukas, M.I., L. Mentaschi, E. Voukouvalas, M. Verlaan, S. Jevrejeva, L.P. Jackson, and L. Feyen, 2018: Global probabilistic projections of extreme sea levels show intensification of coastal flood hazard. *Nature Communications*, 9 (1), 2360. http://dx.doi.org/10.1038/s41467-018-04692-w

Wada, Y., L.P.H. Van Beek, F.C. Sperna Weiland, B.F. Chao, Y.-H. Wu, and M.F.P. Bierkens, 2012: Past and future contribution of global groundwater depletion to sea-level rise. *Geophysical Research Letters*, 39 (9). https://doi.org/10.1029/2012GL051230

Wada, Y., M.-H. Lo, P.J.F. Yeh, J.T. Reager, J.S. Famiglietti, R.-J. Wu, and Y.-H. Tseng, 2016: Fate of water pumped from underground and contributions to sea-level rise. *Nature Climate Change*, 6 (8), 777–780. http://dx.doi.org/10.1038/nclimate3001

Wahl, T., I.D. Haigh, R.J. Nicholls, A. Arns, S. Dangendorf, J. Hinkel, and A.B. Slangen, 2017: Understanding extreme sea levels for broad-scale coastal impact and adaptation analysis. *Nature Communications*, 8 (1), 16075. http://dx.doi.org/10.1038/ncomms16075

Wang, J., Church, J. A., Zhang, X., & Chen, X. (2021). Reconciling global mean and regional sea level change in projections and observations. *Nature Communications*, 12 (1), 1–12. https://doi.org/10.1038/s41467-021-21265-6

WCRP Global Sea Level Budget Group, 2018: Global sea-level budget 1993–present. *Earth System Science Data*, 10, 1551–1590. http://dx.doi.org/10.5194/essd-10-1551-2018

Weaver, C.P., R.H. Moss, K.L. Ebi, P.H. Gleick, P.C. Stern, C. Tebaldi, R.S. Wilson, and J.L. Arvai, 2017: Reframing climate change assessments around risk: Recommendations for the US National Climate Assessment. *Environmental Research Letters*, 12 (8), 080201. https://doi.org/10.1088/1748-9326/aa7494

Werners, S.E., R.M. Wise, J.R.A. Butler, E. Totin, and K. Vincent, 2021: Adaptation pathways: A review of approaches and a learning framework. *Environmental Science & Policy*, 116, 266–275. https://doi.org/10.1016/j.envsci.2020.11.003

Yin, J., M.E. Schlesinger, and R.J. Stouffer, 2009: Model projections of rapid sea-level rise on the northeast coast of the United States. *Nature Geoscience*, 2 (4), 262–266. https://doi.org/10.1038/ngeo462

Zervas, C., 2013: Extreme Water Levels of the United States 1893–2010. NOAA Technical Report NOS CO-OPS 067. National Oceanic and Atmospheric Administration, National Ocean Service, Silver Spring, MD, 212 pp. https://tidesandcurrents.noaa.gov/publications/NOAA_Technical_Report_NOS_COOPS_067a.pdf

Section A1: Tables and Figures

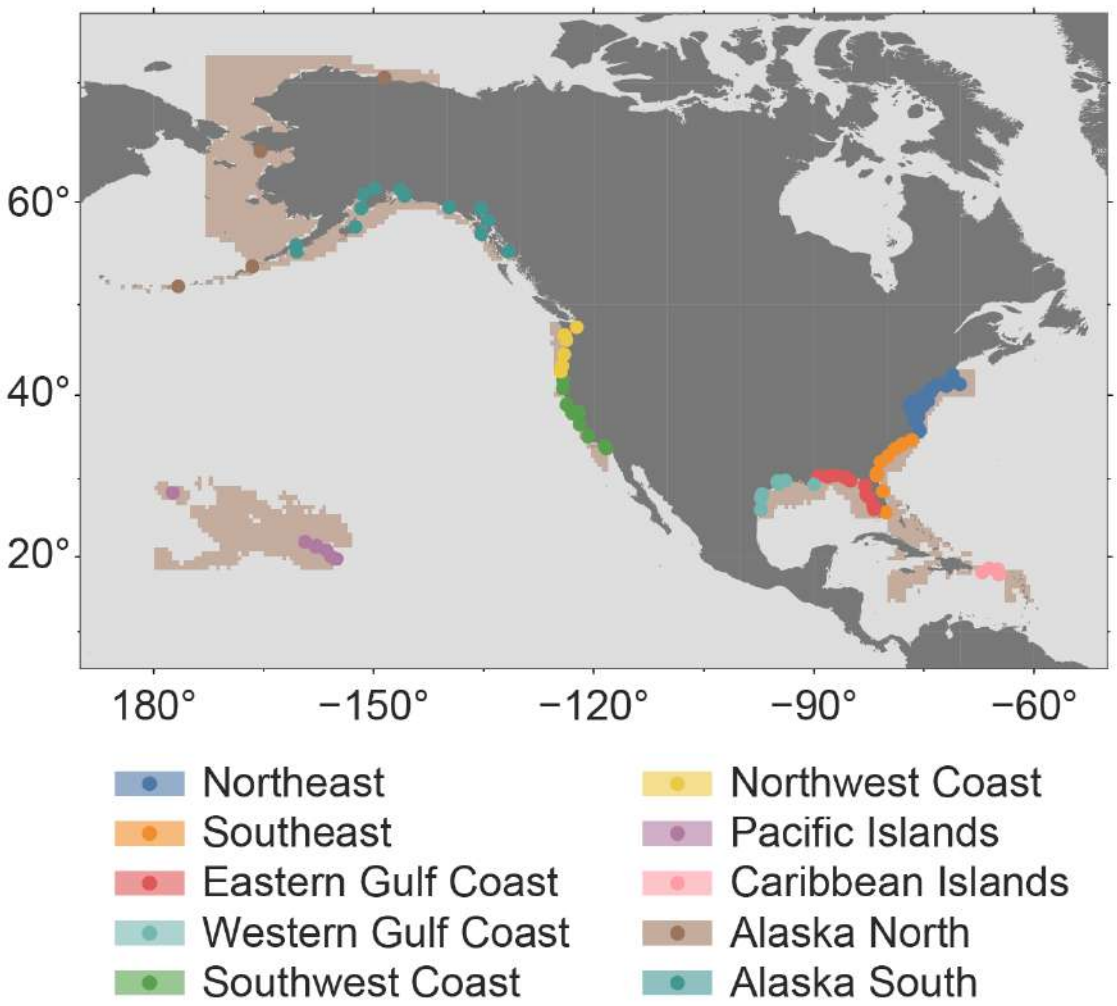

Figure A1.1: Region definitions for observation-based extrapolations and scenarios in Section 2. These regions are used both to group tide gauges and also to generate regional averages for the gridded scenarios. A bathymetry mask is used to define the regions for the gridded scenarios.

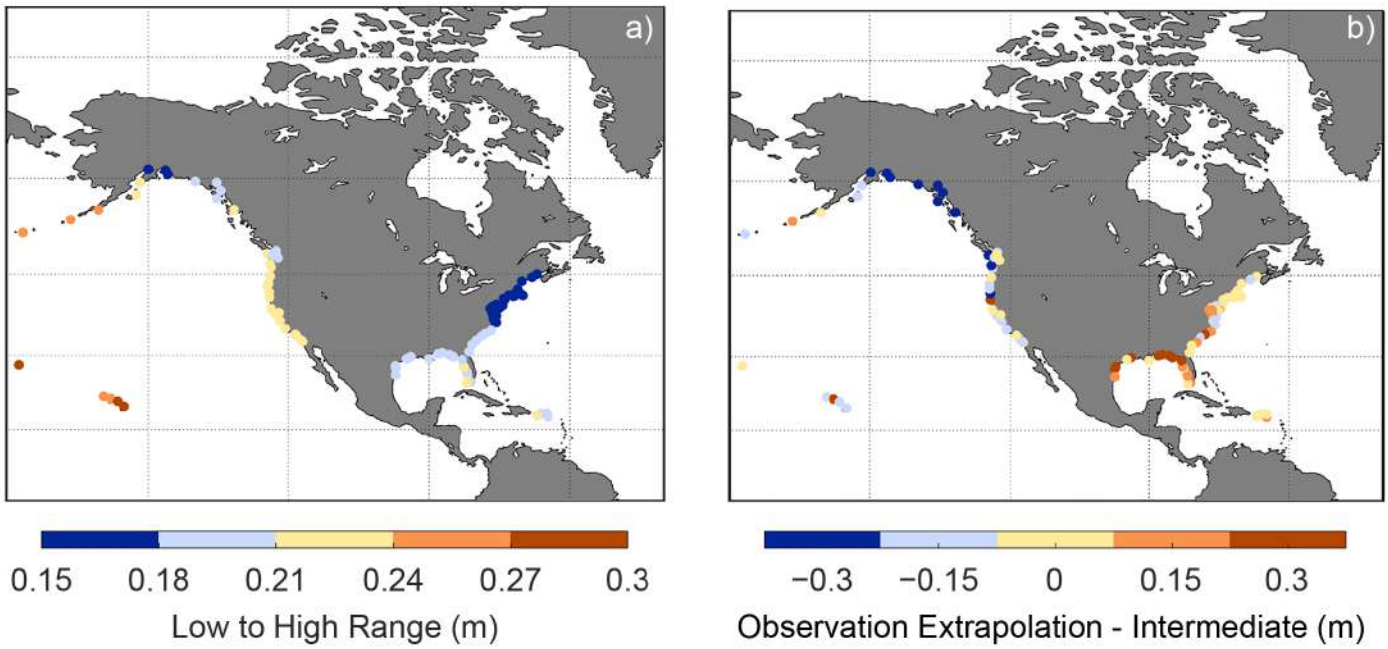

Figure A1.2. Shown for each tide gauge record with at least 30 years of record length between 1970 and 2020 are a) range, in meters, between median projection of Low and High Scenarios in 2050, and b) difference, in meters, between median observation-based extrapolation and Intermediate scenario in 2050.

Table A1.1: Projections methods employed.

Driver of GMSL or RSL change	Kopp et al. (2014) projection method (used in Sweet et al., 2017)	AR6 (Fox-Kemper et al., 2021) projection methods (used here)
Thermal expansion	CMIP5 ensemble drift-corrected zostoga	Two-layer model with climate sensitivity calibrated to the IPCC assessment and expansion coefficients calibrated to emulate CMIP6 models
Greenland ice sheet	*Likely* range from IPCC AR5, with shape of tails based on structured expert judgment (Bamber and Aspinall, 2013)	1. Emulated ISMIP6 simulations through 2100 (Edwards et al., 2021), extended after 2100 based on constant post-2100 rates 2. Structured expert judgment (Bamber et al., 2019)
Antarctic ice sheet	*Likely* range from IPCC AR5, with shape of tails based on structured expert judgment (Bamber and Aspinall, 2013)	1. Emulated ISMIP6 simulations through 2100 (Edwards et al., 2021), extended after 2100 with constant rates based on the IPCC AR5 parametric Antarctic Ice Sheet model (Church et al., 2013) 2. LARMIP-2 simulations (Levermann et al., 2020) augmented by AR5 surface mass balance model (Church et al., 2013), extended past 2100 based on constant rates 3. Single ice-sheet model incorporated marine ice cliff instability (DeConto et al., 2021) 4. Structured expert judgment (Bamber et al., 2019)
Glaciers	Distribution based on Marzeion et al. (2012) surface mass balance model	Emulated GlacierMIP (Marzeion et al., 2020; Edwards et al., 2021) extended after 2100 with IPCC AR5 parametric model refit to GlacierMIP (Marzeion et al., 2020)
Land water storage	Groundwater depletion: Population/groundwater depletion relationship calibrated based on Konikow (2011) and Wada et al. (2012) Water impoundment: Population/dam impoundment relationship calibrated based on Chao et al. (2008)	Groundwater depletion: Updated population/groundwater depletion relationship calibrated based on Konikow (2011) and Wada et al. (2012, 2016) Water impoundment: Population/dam impoundment relationship calibrated based on Chao et al. (2008), adjusted for new construction, following Hawley et al. (2020) for 2020 to 2040
Ocean dynamic sea level	Distribution derived from CMIP5 ensemble zos field	Distribution derived from CMIP6 ensemble zos field after linear drift removal
Gravitational, rotational, and deformational effects	Sea-level equation solver (Mitrovica et al., 2011) driven by projections of ice-sheet and glacier changes	Sea-level equation solver (Slangen et al., 2014) driven by projections of ice-sheet, glacier, and land water storage changes
GIA and other drivers of VLM	Spatiotemporal statistical model of tide-gauge data	Spatiotemporal statistical model of tide-gauge data (updated from Kopp et al., 2014)

Table A1.2: Offsets, in meters, for different time periods and for each region considered in Section 2. These offsets are assessed using the trajectory determined from the available tide-gauge data in each region.

	1992–2000	2000–2005	2005–2020
Contiguous U.S.	0.02	0.03	0.08
Northeast	0.03	0.02	0.09
Southeast	0.03	0.02	0.09
Eastern Gulf	0.03	0.02	0.1
Western Gulf	0.05	0.04	0.14
Southwest	0.01	0.01	0.05
Northwest	0.01	0.01	0.04
Hawaiian Islands	0.02	0.02	0.06
Caribbean	0.02	0.01	0.06

Table A1.3: Regional designation, tide gauge information, extreme water level metadata, and high tide flood heights.

US Region	EWL Grid No.	NOAA ID	Location	Latitude	Longitude	Tide Range (m)	Flood Index u (m, MHHW)	u Trend (mm/yr)	Epoch of u	Minor Flood (m, MHHW)	Moderate Flood (m)	Major Flood (m)
Pacific	39509	1611400	Nawiliwili, HI	21.95	−159.36	0.558	0.244	1.7	1983–2001	0.522	0.817	1.192
	39511	1612340	Honolulu, HI	21.31	−157.87	0.580	0.248	1.3	1983–2001	0.523	0.817	1.193
	39511	1612480	Mokuoloe, HI	21.43	−157.79	0.646	0.265	2.0	1983–2001	0.526	0.819	1.196
	39153	1615680	Kahului, HI	20.90	−156.48	0.686	0.252	2.1	1983–2001	0.527	0.821	1.197
	39154	1617433	Kawaihae, HI	20.04	−155.83	0.659	0.237	7.9	1983–2001	0.526	0.820	1.196
	38795	1617760	Hilo, HI	19.73	−155.06	0.731	0.272	3.1	1983–2001	0.529	0.822	1.199
	37704	1619000	Johnston Atoll	16.74	−169.53	0.674	0.295	2.2	1983–2001	0.527	0.820	1.197
	42004	1619910	Midway Islands	28.21	−177.36	0.381	0.303	1.9	1983–2001	0.515	0.811	1.185
	36941	1630000	Apra Harbor, Guam	13.44	144.65	0.715	0.249	4.2	1983–2001	0.529	0.821	1.199
	36941	1631428	Pago Bay, Guam	13.43	144.80	0.525	0.287	4.2	1983–2001	0.521	0.816	1.191
	26574	1770000	American Samoa	−14.28	189.32	0.848	0.338	3.8	1983–2001	0.497	0.788	1.167
	35169	1820000	Kwajalein	8.73	167.74	1.194	0.446	3.1	1983–2001	0.548	0.836	1.218
	39117	1890000	Wake Island	19.29	166.62	0.718	0.295	2.1	1983–2001	0.529	0.822	1.199
NE	47859	8410140	Eastport, ME	44.90	−66.98	5.874	0.930	2.1	1983–2001	0.735	0.976	1.405
	47858	8411250	Cutler Naval Base, ME	44.64	−67.30	4.133	0.716	2.4	1983–2001	0.665	0.924	1.335
	47857	8413320	Bar Harbor, ME	44.39	−68.21	3.465	0.657	2.1	1983–2001	0.639	0.904	1.309
	47496	8418150	Portland, ME	43.66	−70.25	3.019	0.605	1.9	1983–2001	0.621	0.891	1.291
	47496	8419317	Wells, ME	43.32	−70.56	2.914	0.667	3.5	1983–2001	0.617	0.887	1.287
	47496	8423898	Fort Point, NH	43.07	−70.71	2.864	0.662	3.5	1983–2001	0.615	0.886	1.285
	47136	8443970	Boston, MA	42.35	−71.05	3.131	0.634	2.8	1983–2001	0.625	0.894	1.295
	46777	8447386	Fall River, MA	41.70	−71.16	1.456	0.566	3.5	1983–2001	0.558	0.844	1.228
	46778	8447930	Woods Hole, MA	41.52	−70.67	0.672	0.446	3.2	1983–2001	0.527	0.820	1.197
	46778	8449130	Nantucket Island, MA	41.29	−70.10	1.089	0.418	3.8	1983–2001	0.544	0.833	1.214
	46777	8452660	Newport, RI	41.51	−71.33	1.174	0.478	2.8	1983–2001	0.547	0.835	1.217

Table A1.3 (cont.): Regional designation, tide gauge information, extreme water level metadata, and high tide flood heights.

US Region	EWL Grid No.	NOAA ID	Location	Latitude	Longitude	Tide Range (m)	Flood Index u (m, MHHW)	u Trend (mm/yr)	Epoch of u	Minor Flood (m, MHHW)	Moderate Flood (m)	Major Flood (m)
NE (cont.)	46777	8452944	Conimicut Light, RI	41.72	–71.34	1.398	0.560	3.5	1983–2001	0.556	0.842	1.226
	46777	8454000	Providence, RI	41.81	–71.40	1.476	0.549	2.3	1983–2001	0.559	0.844	1.229
	46777	8454049	Quonset Point, RI	41.59	–71.41	1.249	0.547	3.5	1983–2001	0.550	0.837	1.220
	46776	8461490	New London, CT	41.36	–72.09	0.930	0.468	2.6	1983–2001	0.537	0.828	1.207
	46776	8465705	New Haven, CT	41.28	–72.91	2.045	0.603	3.5	1983–2001	0.582	0.861	1.252
	46775	8467150	Bridgeport, CT	41.17	–73.18	2.231	0.555	3.0	1983–2001	0.589	0.867	1.259
	46777	8510560	Montauk, NY	41.05	–71.96	0.771	0.487	3.4	1983–2001	0.531	0.823	1.201
	46416	8514560	Port Jefferson, NY	40.95	–73.08	2.181	0.527	2.5	1983–2001	0.587	0.865	1.257
	46416	8516945	Kings Point, NY	40.81	–73.76	2.378	0.638	2.5	1983–2001	0.597	0.873	1.267
	46415	8518750	The Battery, NY	40.70	–74.01	1.542	0.546	3.1	1983–2001	0.562	0.846	1.232
	46415	8519483	Bergen Point, NY	40.64	–74.14	1.681	0.549	4.4	1983–2001	0.567	0.850	1.237
	46415	8531680	Sandy Hook, NJ	40.47	–74.01	1.593	0.552	2.7	1983–2001	0.564	0.848	1.234
	46056	8534720	Atlantic City, NJ	39.36	–74.42	1.403	0.534	4.1	1983–2001	0.556	0.842	1.226
	45697	8536110	Cape May, NJ	38.97	–74.96	1.659	0.486	4.7	1983–2001	0.566	0.850	1.236
	46055	8537121	Ship John Shoal, NJ	39.31	–75.38	1.894	0.578	3.5	1983–2001	0.576	0.857	1.246
	46055	8540433	Marcus Hook, PA	39.81	–75.41	1.871	0.563	3.5	1983–2001	0.575	0.856	1.245
	46055	8545240	Philadelphia, PA	39.93	–75.14	2.039	0.462	3.1	1983–2001	0.582	0.861	1.252
	46055	8551762	Delaware City, DE	39.58	–75.59	1.830	0.540	3.5	1983–2001	0.573	0.855	1.243
	46055	8551910	Reedy Point, DE	39.56	–75.57	1.779	0.423	4.1	1983–2001	0.571	0.853	1.241
	45696	8555889	Brandywine Shoal, DE	38.99	–75.11	1.676	0.616	3.5	1983–2001	0.567	0.850	1.237
	45696	8557380	Lewes, DE	38.78	–75.12	1.418	0.530	3.5	1983–2001	0.557	0.843	1.227
	45696	8570280	Ocean City, MD	38.33	–75.08	1.187	0.413	3.5	1983–2001	0.547	0.836	1.217
	45696	8570283	Ocean City Inlet, MD	38.33	–75.09	0.751	0.360	3.5	1983–2001	0.530	0.823	1.200
	45695	8571421	Bishops Head, MD	38.22	–76.04	0.624	0.503	3.5	1983–2001	0.525	0.819	1.195

Table A1.3 (cont.): Regional designation, tide gauge information, extreme water level metadata, and high tide flood heights.

US Region	EWL Grid No.	NOAA ID	Location	Latitude	Longitude	Tide Range (m)	Flood Index u (m, MHHW)	u Trend (mm/yr)	Epoch of u	Minor Flood (m, MHHW)	Moderate Flood (m)	Major Flood (m)
NE (cont.)	45695	8571892	Cambridge, MD	38.57	−76.07	0.622	0.414	4.9	1983–2001	0.525	0.819	1.195
	46054	8573364	Tolchester Beach, MD	39.21	−76.25	0.527	0.484	2.5	1983–2001	0.519	0.814	1.189
	46055	8573927	Chesapeake City, MD	39.53	−75.81	0.980	0.470	3.8	1983–2001	0.539	0.829	1.209
	46054	8574070	Havre De Grace, MD	39.54	−76.09	0.746	0.482	3.5	1983–2001	0.530	0.822	1.200
	46054	8574680	Baltimore, MD	39.27	−76.58	0.506	0.443	3.2	1983–2001	0.520	0.815	1.190
	45695	8575512	Annapolis, MD	38.98	−76.48	0.438	0.430	3.7	1983–2001	0.518	0.813	1.188
	45695	8577330	Solomons Island, MD	38.32	−76.45	0.449	0.398	6.0	1983–2001	0.518	0.813	1.188
	45694	8594900	Washington, DC	38.87	−77.02	0.965	0.461	3.3	1983–2001	0.539	0.829	1.209
	45337	8631044	Wachapreague, VA	37.61	−75.69	1.376	0.508	5.4	1983–2001	0.564	0.850	1.234
	45337	8632200	Kiptopeke, VA	37.17	−75.99	0.896	0.435	4.7	1983–2001	0.536	0.827	1.206
	45695	8635150	Colonial Beach, VA	38.25	−76.96	0.591	0.406	4.7	1983–2001	0.524	0.818	1.194
	45336	8635750	Lewisetta, VA	38.00	−76.46	0.458	0.420	5.6	1983–2001	0.518	0.814	1.188
	45336	8636580	Windmill Point, VA	37.62	−76.29	0.424	0.419	5.2	1983–2001	0.532	0.828	1.202
	45336	8637689	Yorktown, VA	37.23	−76.48	0.786	0.567	3.5	1983–2001	0.531	0.824	1.201
	44977	8638610	Sewells Point, VA	36.95	−76.33	0.841	0.502	4.6	1983–2001	0.534	0.825	1.204
	44977	8638863	CBBT, VA	36.97	−76.11	0.885	0.503	6.0	1983–2001	0.535	0.827	1.205
	44977	8639348	Money Point, VA	36.78	−76.30	0.977	0.528	5.6	1983–2001	0.539	0.829	1.209

Table A1.3 (cont.): Regional designation, tide gauge information, extreme water level metadata, and high tide flood heights.

US Region	EWL Grid No.	NOAA ID	Location	Latitude	Longitude	Tide Range (m)	Flood Index u (m, MHHW)	u Trend (mm/yr)	Epoch of u	Minor Flood (m, MHHW)	Moderate Flood (m)	Major Flood (m)
SE	44978	8651370	Duck, NC	36.18	−75.75	1.124	0.494	4.6	1983–2001	0.545	0.834	1.215
	44619	8652587	Oregon Inlet, NC	35.80	−75.55	0.360	0.384	4.6	1983–2001	0.514	0.811	1.184
	44619	8654400	Cape Hatteras, NC	35.22	−75.64	1.056	0.412	3.2	1983–2001	0.542	0.832	1.212
	44619	8654467	USCG Hatteras, NC	35.21	−75.70	0.186	0.598	3.2	1983–2001	0.507	0.806	1.177
	44259	8656483	Beaufort, NC	34.72	−76.67	1.079	0.362	3.8	1983–2001	0.543	0.832	1.213
	44258	8658120	Wilmington, NC	34.23	−77.95	1.427	0.327	2.3	1983–2001	0.557	0.843	1.227
	44258	8658163	Wrightsville Beach, NC	34.21	−77.79	1.366	0.564	3.2	1983–2001	0.555	0.841	1.225
	43898	8661070	Springmaid Pier, SC	33.66	−78.92	1.707	0.493	2.9	1983–2001	0.568	0.851	1.238
	43897	8662245	Oyster Landing, SC	33.35	−79.19	1.561	0.496	3.2	1983–2001	0.562	0.847	1.232
	43538	8665530	Charleston, SC	32.78	−79.93	1.757	0.453	3.3	1983–2001	0.570	0.853	1.240
	43537	8670870	Fort Pulaski, GA	32.03	−80.90	2.287	0.500	3.3	1983–2001	0.591	0.869	1.261
	42818	8720030	Fernandina Beach, FL	30.67	−81.47	1.999	0.473	2.3	1983–2001	0.580	0.860	1.250
	42818	8720218	Mayport, FL	30.40	−81.43	1.508	0.378	2.6	1983–2001	0.557	0.842	1.227
	42818	8720357	St Johns River, FL	30.19	−81.69	0.312	0.333	3.2	1983–2001	0.512	0.809	1.182
	42459	8720587	St. Augustine Beach, FL	29.86	−81.26	1.569	0.531	3.2	1983–2001	0.563	0.847	1.233
	42101	8721604	Trident Pier, FL	28.42	−80.59	1.193	0.407	5.1	1983–2001	0.537	0.825	1.207
	41024	8723214	Virginia Key, FL	25.73	−80.16	0.667	0.317	5.1	1983–2001	0.518	0.811	1.188
	40664	8723970	Vaca Key, FL	24.71	−81.11	0.297	0.249	4.2	1983–2001	0.512	0.809	1.182
	40664	8724580	Key West, FL	24.56	−81.81	0.551	0.262	2.5	1983–2001	0.522	0.817	1.192

Table A1.3 (cont.): Regional designation, tide gauge information, extreme water level metadata, and high tide flood heights.

US Region	EWL Grid No.	NOAA ID	Location	Latitude	Longitude	Tide Range (m)	Flood Index u (m, MHHW)	u Trend (mm/yr)	Epoch of u	Minor Flood (m, MHHW)	Moderate Flood (m)	Major Flood (m)
E. Gulf	41382	8725110	Naples, FL	26.13	−81.81	0.875	0.323	2.9	1983–2001	0.535	0.826	1.205
	41382	8725520	Fort Myers, FL	26.65	−81.87	0.401	0.325	3.1	1983–2001	0.516	0.812	1.186
	41740	8726384	Port Manatee, FL	27.64	−82.56	0.669	0.260	6.6	1983–2001	0.527	0.820	1.197
	41740	8726520	St Petersburg, FL	27.76	−82.63	0.688	0.337	2.8	1983–2001	0.528	0.821	1.198
	41740	8726607	Old Port Tampa, FL	27.86	−82.55	0.749	0.304	3.2	1983–2001	0.530	0.822	1.200
	41740	8726667	Mckay Bay Entrance, FL	27.91	−82.43	0.814	0.320	3.2	1983–2001	0.533	0.824	1.203
	41740	8726724	Clearwater Beach, FL	27.98	−82.83	0.841	0.294	7.1	1983–2001	0.540	0.831	1.210
	42457	8727520	Cedar Key, FL	29.14	−83.03	1.157	0.415	2.2	1983–2001	0.546	0.835	1.216
	42456	8728690	Apalachicola, FL	29.73	−84.98	0.492	0.390	3.0	1983–2001	0.520	0.815	1.190
	42814	8729108	Panama City, FL	30.15	−85.67	0.409	0.368	2.5	1983–2001	0.516	0.812	1.186
	42814	8729210	Panama City Beach, FL	30.21	−85.88	0.420	0.348	4.3	1983–2001	0.517	0.813	1.187
	42812	8729840	Pensacola, FL	30.40	−87.21	0.383	0.345	2.4	1983–2001	0.515	0.811	1.185
	42812	8732828	Mobile Bay, AL	30.42	−87.83	0.490	0.519	4.3	1983–2001	0.520	0.815	1.190
	42811	8735180	Dauphin Island, AL	30.25	−88.08	0.367	0.354	4.3	1983–2001	0.512	0.808	1.182
	42811	8736897	Mobile, AL	30.65	−88.06	0.517	0.535	4.3	1983–2001	0.521	0.816	1.191
	42811	8737048	Mobile State Docks, AL	30.71	−88.04	0.501	0.439	4.3	1983–2001	0.520	0.815	1.190
	42811	8741533	Pascagoula NOAA Lab, MS	30.37	−88.56	0.466	0.494	4.3	1983–2001	0.519	0.814	1.189
	42810	8747437	Bay Waveland Yacht Club, MS	30.33	−89.33	0.529	0.498	4.6	1983–2001	0.522	0.816	1.192

Table A1.3 (cont.): Regional designation, tide gauge information, extreme water level metadata, and high tide flood heights.

US Region	EWL Grid No.	NOAA ID	Location	Latitude	Longitude	Tide Range (m)	Flood Index u (m, MHHW)	u Trend (mm/yr)	Epoch of u	Minor Flood (m, MHHW)	Moderate Flood (m)	Major Flood (m)
W. Gulf	42092	8760922	Pilots Station East, SW Pass, LA	28.93	−89.41	0.356	0.399	4.3	2012–2016	0.514	0.811	1.184
	42451	8761724	Grand Isle, LA	29.26	−89.96	0.323	0.309	7.8	2012–2016	0.428	0.725	1.098
	42809	8761927	New Canal Station, LA	30.03	−90.11	0.164	0.485	5.6	1983–2001	0.507	0.805	1.177
	42450	8762075	Port Fourchon, LA	29.11	−90.20	0.368	0.298	4.3	2012–2016	0.515	0.811	1.185
	42449	8764227	Amerada Pass, LA	29.45	−91.34	0.487	0.535	4.3	1983–2001	0.519	0.815	1.189
	42449	8765251	Cypremort Point, LA	29.71	−91.88	0.518	0.458	4.3	1983–2001	0.521	0.816	1.191
	42448	8766072	Freshwater Canal Locks, LA	29.56	−92.31	0.657	0.696	4.3	1983–2001	0.526	0.820	1.196
	42806	8767816	Lake Charles, LA	30.22	−93.22	0.427	0.494	4.3	1983–2001	0.517	0.813	1.187
	42447	8768094	Calcasieu Pass, LA	29.77	−93.34	0.589	0.465	6.1	1983–2001	0.524	0.818	1.194
	42447	8770570	Sabine Pass North, TX	29.73	−93.87	0.488	0.368	6.1	1983–2001	0.520	0.815	1.190
	42446	8770613	Morgans Point, TX	29.68	−94.99	0.398	0.488	3.1	1983–2001	0.535	0.831	1.205
	42446	8771013	Eagle Point, TX	29.48	−94.92	0.338	0.331	13.8	1983–2001	0.494	0.790	1.164
	42446	8771341	Galveston Bay Entrance, TX	29.36	−94.72	0.510	0.499	6.1	1983–2001	0.520	0.815	1.190
	42446	8771450	Galveston Pier 21, TX	29.31	−94.79	0.429	0.366	6.5	1983–2001	0.517	0.813	1.187
	42446	8771510	Galveston Pleasure Pier, TX	29.29	−94.79	0.622	0.425	6.5	1983–2001	0.525	0.819	1.195
	42086	8772440	Freeport, TX	28.95	−95.31	0.536	0.391	9.0	1983–2001	0.521	0.816	1.191
	42086	8772447	USCG Freeport, TX	28.94	−95.30	0.549	0.460	6.1	1983–2001	0.522	0.816	1.192
	42084	8774770	Rockport, TX	28.02	−97.05	0.111	0.336	5.7	2002–2006	0.504	0.803	1.174
	41725	8775870	Corpus Christi, TX	27.58	−97.22	0.497	0.391	4.8	1983–2001	0.529	0.824	1.199
	41366	8779770	Port Isabel, TX	26.06	−97.22	0.418	0.337	4.0	1983–2001	0.517	0.813	1.187

Table A1.3 (cont.): Regional designation, tide gauge information, extreme water level metadata, and high tide flood heights.

US Region	EWL Grid No.	NOAA ID	Location	Latitude	Longitude	Tide Range (m)	Flood Index u (m, MHHW)	u Trend (mm/yr)	Epoch of u	Minor Flood (m, MHHW)	Moderate Flood (m)	Major Flood (m)
SW	43500	9410170	San Diego, CA	32.71	−117.17	1.745	0.490	2.2	1983–2001	0.570	0.852	1.240
	43500	9410230	La Jolla, CA	32.87	−117.26	1.624	0.468	2.1	1983–2001	0.565	0.849	1.235
	43858	9410660	Los Angeles, CA	33.72	−118.27	1.674	0.472	1.0	1983–2001	0.567	0.850	1.237
	44217	9410840	Santa Monica, CA	34.01	−118.50	1.654	0.489	1.8	1983–2001	0.566	0.850	1.236
	44216	9411340	Santa Barbara, CA	34.41	−119.69	1.645	0.485	0.6	1983–2001	0.566	0.849	1.236
	44574	9412110	Port San Luis, CA	35.18	−120.76	1.623	0.449	1.0	1983–2001	0.565	0.849	1.235
	44932	9413450	Monterey, CA	36.61	−121.89	1.627	0.431	1.6	1983–2001	0.565	0.849	1.235
	45290	9414290	San Francisco, CA	37.81	−122.47	1.780	0.375	1.9	1983–2001	0.571	0.853	1.241
	45290	9414523	Redwood City, CA	37.51	−122.21	2.501	0.400	2.7	1983–2001	0.600	0.875	1.270
	45290	9414750	Alameda, CA	37.77	−122.30	2.010	0.411	0.4	1983–2001	0.580	0.860	1.250
	45290	9414863	Richmond, CA	37.93	−122.40	1.846	0.359	3.1	1983–2001	0.574	0.855	1.244
	45290	9415020	Point Reyes, CA	38.00	−122.98	1.758	0.447	2.1	1983–2001	0.570	0.853	1.240
	45649	9415144	Port Chicago, CA	38.06	−122.04	1.498	0.388	1.4	1983–2001	0.560	0.845	1.230
	45648	9416841	Arena Cove, CA	38.91	−123.71	1.787	0.500	0.6	1983–2001	0.573	0.856	1.243
	46365	9418767	North Spit, CA	40.77	−124.22	2.090	0.491	4.8	1983–2001	0.584	0.863	1.254
	46724	9419750	Crescent City, CA	41.75	−124.18	2.095	0.548	-0.8	1983–2001	0.584	0.863	1.254
	47083	9431647	Port Orford, OR	42.74	−124.50	2.220	0.594	0.2	1983–2001	0.572	0.850	1.242
	47442	9432780	Charleston, OR	43.35	−124.32	2.323	0.586	1.1	1983–2001	0.593	0.870	1.263
	47801	9435380	South Beach, OR	44.63	−124.04	2.543	0.579	1.7	1983–2001	0.602	0.876	1.272
	48161	9437540	Garibaldi, OR	45.55	−123.92	2.536	0.597	2.4	1983–2001	0.601	0.876	1.271
	48520	9439040	Astoria, OR	46.21	−123.77	2.624	0.629	−0.2	1983–2001	0.605	0.879	1.275

Table A1.3 (cont.): Regional designation, tide gauge information, extreme water level metadata, and high tide flood heights.

US Region	EWL Grid No.	NOAA ID	Location	Latitude	Longitude	Tide Range (m)	Flood Index u (m, MHHW)	u Trend (mm/yr)	Epoch of u	Minor Flood (m, MHHW)	Moderate Flood (m)	Major Flood (m)
NW	48520	9440910	Toke Point, WA	46.71	−123.97	2.720	0.807	0.6	1983–2001	0.609	0.882	1.279
	48519	9441102	Westport, WA	46.90	−124.11	2.786	0.670	1.9	1983–2001	0.611	0.884	1.281
	48878	9442396	La Push, WA	47.91	−124.64	2.577	0.766	1.9	1983–2001	0.603	0.877	1.273
	49237	9443090	Neah Bay, WA	48.37	−124.61	2.425	0.688	−1.7	1983–2001	0.597	0.873	1.267
	49238	9444090	Port Angeles, WA	48.13	−123.44	2.153	0.562	0.2	1983–2001	0.586	0.865	1.256
	49239	9444900	Port Townsend, WA	48.11	−122.76	2.597	0.538	1.7	1983–2001	0.604	0.878	1.274
	48880	9446484	Tacoma, WA	47.27	−122.41	3.595	0.517	3.4	1983–2001	0.644	0.908	1.314
	48880	9447130	Seattle, WA	47.60	−122.34	3.462	0.541	2.1	1983–2001	0.639	0.904	1.309
	49239	9449424	Cherry Point, WA	48.86	−122.76	2.788	0.585	0.4	1983–2001	0.612	0.884	1.282
	49238	9449880	Friday Harbor, WA	48.55	−123.01	2.364	0.554	1.2	1983–2001	0.595	0.871	1.265
Alaska	51743	9450460	Ketchikan, AK	55.33	−131.63	4.708	1.086	−0.4	1983–2001	2.059	2.359	2.759
	52099	9451054	Port Alexander, AK	56.25	−134.65	3.329	0.738	−5.8	1983–2001	1.031	1.331	1.731
	52457	9451600	Sitka, AK	57.05	−135.34	3.029	0.768	−2.4	1983–2001	0.883	1.183	1.583
	52817	9452210	Juneau, AK	58.30	−134.41	4.970	1.152	−15.1	2012–2016	2.319	2.619	3.019
	53175	9452400	Skagway, AK	59.45	−135.33	5.100	1.218	−19.9	2012–2016	2.456	2.756	3.156
	52815	9452634	Elfin Cove, AK	58.19	−136.35	3.360	1.149	−5.8	1983–2001	1.048	1.348	1.748
	53171	9453220	Yakutat, Yakutat Bay, AK	59.55	−139.73	3.070	0.891	−10.7	2012–2016	0.902	1.202	1.602
	53524	9454050	Cordova, AK	60.56	−145.75	3.838	0.937	0.8	1983–2001	1.344	1.644	2.044
	53882	9454240	Valdez, AK	61.13	−146.36	3.702	0.878	−5.8	1983–2001	1.253	1.553	1.953
	53520	9455090	Seward, AK	60.12	−149.43	3.238	0.884	−4.0	1983–2001	0.983	1.283	1.683
	53159	9455500	Seldovia, AK	59.44	−151.72	5.499	1.350	−9.8	2012–2016	2.906	3.206	3.606
	53518	9455760	Nikiski, AK	60.68	−151.40	6.262	1.254	−9.9	2012–2016	NaN	NaN	NaN
	53879	9455920	Anchorage, AK	61.24	−149.89	8.889	1.269	−2.7	1983–2001	NaN	NaN	NaN
	52440	9457292	Kodiak Island, AK	57.73	−152.51	2.675	0.715	−9.2	2012–2016	0.743	1.043	1.443

Table A1.3 (cont.): Regional designation, tide gauge information, extreme water level metadata, and high tide flood heights.

US Region	EWL Grid No.	NOAA ID	Location	Latitude	Longitude	Tide Range (m)	Flood Index u (m, MHHW)	u Trend (mm/yr)	Epoch of u	Minor Flood (m, MHHW)	Moderate Flood (m)	Major Flood (m)
Alaska (cont.)	52079	9457804	Alitak, AK	56.90	−154.25	3.578	0.908	−5.8	2012–2016	1.174	1.474	1.874
	51714	9459450	Sand Point, AK	55.34	−160.50	2.204	0.737	1.4	1983–2001	0.615	0.915	1.315
	51712	9459881	King Cove, AK	55.06	−162.33	2.082	0.753	−5.8	1983–2001	0.592	0.892	1.292
	50262	9461380	Adak Island, AK	51.86	−176.63	1.131	NaN	NaN	NaN	0.572	0.872	1.272
	50623	9461710	Atka, AK	52.23	−174.17	1.041	0.424	−5.8	1983–2001	0.584	0.884	1.284
	50629	9462450	Nikolski, AK	52.94	−168.87	1.213	0.537	−5.8	1983–2001	0.563	0.863	1.263
	50990	9462620	Unalaska, AK	53.88	−166.54	1.098	NaN	NaN	NaN	0.576	0.876	1.276
	51714	9463502	Port Moller, AK	55.99	−160.57	3.175	0.697	−5.8	1983–2001	0.952	1.252	1.652
	52422	9464212	Village Cove, AK	57.13	−170.29	1.005	NaN	NaN	NaN	0.589	0.889	1.289
	54940	9468756	Nome, AK	64.50	−165.43	0.464	NaN	NaN	NaN	0.719	1.019	1.419
	56018	9491094	Red Dog Dock, AK	67.58	−164.07	0.269	NaN	NaN	NaN	0.787	1.087	1.487
	57111	9497645	Prudhoe Bay, AK	70.40	−148.53	0.214	NaN	NaN	NaN	0.808	1.108	1.508
Carib	38168	9751364	St. Croix, VI	17.75	−64.71	0.226	0.205	2.4	1983–2001	0.509	0.807	1.179
	38527	9751381	St. John, VI	18.32	−64.72	0.252	0.210	2.4	1983–2001	0.510	0.808	1.180
	38168	9751401	Lime Tree Bay, VI	17.69	−64.75	0.216	0.154	3.0	1983–2001	0.509	0.806	1.179
	38527	9751639	Charlotte Amalie, VI	18.34	−64.92	0.240	0.172	2.3	1983–2001	0.510	0.807	1.180
	38526	9752695	Vieques Island, PR	18.09	−65.47	0.225	0.190	2.4	1983–2001	0.509	0.807	1.179
	38525	9755371	San Juan, PR	18.46	−66.12	0.481	0.191	2.4	1983–2001	0.519	0.814	1.189
	38165	9759110	Magueyes Island, PR	17.97	−67.05	0.204	0.157	1.9	1983–2001	0.508	0.806	1.178
	38524	9759938	Mona Island, PR	18.09	−67.94	0.247	0.257	2.4	1983–2001	0.510	0.807	1.180

Section A2: Methods Appendix: Extreme Water Levels and Alaska Coastal Flood Height

A2.1: Data and Regional Frequency Analysis

A regional frequency analysis (RFA) of NOAA tide gauges is used to estimate extreme water levels (EWLs) along U.S. coastlines at and away from tide gauges. The RFA method (Hosking and Wallis, 1997) is based on the assumption that similar physical forcing across a region will produce a similar frequency of events and a probability density up to a local index (u), which is a local scaling factor that captures response peculiarities (Dalrymple, 1960). An RFA uses regional sets of data that have been locally normalized by their respective local index with a statistical heterogeneity test (H value) to assess the extent that the data are sufficiently similar. Using statistical L-moments, heterogeneity is a measure of the variation between sites of a location's summary distribution statistics and the amount of dispersion expected if the locations were indeed a homogeneous region (Hosking and Wallis, 1997). If $H < 1$, the region is considered acceptably homogeneous. If $1 \leq H < 2$, the region is considered possibly heterogeneous but acceptable for our study. If $H \geq 2$, then the tide-gauge group is definitely heterogeneous and not suitable for analysis. Once the regional bounds are established whose data are acceptably homogeneous, the aggregated data are fit with an extreme value distribution.

This study uses hourly and "top ten" data from all NOAA tide gauges[46] with at least 10 years of record (Figure A2.1). Water levels are put onto the mean higher high water (MHHW) tidal datum and detrended (the trend value is retained and shown in Table A1.3) relative to the midpoint of the current national datum tidal epoch (1983–2001), which is similar for NOAA EWL procedures using a single-gauge analysis (Zervas, 2013; Extreme Water Levels[47]). From the datasets, daily highest water levels are picked and declustered at each tide gauge using a 4-day storm window to ensure event independence. The 98th percentile of the

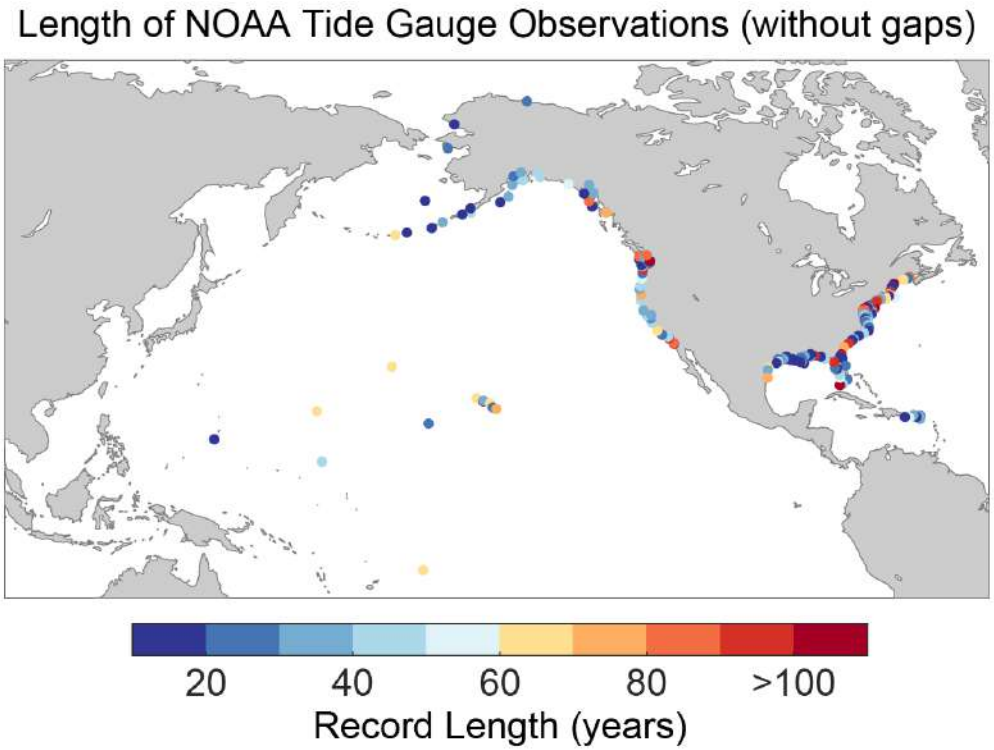

Figure A2.1: NOAA tide gauges used in the regional frequency analysis to generate extreme water level probabilities for U.S. coastlines.

[46] https://tidesandcurrents.noaa.gov/
[47] https://tidesandcurrents.noaa.gov/est/

declustered daily highest levels at each tide gauge is used as the local index (u) to normalize the data for the RFA process.

To form regions, the tide-gauge data is aggregated across a 400 km radius, similar to methods of Hall et al. (2016) but from the midpoint of a continuous set of coastline-intersecting 1-degree grids instead of site-specific installations. A maximum of 10 and a minimum of 3 tide gauges are included for each grid. Next, the regional data are spatially declustered with an additional 4-day event (i.e., storm) window to ensure that only the maximum water level within a region is retained (keep only the highest peak water levels for a particular event). Then, the statistical heterogeneity measure is estimated to ensure that the grouped tide-gauge data are sufficiently homogeneous (H < 2). In some instances, when a region surrounding a grid centroid

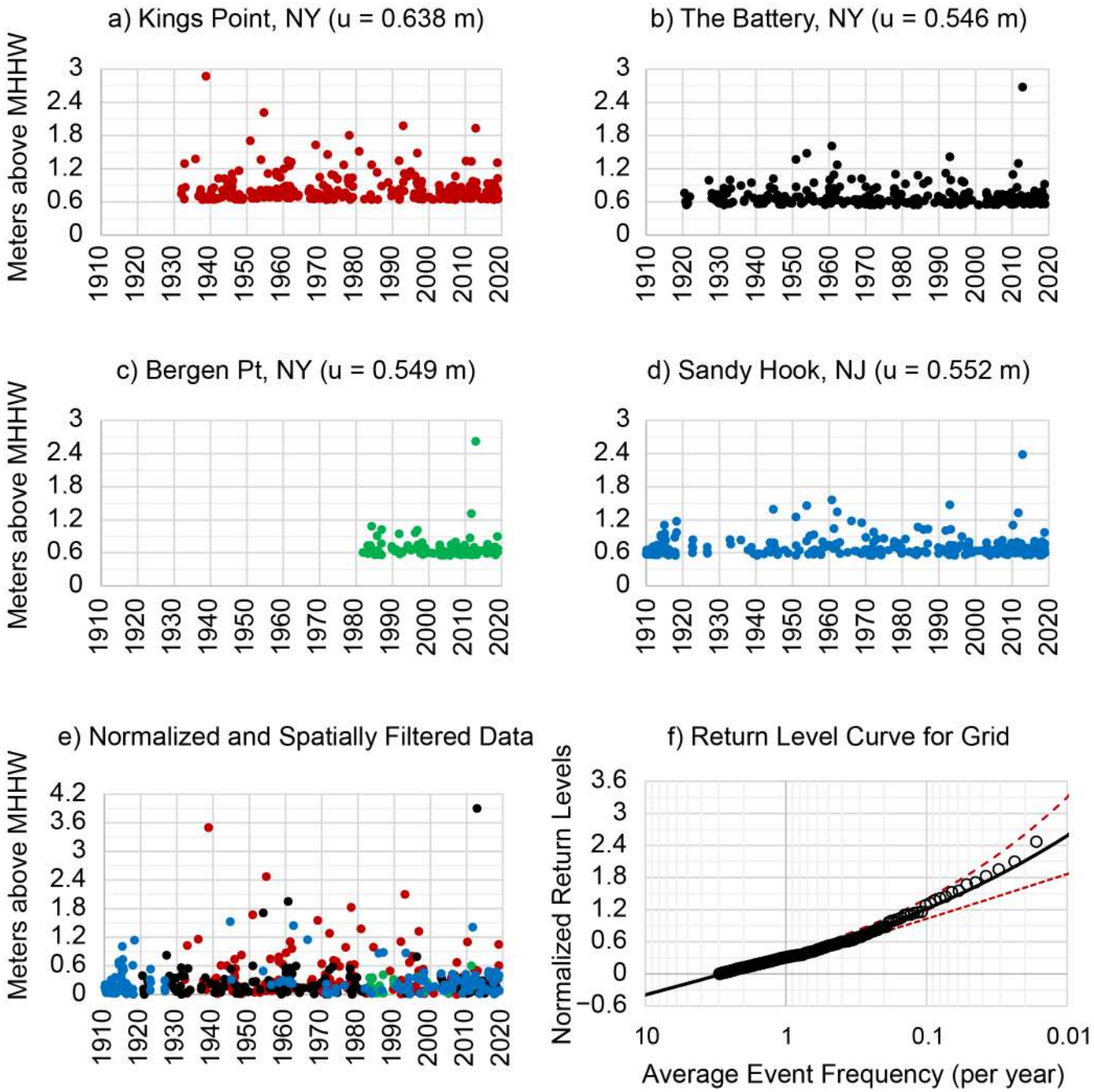

Figure A2.2: Example of data from grid number 46415 showing exceedances above each local index (u) relative to the 1983–2001 mean higher high water (MHHW) tidal datum at a) Kings Point, New York; b) The Battery, New York; c) Bergen Point, New York; and d) Sandy Hook, New Jersey, which are e) aggregated into a single dataset and f) fit by a Generalized Pareto Distribution to form a return level interval curve for the grid.

has H ≥ 2, tide gauges farthest away are sequentially dropped until homogeneity is achieved. In the end, all 1-degree grids along the contiguous United States (CONUS) had H < 2 (considered acceptably homogeneous) except a grid (number 48519) along the Northwest Pacific coastline, which, along with the Hawaiian and other U.S. Pacific Islands, uses the much larger physical-process regions identified and quantified in Sweet et al. (2020b). Grids along the Alaska coastline are fairly well resolved by the RFA except along the western and northern coasts.

An example is shown for grid number 46415, which is where the NOAA tide gauge at The Battery in New York City (NYC) is located (Figure A2.2). Four tide gauges are included in this grid (Kings Point, New York; The Battery, New York; Bergen Point, New York; and Sandy Hook, New Jersey [Figure A2.2a–d]), and their data are considered homogeneous (H value of 0.32). After the 4-day spatial filtering for events, each of the tide-gauge datasets is normalized by (divided by) its respective local index (u) value and aggregated as shown in Figure A2e.

A2.2: Gridded (Regional) Extreme Water Level Probabilities

With the tide gauges identified for each 1-degree grid, the aggregated and normalized datasets are fit with a Generalized Pareto Distribution (GPD; Coles, 2001). Using the penalized maximum likelihood method (Coles and Dixon, 1999; Frau et al., 2018; Sweet et al., 2020b), expected and 95% confidence interval (2.5th% and 97.5th% levels) values are estimated for the gridded EWL probabilities and defined as:

1)
$$G\,(Z;\,u,\alpha,\xi)\;=\;\lambda\left[1+\;\xi\left(\frac{z-u}{\alpha}\right)\right]^{-1/\xi}$$

where G is the exceedance probability (P[Z > z]), λ is the probability of an individual (normalized) observation exceeding the local index (u), α is the scale parameter, and ξ is the shape parameter. It is assumed that the distribution of the number of exceedances per year follows a Poisson distribution and that the return level for an EWL of height (Z) is given by:

2)
$$Z_N = u + \frac{\alpha}{\xi}\left[\left(Nn_y\lambda\right)^{\xi} - 1\right]$$

where N is the average recurrence interval (referred to in this study as the average event frequency, which is the reciprocal value), n_y is number of days per year (365.25), and λ is the average number of event exceedances per year (about 3 on average across all tide gauges in the study). To estimate EWLs with return levels with a 10 events/year frequency, we extrapolate the gridded GPD model with a logarithmic fit for return levels between the 0.5–3 events/year frequencies. A return level interval curve fit to the aggregated data (Figure A2.2e) for the grid where NYC is located is shown in Figure A2.2f.

A2.3: Localized Extreme Water Level Probabilities

When fitting a GPD to the RFA of aggregated tide-gauge data, the local EWL (EWL_{local}) probabilities including the model of expected values and their 95% confidence interval at a particular location are given as

3)
$$EWL_{local} = EWL_{gridded} * u_{local} + u_{local}$$

where $EWL_{gridded}$ is the gridded return level for a particular coastal 1-degree grid and u_{local} is the local index used in both the RFA and GPD processes. The value of u is a height (98th percentile of 4-day event filtered daily highest water level) above the local MHHW tidal datum for the current (1983–2001) national tidal datum epoch (NTDE) or for a modified 5-year epoch. The associated uncertainty of the $EWL_{gridded}$ estimated during the RFA is expressed as $\sigma_{gridded.}$ When localized at a tide gauge used in the formulation of the grids (see Figure A1), u is assumed to have no uncertainty. However, just as the location parameters in generalized extreme value (GEV) have time-dependent characteristics (Menéndez and Woodworth, 2010), it is recognized that u would experience similar behavior, but that is not quantified in this study.

In this RFA framework, it is possible to estimate EWL_{local} from the $EWL_{gridded}$ probabilities (expected values and 95% confidence interval) through the use of other sources of data. Specifically, the local indices needed to localize the $EWL_{gridded}$ values can either be 1) obtained from short-term tide-gauge data (or by targeted deployments) within a particular grid that is not included in the RFA formulation (<10 years; Figure A2.3) or 2) based on an underlying relationship between regional sets of local index (u) values and tide range available from, for example, NOAA VDatum.[48] In both cases, we establish large U.S. coastal regions (note: these are slightly different than the regions discussed in Sections 2 and 3 of the report and shown in Figure A1.1) that encompass several 1-degree grids to quantify information needed to obtain local indices and/or estimate variance/uncertainties (e.g., RMSE). These alternative methods, which are discussed below, may be of interest to coastal communities that are not co-located to a tide gauge used in this study but have predictions of tide range or have access to or are planning temporary tide-gauge installations to establish tidal datums and/or EWLs.

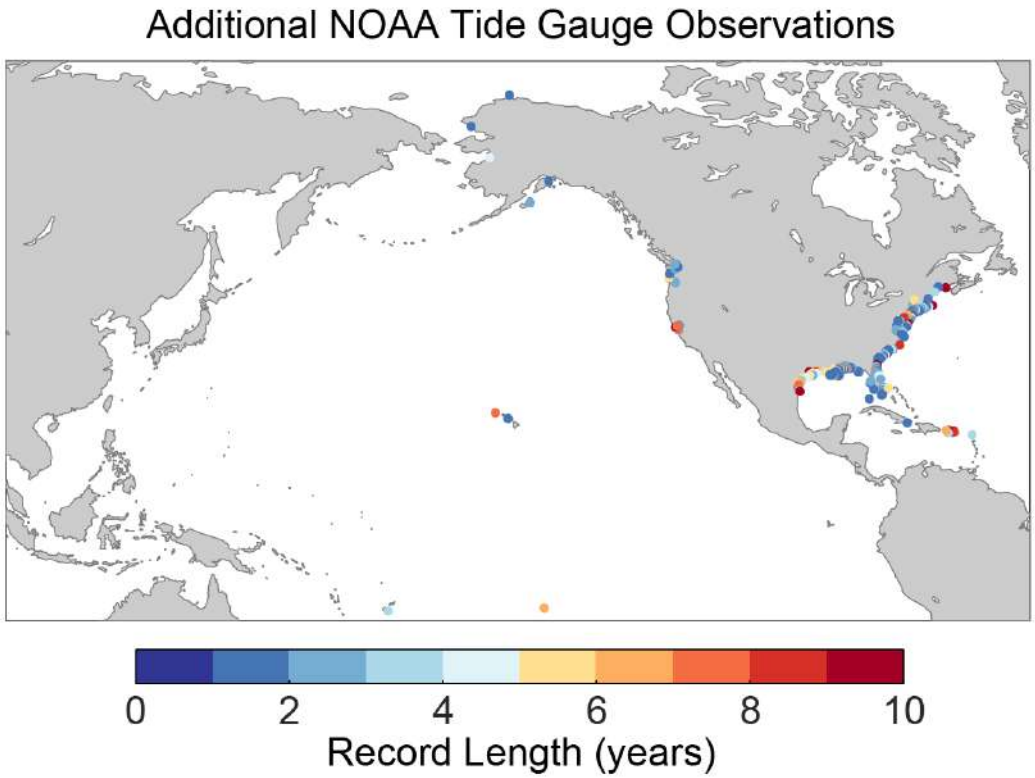

Figure A2.3: Additional tide-gauge data available from NOAA that can be used to localize the 1-degree gridded set of regional frequency analysis-based extreme water level probabilities. See https://tidesandcurrents.noaa.gov/.

A2.3.1: Local Index Estimates from Short-Term Installations

When other sets of tide/water level data are available, a local index can be directly estimated to obtain EWL_{local} probabilities from the $EWL_{gridded}$ probabilities. The first step for using data that are not from NOAA would be to estimate a local MHHW tidal datum using, for example, NOAA's online datum tool.[49] Following Equation 3 above, there will be some uncertainty in the local index value that is dependent on record length (e.g., 1–10 years). To account for short-record uncertainty in the local indices (u), RMSE (1 standard error) is estimated for regional estimates of u for the tide gauges used in the RFA (see Figure A2.1). Root mean square error is estimated using a logarithmic fit over a 19-year record length (Figure A4). To compute the RMSE, the maximum absolute differences are computed between u derived over the entire record and for progressively longer consecutive record lengths between 2001 and 2019 at each tide gauge (e.g., 19 discrete 1-year

[48] https://vdatum.noaa.gov/
[49] https://access.co-ops.nos.noaa.gov/datumcalc/

records; 18 consecutive 2-year records). The maximum (absolute) difference is used to account for interannual variability that can be significant (e.g., during phases of El Niño–Southern Oscillation [ENSO]). This difference is considered the error in estimating u for shorter records, and the average of the absolute differences across the regional set of tide gauges is considered the bias. The standard deviation of the absolute differences is also computed across all tide gauges, and an estimate of the RMSE is then computed as the square

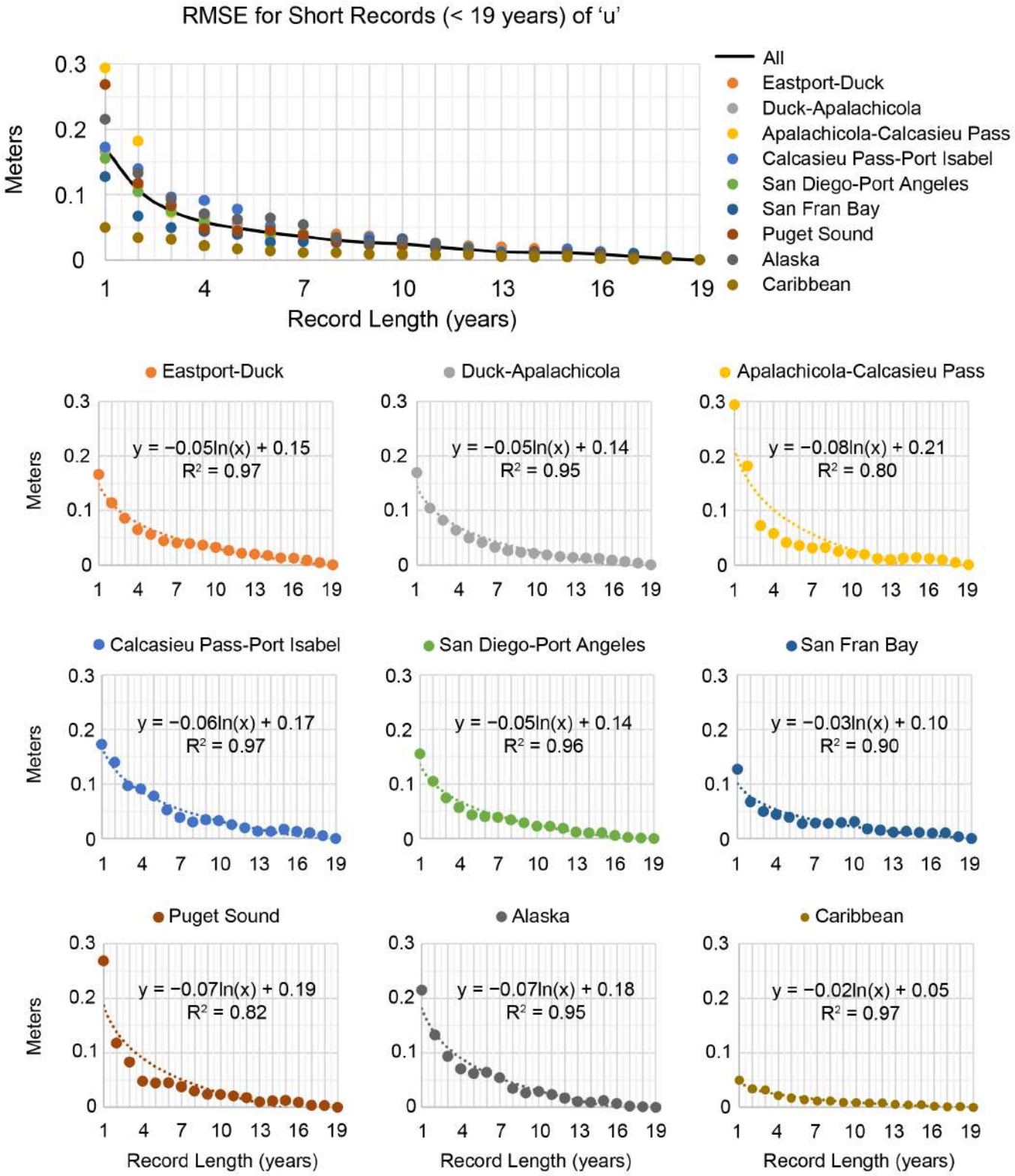

Figure A2.4: Root mean square error for regional estimates of flood indices (u) based on 1–19 years of consecutive data over the 2001–2019 period, based on regional sets of tide gauges used in this study. Note: these regions are not the same as those shown in Figure A1.1 and used to describe results in Sections 2 and 3 of the report.

root of the sum of the square of the bias and the standard deviation (variance). The estimates for Hawaiian and U.S. Pacific Islands follow estimates of Sweet et al. (2020b).

A2.3.2: Obtaining a Local Index from Tide Range Information

Another method to obtain an estimate of a local index (u) and its uncertainty is based on a dependency (correlation) that exists with tide range (great diurnal [GT]) along most coastal regions similar to findings of Merrifield et al. (2013). In essence, tide range (GT), which represents the spread between MHHW and mean lower low water (MLLW), partially quantifies the variance of the daily highest water level distribution and the height of the local index u. Figure A2.5 illustrates the regression-based relationships between tide range and u along U.S. coastal regions (these are the same regions used in Figure A2.4). All regressions are significant above the 90% significance level (p values < 0.1) and applicable for the 1983–2001 tidal epoch. For the Hawaiian and U.S. Pacific Islands, the Pacific-wide regression of Sweet et al. (2020b) is used.

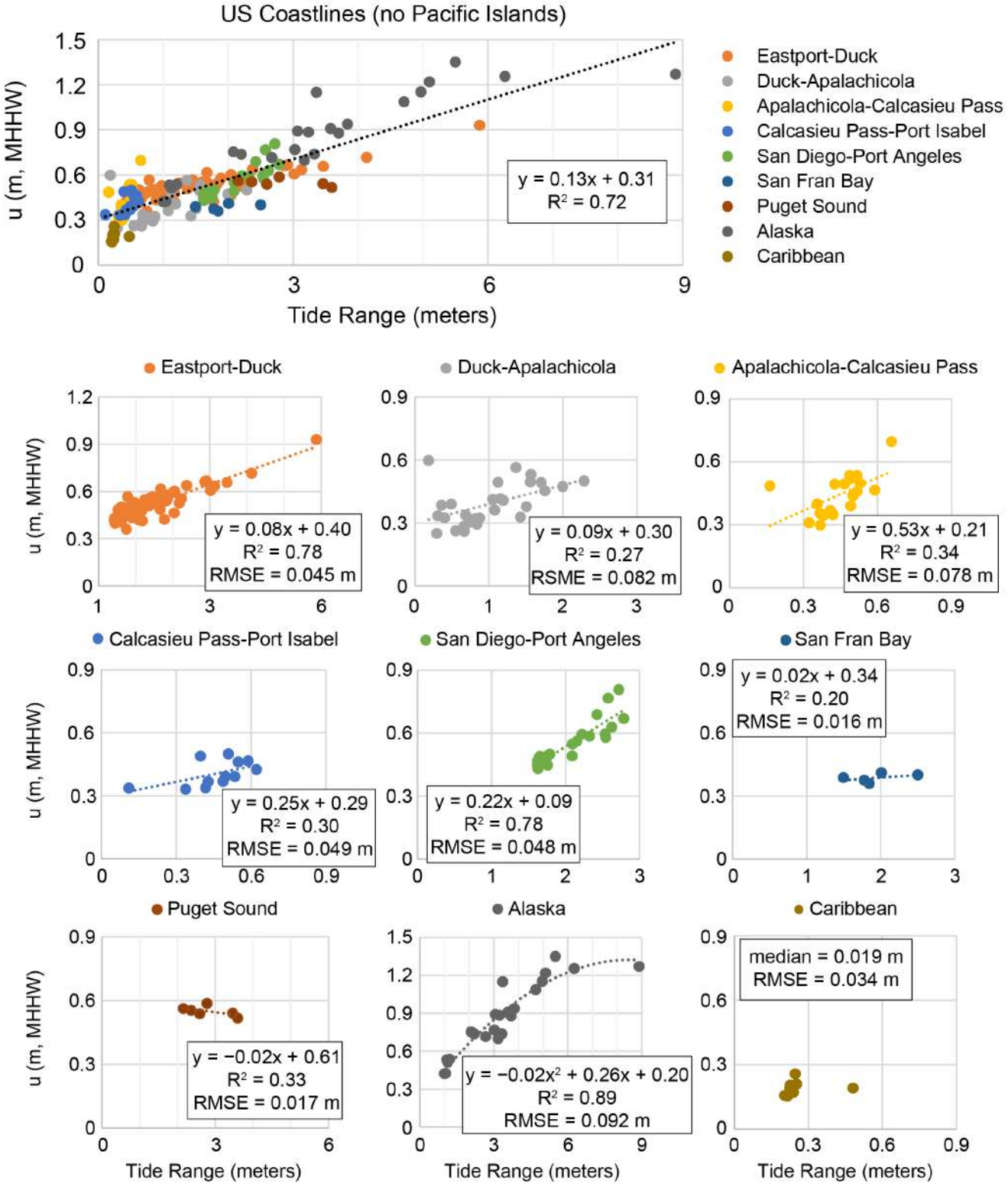

Figure A2.5: Tide range to local index (u) regressions with equations, goodness of fit (R^2), and root mean squared error (RMSE) shown by regions. Note: all local indices (u) are relative to the 1983–2001 tidal datum epoch. In the equations, y represents the local index (u) and x represents tide range.

A2.3.3: Uncertainties Using Alternative Methods to Estimate EWL_{local} Probabilities

When using either alternative method (tide range or short-record estimates) to obtain a local index (u), the uncertainty estimates of EWL_{local} probabilities will include additional uncertainty in u (σ_u). Following methods of Sweet et al. (2020b), it can be shown that

4) $$\sigma_{EWL(local)} = [(1 + \mu_{EWLgridded})^2 + \sigma^2_{EWLgridded}]\sigma_u^2 + \mu_u^2\sigma^2_{EWLgridded}$$

where $\mu_{EWLgridded}$ and μ_u are the expected values of the gridded return levels and the expected value of u, for example, estimated by the tide-range and u dependency (see Figure A2.5), respectively, σ_u^2 is the uncertainty inherent to any u-prediction relationship (e.g., RMSE). Thus, there is an additive uncertainty in u as estimated from this relationship, which would introduce additional uncertainty in estimates of EWL_{local}.

A2.3.4: Adjusting Local Extreme Water Level Probabilities to Time Periods

To adjust the EWL_{local} probabilities to a different sea level other than the current tidal epoch (e.g., from 1992 to 2000 or 2005 so as to apply the sea level rise scenarios), RSL estimates using the trends inherent to the hourly data used to compute the local index (u) should be applied (Table A1.3) to the epoch-specific EWL_{local} probabilities themselves. For tide gauges used in the RFA analysis and with more than 20 years of data, the local u trend can be used; otherwise, a median regional trend as defined in Figures A2.4 and A2.5 can be used. Alternatively, the RSL offsets derived from the regional observational RSL data (Table A1.2) could be used with differences between methods considered insignificant. For example, to estimate probabilities for the year 2000, the EWL_{local} probabilities values would be increased by an amount equal to the trend in u (or the median u trend value for the region) multiplied by 8 years (since 1992, which is the midpoint of the 1983–2001 epoch). The same procedure should be followed to adjust EWL_{local} probabilities for a given location estimated via the tide range regression (see Figure A5). In the case of a short-term estimate of u, similar procedures should be followed if local tidal datums have been computed and adjusted to the national tidal datum epoch (e.g., using the CO-OPS Tidal Analysis Datum Calculator[50]); in the case where no epoch can be established (see the CO-OPS Tidal Analysis Datum Calculator for guidance), then the measurements will be assumed to be referenced to the period of collection, and trend adjustment may be less straightforward.

A2.4: Alaska Coastal Flood Heights

To assess flood exposure, the coastal high tide flooding (HTF) heights of Sweet et al. (2018) are used for all U.S. coastlines outside of Alaska. Used in NOAA annual outlooks (e.g., Sweet et al., 2021; The State of High Tide Flooding and Annual Outlook[51]), these heights are a best-fit solution (regression) to the dozens of National Weather Service (NWS) emergency response warning thresholds established at many (but not all) NOAA tide gauges along the country's coastline. The NWS thresholds are used to communicate expected or ongoing coastal flood hazards to the public (NOAA, 2020), but often their depth-severity thresholds vary according to specific features near the tide gauge that affect both the associated flood frequency and the degree of broader vulnerabilities. Along the Alaska coastline, we follow the methodologies of Sweet et al. (2020b), who used a slight modification to assess "damaging flood heights" for the Pacific Basin coastlines. Here, the Alaska flood heights are based on a quadratic regression model using only Pacific Coast NWS minor flood heights and considered for only tide ranges below 6 meters (Figure A2.6a). To obtain moderate and major flood heights for Alaska, 0.3 m and 0.7 m are added to the regression, which is approximately the median difference between these heights and those for minor flooding along CONUS (Sweet et al., 2018). With flood heights defined nationally, minor, moderate, and major HTF are defined as occurring when water levels reach or exceed heights of about (median values) 0.55 m, 0.85 m, and 1.2 m above MHHW, respectively, and linearly vary with tide range (Figures A2.6b–d).

[50] https://access.co-ops.nos.noaa.gov/datumcalc/index.jsp
[51] https://tidesandcurrents.noaa.gov/HighTideFlooding_AnnualOutlook.html

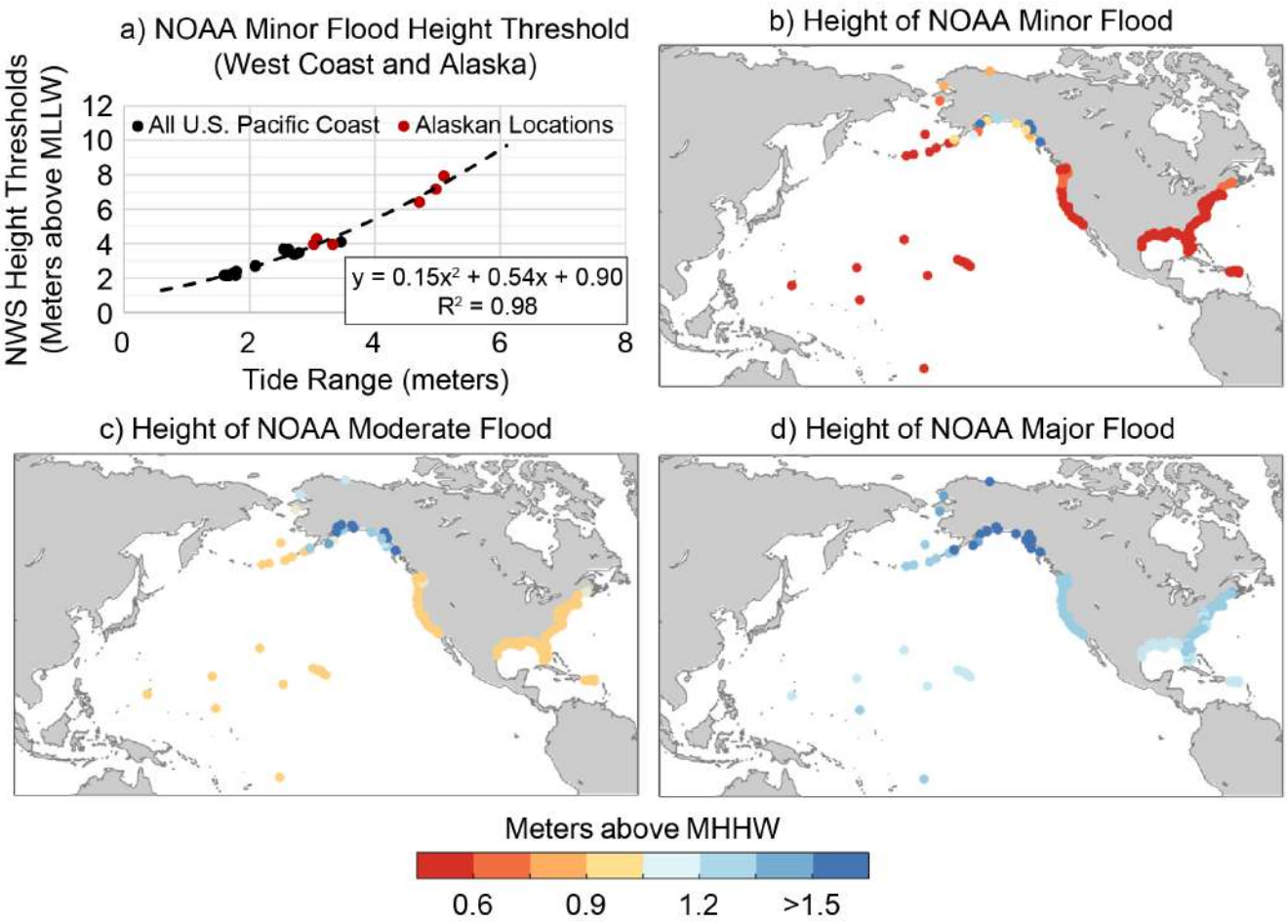

Figure A2.6: a) Quadratic regression of U.S. West Coast minor flood heights of NOAA's National Weather Service, following methods of Sweet et al. (2020b), to obtain a minor HTF definition for Alaska's coastline. The NOAA flood heights for b) minor, c) moderate, and d) major HTF are shown relative to mean higher high water.

8. Acronyms

Note: state abbreviations have been omitted

AIS: Antarctic ice sheet
AEF: average event frequency
AMOC: Atlantic meridional overturning circulation
AR5: [IPCC] Fifth Assessment Report
AR6: [IPCC] Sixth Assessment Report
ARI: average return interval
C: celsius
CDF: cumulative distribution function
cm: centimeter
CMIP5: Coupled Model Intercomparison Project Phase 5
CMIP6: Coupled Model Intercomparison Project Phase 6
CONUS: contiguous United States
CO-OPS: Center for Operational Oceanographic Products and Services
CoSMoS: Coastal Storm Modeling System
DRSL: Department of Defense Regional Sea Level [database]
ENSO: El Niño–Southern Oscillation
EPA: Environmental Protection Agency
EWL: extreme water level
FEMA: Federal Emergency Management Agency
FFRD: Future of Flood Risk Data
GCM: global climate model
GEV: generalized extreme value
GHG: greenhouse gas
GIA: glacial isostatic adjustment
GlacierMIP: Glacier Model Intercomparison Project
GMSL: global mean sea level
GPD: Generalized Pareto Distribution
GPS: Global Positioning System
GRD: gravitational, rotational, and deformational
GT: great diurnal tide range
HTF: high tide flood, flooding
HUC: hydrologic unit code
InSAR: Interferometric Synthetic Aperture Radar
IPCC: Intergovernmental Panel on Climate Change
ISMIP6: Ice Sheet Model Intercomparison Project for CMIP6
JPM–OS: joint probability method–optimal sampling [procedure]
LARMIP-2: Linear Antarctic Response Model Intercomparison Project [version 2]
m: meter
MHHW: mean higher high water
MICI: marine ice cliff instability
MLLW: mean lower low water
mm: millimeter
NASA: National Aeronautics and Space Administration
NAVD88: North American Vertical Datum of 1988
NCA: National Climate Assessment
NCA5: Fifth National Climate Assessment
NCA4: Fourth National Climate Assessment
NOAA: National Oceanic and Atmospheric Administration
NOC: National Ocean Council

NSRS: National Spatial Reference System
NTDE: national tidal datum epoch
NWS: National Weather Service
NYC: New York City
PDO: Pacific Decadal Oscillation
R^2: goodness of fit
RFA: regional frequency analysis
RMSE: root mean square error
RSL: relative sea level
SOST: Subcommittee on Ocean Sciences and Technology
SSP: Shared Socioeconomic Pathway
USACE: U.S. Army Corps of Engineers
USGCRP: U.S. Global Change Research Program
USGS: U.S. Geological Survey
VDatum: Vertical Datum Transformation
VLM: vertical land motion


NOAA
NASA
US Army Corps of Engineers
USGS
science for a changing world
RUTGERS
UNIVERSITY | NEW BRUNSWICK
FEMA
FIU
Institute of Environment
Florida International University